Self-consistent-field ensembles of disordered Hamiltonians: Efficient solver and application to superconducting films

Dissertation zur Erlangung des Doktorgrades der Naturwissenschaften (Dr. rer. nat.) der Fakultät für Physik

der Universität Regensburg

vorgelegt von

Matthias Stosiek aus

Neumarkt i.d.Opf.

im Jahr 2020

Promotionsgesuch eingereicht am: 17.06.2020
Die Arbeit wurde angeleitet von: Prof. Dr. Ferdinand Evers

Prüfungsausschuss:
Prof. Dr. Christoph Strunk
Prof. Dr. Jaroslav Fabian
Prof. Dr. Vladimir Braun

Datum Promotionskolloquium: 23.07.2020

Contents

Chapter 1

Introduction

The general topic of this thesis is the study of interaction effects in disordered metals. Disorder in this case means impurities, lattice distortions and similiar phenomena that appear in metals. The electronic behavior may be changed profoundly in the presence of disorder: in the strongly disordered case a localization transition may occur, where all eigenstates change from plane-wave-like extended states to localized states that only exhibit appreciable weight in some region of space characterized by a localization scale.

We are interested in the effects that interactions have on systems in the localized and diffusive regimes. The description of interacting particles is a very challenging endeavor. Exact analytical solutions are not known for most disordered interacting system of appreciable system size. A major challenge for numerical approaches is the exponential growth of the Fock space of interacting systems with their size. Mean-field theory, which we will employ throughout this thesis, is an important approximate approach to handle interactions. Here the aggregated effect of the interactions of all involved particles is described with mean-fields that enter an effective single-particle Hamiltonian. As these mean-fields are functionals of observables, they have to be determined self-consistently.

Many systems are well described within a mean-field approach. Beyond their immediate usefulness mean-field theories bear importance because they provide a tractable reference point for a perturbative analysis of interaction effects, as they typically appear in analytical approaches. Thus, they are a generic encounter in all theories of disordered fermions that try to incorporate interactions.

A major focus of this thesis will be placed on phase transitions that these

disordered interacting systems undergo. An example for such a transition that has received considerable attention recently is many-body localization. Many-body localized systems are not able to thermalize on any time-scale that could be studied so far. This illustrates the fascinating novel physics that disordered interacting systems exhibit.

Phase transitions can be characterized by the critical behavior in the vicinity of the transition. There may be various microscopic realizations for a specific kind of critical behavior. Systems that exhibit the same criticality are categorized in the same universality class. A systematic description of all universality classes of disordered systems remains unkown. We hope to contribute to a more complete understanding of an exhaustive classification of transitions in disordered metals by finding transitions that belong to as of yet unknown universality classes.

A very important category to distinguish universality classes is the symmetry class of the underlying system. A complete symmetry classification of disordered metals has been devised by Altland and Zirnbauer[1, 2, 3]. The ten symmetry classes are distinguished by their combination of the four basic symmetries: time-reversal, spin-rotation, chiral or sub-lattice and particle-hole symmetry. In the past, symmetry classes were sometimes identified with universality classes. Today it is widely appreciated that transitions that belong to the same symmetry class can differ in universality class. As an example where the symmetry classification does not give a good hint on the universality class, we mention disordered superconductors with broken time-reversal and spin-rotational symmetry (symmetry class D). In these systems different types of disorder can lead to different universality classes, even if the type of disorder does not affect the symmetry class.[4].

In order to study novel universality classes, we will investigate special kinds of random matrix ensembles. Random matrix theory is an important formalism to describe disordered systems. With the help of suitable random matrix ensembles many of the low-energy properties of disordered Hamiltonians can be described. A generic random matrix ensemble can be found for all symmetry classes[1, 2, 3]. We are interested in sub-ensembles of these generic random matrix ensembles. These ensembles can exhibit various kinds of critical behavior. A well studied example of such an ensemble is constituted by the power-law random-banded matrices (PRBM).[5] Criticality in PRBM can be studied relatively easily with numerical and analytical techniques. [5, 6]

It is a synthetic property that criticality appears in the PRBM-ensemble; it is imposed by introducing long-range hoppings into a tight-binding Hamil-

tonian. The criticality is tuned by a parameter, the hopping distance. Physical realizations have been suggested[7] but the systems it is applicable to are limited.

It therefore is interesting to explore properties of other ensembles that arise in a broader range of physical contexts. The ensembles that we have in mind are those that naturally appear in the mean-field treatment of disordered interacting systems. As an illustration of their appearance in this context and the novel critical behavior that they can exhibit, we give the example of a disordered one-dimensional wire. Without interactions such a system is in a localized phase, which impedes screening. For that reason long-range Coulomb interaction has to be considered. Within a mean-field description the long-range nature of the Coulomb interaction will lead to long-range correlations in the effective mean-field potential. The disorder on the other hand can be modelled by a random modulation of the potential. Each realization of the disorder potential corresponds then to one Hamiltonian matrix of the matrix ensemble. It has been shown that a linear system with a long-range correlated random potential can delocalize[8]. Thus in this ensemble interactions may change the universality class even in the case of symmetry-preserving effective potentials. Furthermore, the criticality may be tuned by parameters associated to the interaction, e.g. an interaction strength energy scale.

The self-consistent field (scf) ensemble of random Hamiltonians described above is only one of many candidates for such a novel kind of ensembles. It was chosen as an example, because the appearance of long-range correlations is immediately obvious in it. As we show in this thesis, even short-range interactions can lead to long-range correlations in the mean-fields. Thus, the appearance of novel critical behavior can be expected in a very wide range of physical contexts, in which these ensembles arise naturally within a mean-field description. We believe that their study will contribute to a more complete understanding of universality classes in disordered fermionic systems.

1.1 Motivation for numerics and challenges

Parts of this introduction can already be found in an earlier publication with copyright by the American Physical Society[9]. The investigation of scf-ensembles is a very challenging endeavor. The difficulty is that each

disorder configuration requires to find its own self-consistent fields. The solution of the scf-cycle is very difficult to do with analytical techniques. But also numerically it is demanding already at moderate system sizes of a few thousand sites. The solution has to be found in an iterative fashion with a large number of self-consistency cycles ($\sim 10^3$). Furthermore, to compute disorder-averaged observables many disorder realizations have to be considered ($\sim 10^2$). Presumably, this is the main reason why numerical studies of scf-ensembles have been performed infrequently in the past, despite of their obvious fundamental relevance.

Thus motivated, we have developed a state-of-the-art implementation of the scf-problem. With it the system sizes that we can address at an affordable numerical cost exceed the ones of prior studies by two orders of magnitude. The interplay of disorder induced quantum-interference and mean-field interactions can be studied on length scales that exceed the lattice constant by two orders of magnitude.

In the following we give two interesting applications of our software package to the physical systems that we consider throughout this thesis.

1.2 Appetizer: superconductors with a single impurity

As a first application of our code we have considered s-wave superconductors with a single impurity. We are motivated by a collaboration with the experimental group of Wulf Wulfhekel at the Karlsruhe Institute of Technology. In this group scanning tunneling microscopy(STM) measurements of superconducting bulk Al(111) around a Fe impurity have been conducted. In Fig. 1.1 (b) the raw experimental data of the differential conductance is shown. By a fit of the resulting local density of states to a temperature broadened BCS density of states, the value of the superconducting gap has been obtained. In Fig. 1.1 (c) this gap as a function of the distance from the impurity is shown. It is clearly enhanced ($\sim 9\%$) at the impurity position. The decay is non-monotonic, as is evidenced by the local maximum at 3 nm distance. The Wulfhekel group attributed this to a oscillatory contribution in the response function.

The self-consistency requirement complicates the description of the response to an impurity at the surface of a bulk superconductor. An analytical

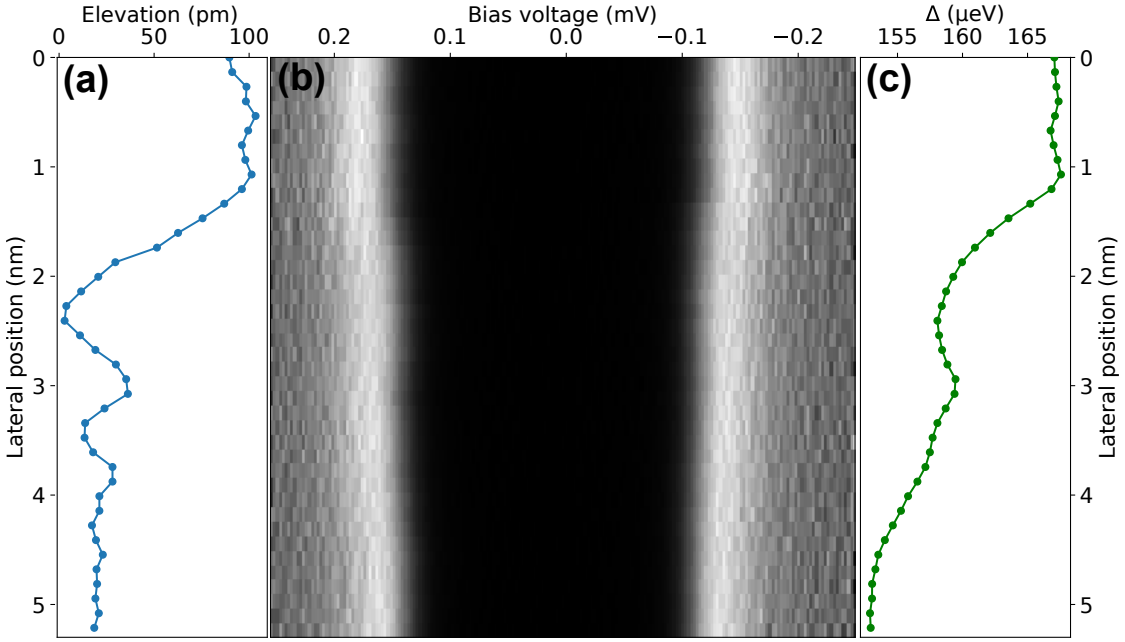

Figure 1.1: (a) Change of the STM tip elevation in constant current mode as a function of distance from the impurity. (b) Color encoded dI/dV recorded as function of distance from the impurity on the same lateral positions as a). (c) Superconducting gap Δ fitted to data of b) as function of position from the impurity. The experiments were conducted by the Wulfhekel group of the Karlsruhe Institute of Technology and are as of yet unpublished.[10]

formalism remains unknown. With our numerical simulations we could confirm the oscillatory nature of the response function. It shows a frequency of twice the Fermi wave vector, $2k_{\mathrm{F}}$. We find an increase of the gap at the impurity of $\sim 6\%$. Thus the enhancement of superconductivity around the impurity was reproduced semi-quantitatively as well. Furthermore we also determine the exponent of the power-law decay of the gap response. An exhaustive and detailed comparison with the experimental data including the decay is in progress[10].

1.3 Appetizer: dirty superconductors

Parts of this introduction can already be found in an earlier publication with copyright by the American Physical Society[9]. As the second application of our code we choose disordered s-wave superconductors with screened Coulomb interaction.

The interplay of disorder and superconductivity provides a fascinating field of inquiry. Disorder may lead to localization and thus an insulating phase with vanishing conductivity. Superconductivity on the other hand leads to conduction with vanishing resistance. In that sense the two phases are polar opposites. In systems exhibiting both phenomena a Superconductor-Insulator-Transition (SIT) is possible. Despite considerable effort there is no consensus on a critical theory describing the SIT. Multiple theories and mechanisms are being discussed and the relation between them remains unknown.

Since the seminal papers by Ghosal, Randeria, and Trivedi [11, 12] the disordered attractive Hubbard model has been employed extensively to study the SIT both with computational[13, 14, 15, 16, 17, 18, 19, 20, 21, 22, 23] and analytical[24, 25, 26] means.

Important insights have been gained within the mean-field description of the disordered attractive Hubbard model. The most striking findings include (i) the granularity of the pairing amplitude ("islands") emergent on the scale of the coherence length even for short-range disorder[12]. Since this theoretical prediction the effect has been observed experimentally[27, 28]; (ii) the parametric decoupling of the spectral gap from the mean pairing amplitude at large disorder: while the first remains relatively large, the second decays to zero. [12] Only recently direct evidence of the existence of separate pairing and spectral gap energy scales has become available[29]. (iii) A parameter regime was predicted where the typical size of pairing amplitude is increased as compared to the clean limit, so disorder has a pronounced tendency to *enhance* superconductivity. The mechanism was explored in 3D near the Anderson transition[24, 25] but also in 2D samples with short and long-range interactions[30, 31, 32]. Several predictions are broadly consistent with numerical results obtained on a honeycomb lattice [18] and have been confirmed recently on a square lattice as well [23]. Recently this phenomenon was observed experimentally as well[33]. (iv) At large interactions the coherence length was reported to exhibit a non-monotonous behavior with increasing disorder strength.[19]

Despite the progress, the current situation is not fully satisfying: On

the one hand, computational mean-field studies of the Hubbard model have been limited to system sizes L that do not allow to study the most interesting regime of length scales where the coherence length exceeds the lattice spacing: $\xi \gg a$. While analytical approaches, on the other hand, operate in this regime, they rely on partial self-consistency in order to become tractable.

Motivated by this observation, we investigate the Bogoliubov-deGennes(BdG) theory of disordered superconductors focussing on s-wave pairing in thin films. The full parameter plane of disorder, W, and interaction, U, is considered in which we study the distribution function and autocorrelations of the local gap function, $\Delta(\mathbf{r})$. Our computational machinery allows us to cover the full parameter space from the extreme regimes, which have been addressed computationally before, to the analytically tractable weak coupling limit. In this effort we observe the formation of islands in large regions of the parameter space, for the first time on mesoscopic scales considerably exceeding the lattice constant. Regimes are included with parameters relatively close to the one where strong inhomogeneity has been observed experimentally.[28].

Our observation might indicate that islands play a crucial role for the stability of the superconducting phase in actual experiments. Namely, islands imply localized Cooper pairs and therefore a diminishing of the phase-stiffness. In other words, islands go together with enhanced phase-fluctuations that destabilise long-range superconducting order. This connection between island-formation and stability has been emphasized before.[12, 13]

Calculating the autocorrelation function of the spectral gap, $|\Delta(\mathbf{q})|^2$ we can extract a characteristic inverse length scale $\xi^{-1}(W, U)$ with the physical meaning of a correlation length. We study ξ within the full phase diagram. Interestingly, concomitantly with island formation we find an enhanced correlation length. A similar observation, if only at very large interaction strength, U=5, has been made by Seibold et al. [19]. To what extent the enhancement of ξ is an artefact of mean-field theory that is removed when adding phase fluctuations remains to be seen.

A second focus we put on the investigation of the mesoscopic fluctuations of the local and global density of states at different disorder and temperature regimes. Strong fluctuations in disordered superconductors have been demonstrated experimentally[27, 28, 34]. Analytical treatments are available in a field theoretical framework, where strong fluctuations have been found, in particular close to the critical temperature[35]. The perturbative nature of this non-linear-σ model approach does not allow for predictions beyond the weakly disordered limit.

We for the first time investigate the fluctuations in regimes from weak to strong disorder, where the fluctuations are particularily pronounced. We find that the fluctuations generically get enhanced as the critical temperature is approached. Furthermore the energy range, where the enhancement is appreciable, is broadened significantly with increasing disorder.

In addition we will address open questions concerning the enhancement of superconductivity by disorder. While an increase of the gap has been demonstrated within BdG-theory on a square lattice [23], it is not certain that this translates to an increase in critical temperature. As the authors state themselves, phase fluctuations have to be taken into account in critical temperature predictions. The small increase ($< 1\%$) of the zero temperature gap might be outweighed by a decrease in the phase stiffness. We for the first time identify a regime, where the gap is strongly enhanced (up to $\sim 20\%$).

We complement this zero temperature investigation with a determination of the mean-field critical temperature. While such an investigation has been conducted before [22], the small system sizes ($\sim 10^3$ sites) did not permit an analyzation of the low coupling regime, where an enhancement of the gap can be found.

To investigate the importance of phase fluctuations for the finite temperature transition, we consider the evolution of the spatial distribution of the gap with increasing temperature. In agreement with experimental findings[33], we conclude that a regime with increased critical temperature is plausible.

Finally, like earlier authors[12] we also pay a special attention to the sensitivity of the behavior of computational observables to approximations made in the self-consistency procedure. We identify key effects for which only full self-consistency provides the correct description: (i) island formation when observed in moderate parameter regions is a characteristic hallmark of full self-consistency. It escapes partial ("energy-only") self-consistent schemes; (ii) The gap is monotonically enhanced in the partial ("energy-only"), while with full self-consistency we find a maximum at a certain disorder strength. It turns out that the inhomogeneous Hartree shift is key in this qualitative feature. We conclude that the renormalization of wavefunctions associated with full self-consistency will probably be an important ingredient of a qualitative theory of the superconductor-insulator transition.

At the same time we show that in the weakly disordered limit even approaches without any self-consistency can describe certain features of disordered superconductors quantitatively. We do this on the example of the

fluctuations of the local density of states employing an unpublished analytical approach developed by Igor Burmistrov of the Landau institute.

Overview

We will start in **Chapter 2** with review on the description of inhomogeneous superconductors. We will give theoretical background on phase transitions, superconductivity and mean-field theories in general. Furthermore the attractive Hubbard model will be discussed and a solution within mean-field theory will be provided.

In **Chapter 3** the details of our numerical implementation will be presented. We will discuss the iterative solution for the self-consistent fields. In addition the Kernel Polynomial Method will be discussed both in general and specifically applied to the Hubbard Hamiltonian within mean-field theory. We will contrast different approaches and discuss the errors involved in our numerical approximations.

We will follow in **Chapter 4** with superconductivity in the presence of a single impurity. The known results both for Friedel oscillations in the density and the pairing amplitude will be discussed, followed by a presentation of our results. We will close with a discussion.

Chapter 5 will be devoted to superconductivity in the presence of homogeneous on-site disorder. We will start with a review of both localization and Superconductor-Insulator-Transitions (SIT). We will present our results and conclude with a discussion.

In **Chapter 6** we will summarize what has been achieved and close in **Chapter 7** with an outlook on physical questions that we would like to address in the future.

Chapter 2

Inhomogeneous Superconductors

In this chapter we will discuss theoretical aspects of the description of inhomogeneous superconductors. We will review the theory of phase transitions, superconductors and mean-field approximations. Furthermore we will introduce and discuss the Hamiltonian that will be studied throughout this thesis.

2.1 Phase Transitions

The concept of phase transitions is absolutely central to our understanding of physics today. The nucleation of a crystal, the magnetization of a ferromagnet and the formation of a superconducting condensate can all be understood as a transition towards higher order.

The SIT, which we will study in this thesis, is believed to be a second-order phase transition. The ordered phase can be described by an order parameter. For instance the complex order parameter of a superconducting phase is the pairing amplitude. Its modulus is associated with the pair energy with which electrons are bound together, while its phase corresponds to the complex phase of the condensate. The free energy functional in the superconducting state with respect to this order parameter has the famous mexican hat form seen in Fig. 2.1. It is symmetric with respect to the phase of the order parameter. At the transition this continuous $U(1)-$symmetry is spontaneously broken and a specific phase is chosen.

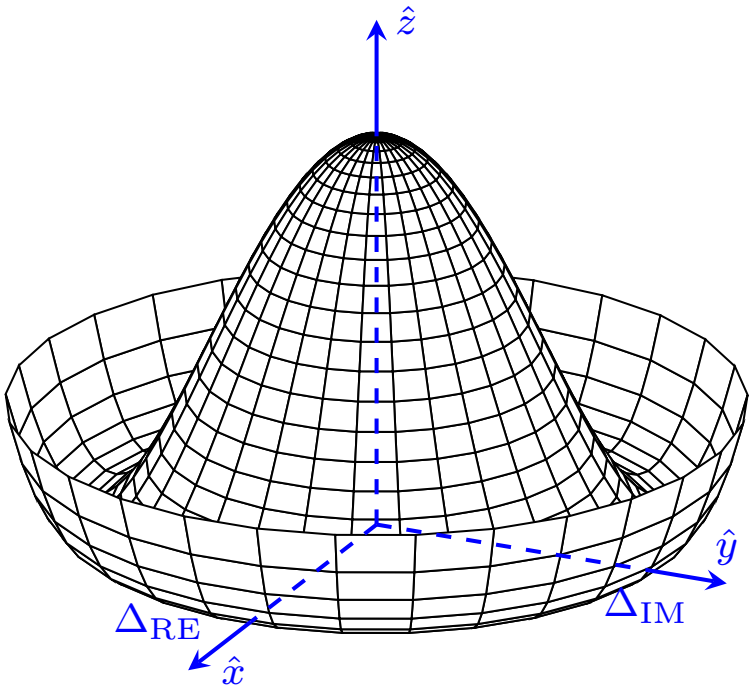

Figure 2.1: Free energy functional (z-axis) of a superconductor with respect to its complex order parameter Δ.

We can characterize a second-order phase transition by a set of critical exponents. Close to the transitions all relevant thermodynamic quantities scale with these exponents. For instance the correlation length, which is the length scale associated to fluctuations, of a thermal second-order phase transition scales according to

$$\xi \propto |T - T_{\mathrm{c}}|^{-\nu}, \tag{2.1}$$

with critical exponent $\nu > 0$ and critical temperature T_{c}. As seen from the equation, the correlation length diverges as the critical point is approached. The resulting power-law correlation across all of space, even in the thermodynamic limit, is another key property of these transitions.

It has been found that these exponents are not unique to every phase transition. Many transitions that seem entirely unrelated microscopically share the same exponents and thus the same critical behavior. This property was attributed to the irrelevance of microscopic details at a phase transition. The sets of unique critical exponents are called universality classes.

Important characteristics that distinguish these universality classes are the symmetry class, the dimensionality and the range of interactions.

Another important aspect of the SIT is its quantum nature. Quantum phase transitions are characterized by a discontinuous change in ground state at $T = 0$. This change is controlled by a material parameter, say the particle density or strength of disorder. The transition is driven by quantum fluctuations in contrast to thermal fluctuations, as in thermal phase transitions.

2.2 Superconductivity

Superconducting phases are characterized by a condensation of electrons to a degenerate ground state constituted of bosonic Cooper pairs. This leads to extraordinary electromagnetic properties that superconductors can exhibit:

- A complete vanishing of the dc resistance. In that sense superconductors are perfect conductors.

- An exponential decay of the penetration depth of magnetic fields inside a superconductor. In that sense they are perfect diamagnets.

Throughout this thesis we will be mainly concerned with thin superconducting films. The two-dimensional nature of theses systems has profound implications on the resulting superconducting state. According to the Mermin-Wagner theorem, there can be no continuous symmetry breaking in $d \leq 2$ in a system with short-range interactions at finite temperatures.

The existance of a superconducting state in 2d is still possible through the BKT-transition. It is a topological phase transition towards a quasi-ordered state. It is quasi-ordered in the sense that correlations decay by a power-law in contrast to constant correlations in the infinite distance limit in conventionally ordered systems.

The inclusion of phase fluctuations is key to arrive at such a transition. In our mean-field description we neglect these fluctuations and arrive at a conventional superconducting phase even for $T > 0$. Our zero temperature results are not affected by this but we want to argue that our conclusions bear relevance even in the finite temperature case. In particular, we do not expect the modulus of the pairing amplitude to be strongly affected by phase fluctuations. The critical temperature on the other hand we expect to depend

on the strength of disorder. At low disorder the critical temperature of the BKT transition T_{BKT} takes the form[36]

$$T_{\mathrm{BKT}} = T_{\mathrm{BCS}}(1 - 4Gi), \tag{2.2}$$

with the BCS critical temperature T_{BCS} and the Ginzburg-Levanyuk number $Gi \ll 1$. Thus in this regime we can expect our mean-field critical temperature T_{c} to be a reasonable estimate for the critical temperature even in the presence of phase fluctuations. As we move towards the strong disorder case $T_{\mathrm{BKT}} \ll T_{\mathrm{c}}$ holds. Physically, this corresponds to a loss of phase coherence of the superconducting condensate before the modulus of the pairing amplitude vanishes. This will be discussed in conjuction with our finite temperature results.

2.3 Mean-field theories

Making interacting systems tractable is one of the major challenges in physics. We will discuss this on the example of an attractive on-site interaction term, as we will consider in the Hubbard model. It reads

$$\hat{H}_{\mathrm{I}} = -U \sum_{i=1}^{N_{\mathrm{bf}}} \hat{c}^{\dagger}_{i,\uparrow} \hat{c}_{i,\uparrow} \hat{c}^{\dagger}_{i,\downarrow} \hat{c}_{i,\downarrow}, \tag{2.3}$$

with number of basis functions N_{bf}, and annihilation (creation) operator $\hat{c}^{(\dagger)}_{i,\sigma}$ at site i with spin σ. Analytical solutions to interacting problems are often unknown, especially for an inhomogeneous problem, as the one that we will consider. To numerically diagonalize a Hamiltonian that contains such an interaction term is challenging as well, as the Fock space size grows exponentially with the size of the lattice N_{bf}. In most cases approximate solutions have to be found.

Mean-field theory is based on the idea to find an effective single-particle Hamiltonian with a much smaller Hilbert space that absorbs the mean interaction effect of all particles in effective potentials, the mean-fields. For instance in our mean-field decoupling we will choose

$$\hat{H}_{\mathrm{I}} = -U \sum_{i=1}^{N_{\mathrm{bf}}} \hat{c}^{\dagger}_{i,\uparrow} \hat{c}_{i,\uparrow} \hat{c}^{\dagger}_{i,\downarrow} \hat{c}_{i,\downarrow} \approx -\frac{U}{2} \sum_{i=1,\sigma}^{N_{\mathrm{bf}}} n(\mathbf{r}_i) c^{\dagger}_{i,\sigma} c_{i,\sigma} - \sum_{i=1}^{N_{\mathrm{bf}}} \Delta(\mathbf{r}_i) \hat{c}^{\dagger}_{i,\uparrow} \hat{c}^{\dagger}_{i,\downarrow} + \mathrm{h.c.}, \tag{2.4}$$

with particle density $n(\mathbf{r}_i)$ and pairing amplitde $\Delta(\mathbf{r}_i)$, which will be our mean-fields. In order to find an optimal representation of the many-body Hamiltonian in terms of the effective Hamiltonian, the mean-fields then have to be determined self-consistently. This self-consistency requirement will ensure that the free energy of the many-body Hamiltonian with respect to the eigenstates of the mean-field Hamiltonian will be minimal for the particular choice of mean-fields that fulfill self-consistency.

Note that the mean-field Hamiltonian does not conserve particle number, even though the many-body Hamiltonian does. The mean-field Hamiltonian explicitly breaks the symmetry that is spontaneously broken in the many-body Hamiltonian.

In mean-field theory we neglect fluctuations around this mean value of the fields. Consequently, how well a mean-field Hamiltonian approximates the many-body Hamiltonian depends on the importance of these fluctuations. A very important factor that determines the size of these fluctuations is the dimensionality of the problem. A higher dimensionality leads to lower strength of fluctuations. At a certain upper critical dimension the mean-field Hamiltonian can even reproduce the critical behavior, i.e. the critical exponents of its respective universality class. Below this upper critical dimension mean-field theory will yield different mean-field critical exponents, due to the rise of fluctuations close to a phase transition. Additionally, there is a lower critical dimension at which mean-field theory might predict a phase transition towards an ordered phase, even though, when fluctuations are taken into account, no such transition can occur.

In the case of the superconducting phase transition the upper critical dimension is 4, while the lower critical dimension is 2. As already discussed in the two-dimensional case superconductivity is still possible in the form of a BKT transition towards a quasi-ordered state.

Even though the critical exponents are not correctly reproduced in 2D and 3D for a superconducting system in mean-field theory, BCS theory, many aspects are described remarkably well, at least in the case of conventional superconductivity. This is for instance true for the critical temperature, the superconducting gap and the coherence length.

Beyond the relevance of mean-field theories in the direct description of interacting systems, they are also the starting point for many other approaches that go beyond it. In quantum field theoretical approaches the object of in-

quiry is a path integral over some action

$$\int \mathcal{D}\Delta e^{-S[\Delta]}, \tag{2.5}$$

with action S that is a functional of some field Δ. The above functional integral is typically solved by a perturbative approach. One starts with a saddle point approximation

$$\int \mathcal{D}\Delta e^{-S[\Delta]} \sim e^{-S[\Delta_0]}, \tag{2.6}$$

i.e. only taking the field configuration Δ_0 that minimizes S. This field configuration is equivalent to our mean-field and starting from that fluctuations around that field can be then taken into account perturbatively.

Apart from mean-field theories, there are other self-consistent field theories. We here want to discuss the example of density functional theory (DFT) and what its advantages and disadvantages are compared to mean-field theories. In density functional theory an effective single particle system, the Kohn-Sham system, is being studied.

$$\left(-\frac{\hbar}{2m}\nabla^2 + V_{\text{eff}}[n(\mathbf{r})](\mathbf{r})\right)\Psi(\mathbf{r}) = E\Psi(\mathbf{r}), \tag{2.7}$$

with some effective potential V_{eff} that is a functional of the particle density of the Kohn-Sham states $\Psi(\mathbf{r})$. There are important differences with respect to mean-field theory:

- Only the density of the Kohn-Sham states bears a direct physical relevance. In mean-field theory the single-particle states are optimized as well to represent the underlying many-body system.

- In DFT in principle more correlation effects can be taken into account than in mean-field theory. Theoretically all properties of the exact many-body ground state can be encoded in a density functional. In practice the density functional is not known and finding an approximate functional is less easily controlled than a mean-field approximation. So on the one hand in many cases the many-body ground state energy E_g can be approximated more accurately than in mean-field theory. On the other an advantage of mean-field theory is that its ground state energy $E_{\text{mf}} \geq E_g$ is always an upper bound, while that is not true for DFT.

2.4 The attractive Hubbard model

2.4.1 Free particles

The tight-binding Hamiltonian of free particles on a lattice with nearest neighbor hopping reads

$$\hat{H}_{\text{free}} = -t \sum_{\langle i,j\rangle,\sigma} \hat{c}^{\dagger}_{i,\sigma}\hat{c}_{j,\sigma}, \tag{2.8}$$

with hopping parameter t and electron annihilation operator $c_{i,\sigma} = c_{\sigma}(\mathbf{r}_i)$ with spin σ at position $\mathbf{r}_i$. With $\langle i,j\rangle$ we denote a sum over the nearest-neighbor sites on a rectangular lattice in d dimensions

$$\sum_{\langle i,j\rangle} \hat{c}^{\dagger}_{i,\sigma}\hat{c}_{j,\sigma} = \sum_{l=1,\sigma}^{L^d}\sum_{D=1}^{d} \hat{c}^{\dagger}_{\sigma}(\mathbf{r}_l + \hat{r}_D)\hat{c}_{\sigma}(\mathbf{r}_l) + \text{h.c.} \tag{2.9}$$

with number of lattice sites along each axis L and unit vector along the D-th axis $\hat{r}_D$ with components

$$(\hat{r}_D)_l = \delta_{l,D}a, \tag{2.10}$$

with lattice spacing a. We impose periodic boundary conditions, thus

$$c_{\sigma}(\mathbf{r}_l + L\hat{r}_D) = c_{\sigma}(\mathbf{r}_l) \;\forall\; D, l. \tag{2.11}$$

We define the discrete Fourier transform of spatial dimension $(\mathbf{r})_l$ as

$$\hat{c}^{\dagger}_{\sigma}(\mathbf{r}) = \hat{c}^{\dagger}_{\sigma}((\mathbf{r})_1, ..., (\mathbf{r})_l, ..., (\mathbf{r})_d) = \sum_{m=1}^{L} \hat{c}^{\dagger}_{\sigma}((\mathbf{r})_1, ..., k_m, ..., (\mathbf{r})_d)e^{-ik_m(\mathbf{r})_l}, \tag{2.12}$$

with momenta k_m taking values

$$k_m = \frac{(m-1)2\pi}{La}. \tag{2.13}$$

Employing Eq. (2.12) the Hamiltonian is readily diagonalized

$$\begin{aligned}
\hat{H}_{\text{free}} &= -t\sum_{l=1}^{L^d}\sum_{\sigma}\sum_{D=1}^{d}\hat{c}_\sigma^\dagger(\mathbf{r}_l+\hat{r}_D)\hat{c}_\sigma(\mathbf{r}_l)+\text{h.c.}= \\
&= -t\sum_{l,\sigma,D}\sum_{m,p=1}^{L^d}\hat{c}_\sigma^\dagger(\mathbf{k}'_\mathbf{m})\hat{c}_\sigma(\mathbf{k_p})e^{i\mathbf{k}'_p\cdot(\mathbf{r}_l+\hat{r}_D)-i\mathbf{k}_m\cdot\mathbf{r}_l}+\text{h.c.}= \\
&= -t\sum_{D=1}^{d}\sum_{p,p=1}^{L^d}\hat{c}_\sigma^\dagger(\mathbf{k}'_\mathbf{p})\hat{c}_\sigma(\mathbf{k_p})e^{i\mathbf{k}'_p\cdot\hat{r}_D}\delta(\mathbf{k}'_p-\mathbf{k}_p)+\text{h.c.}= \\
&= -2t\sum_{m,\sigma}\left[\sum_{D=1}^{d}\cos(\mathbf{k}_m\cdot\hat{r}_D)\right]\hat{c}^\dagger_{\mathbf{k}_m,\sigma}\hat{c}_{\mathbf{k}_m,\sigma}, \qquad (2.14)
\end{aligned}$$

where the components of the wave vector are quantized according to

$$(\mathbf{k}_m)_D\in\left[0,\frac{2\pi}{La},\frac{4\pi}{La},...,\frac{2(L-1)\pi}{La}\right]\ \forall\ m,d. \qquad (2.15)$$

For the band width B of the system we thus get

$$B=\begin{cases}-2t\sum_{D=1}^{d}\left[\cos(\pi)-\cos(0)\right]=4dt & \text{L even}\\ -2t\sum_{D=1}^{d}\left[\cos(\frac{(L-1)\pi}{L})-\cos(0)\right]=2dt(1-\cos(\frac{(L-1)\pi}{L})) & \text{L odd.}\end{cases} \qquad (2.16)$$

We define the density of states (DoS) per spin

$$\rho_\sigma(E)=\frac{1}{L^d}\sum_n\delta(E-E_{\sigma,n})\approx\frac{1}{L^d}\sum_n\frac{1}{\sqrt{2\pi\gamma^2}}\exp\left(\frac{-\left[E-E_{\sigma,n}\right]^2}{2\gamma^2}\right), \qquad (2.17)$$

with eigenenergies $E_{\sigma,n}$ for states with spin σ. As all the systems that we will discuss are time-reversal symmetric and spin-rotational symmetric, we will omit the spin index from now on. In numerical computations we approximate the delta distributions by a Gaussian of width γ, as defined in Eq. 2.17. We define the filling factor as

$$n=2\int_{-\infty}^{E_F}dE\rho(E), \qquad (2.18)$$

with Fermi energy E_F.

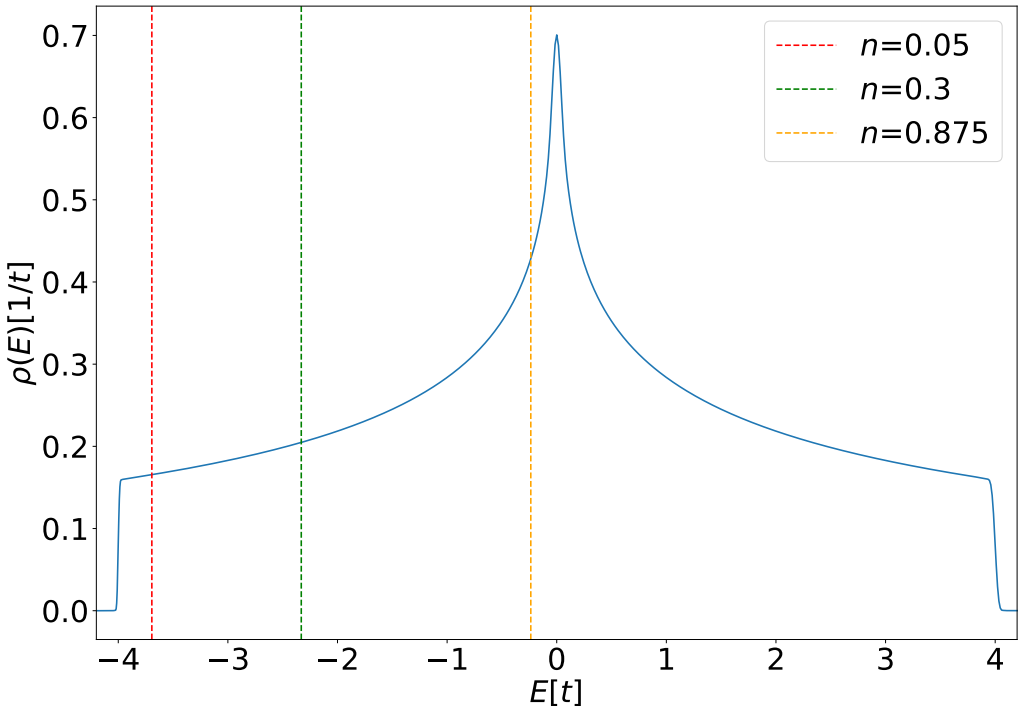

Figure 2.2: The DoS of $\hat{H}_{\text{free}}$ on a 2D lattice of linear size $L = 256$. The delta distributions are approximated by a Gaussian of width $\gamma = 0.025t$ as described in Eq. 2.17. The vertical lines mark the Fermi energies at given filling n, where the Fermi surfaces and Fermi velocities are plotted in Fig. 2.3

.

Notes

- In Fig. 2.2 the density of states (DoS) of $\hat{H}_{\text{free}}$ on a 2D lattice is plotted. Far away from $E = 0$ the DoS is only weakly dependent on energy and the particles behave as though in free space with approximately parabolic dispersion. Going towards $E = 0$ the dependence on energy becomes strong, as the wave length of corresponding states becomes comparable to the lattice spacing.

- In Fig. 2.3 the Fermi surfaces and Fermi velocities at different Fermi energies for a 2D lattice are shown. Again the effect of the lattice is apparent going from approximately isotropic behaviour close to the band edges to a four-fold symmetric behaviour at $E = 0$.

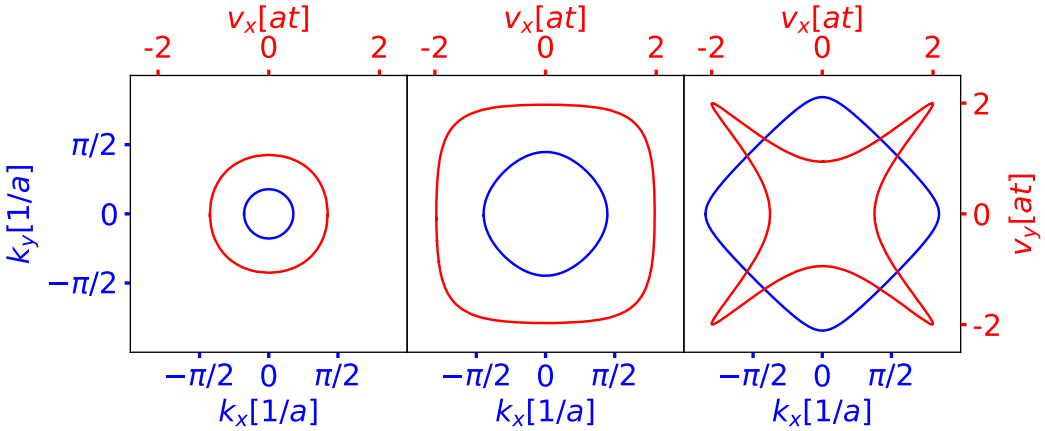

Figure 2.3: The Fermi surfaces and Fermi velocities of Hamiltonian $\hat{H}_{\text{free}}$ in the continuum limit $L \to \infty$ at filling factors $n = 0.05$(left), 0.3,(center) 0.875(right). The corresponding energies are marked in the DoS in Fig. 2.2

- The Hamiltonian is time-reversal symmetric. For an even number of sites or $L \to \infty$ it is also chiral and particle-hole symmetric.

2.4.2 Attractive interaction

In this section we will ad an attractive onsite interaction term and an inhomogeneous onsite potential to the free particle Hamiltonian (Eq. (2.8)). Thus we arrive at the inhomogeneous attractive$-U$ Hubbard model [37]

$$H_{\text{Hubbard}} = \hat{H}_{\text{free}} + \hat{H}_{\text{I}} + \sum_{i=1}^{N_{\text{bf}}} V_i \hat{n}_i \tag{2.19}$$

$$\hat{H}_{\text{I}} = -U \sum_{i=1}^{N_{\text{bf}}} \hat{n}_{i,\uparrow} \hat{n}_{i,\downarrow}, \tag{2.20}$$

with $U > 0$, $\hat{n}_{i,\sigma} = \hat{c}^{\dagger}_{i,\sigma} \hat{c}_{i,\sigma}$, number of real space basis functions $N_{\text{bf}} = L^d$ and some inhomogeneous potential V_i.

Despite its seeming simplicity the Hubbard Hamiltonian has a rich phase diagram and is employed to describe a wide range of physical systems. We are interested in the superconducting s-wave ground state that it can support in its attractive form. It is important to note here that at half filling the superconducting ground state is degenerate with a charge density wave

ground state. For that reason we will choose filling factors smaller than 1 throughout this thesis.

The potential will either serve the role of a single impurity at some site or homogeneous disorder. We will specify it further in the respective chapters.

2.4.3 BdG-treatment of the Hubbard model

In this section we want to move from the interacting many-body Hamiltonian $\hat{H}_{\text{Hubbard}}$ in Eq. (2.19), to an effective single-particle Hamiltonian, as described in 2.3. We will only briefly outline the steps to arrive at a mean-field description of the Hubbard Hamiltonian. A complete derivation can be found in standard textbooks[38].

The effective mean-field Hamiltonian reads

$$\begin{aligned} \hat{H}_{\text{BdG}} &= \hat{H}_0 + \hat{H}_{\text{I}} \\ \hat{H}_0 &= -t \sum_{\langle i,j\rangle,\sigma} \hat{c}^\dagger_{i,\sigma}\hat{c}_{j,\sigma} + \text{h.c.} + \sum_{i=1,\sigma}^{N_{\text{bf}}} (V_i - \mu)\, \hat{n}_{i,\sigma} \\ \hat{H}_{\text{I}} &= -\frac{U}{2} \sum_{i=1,\sigma}^{N_{\text{bf}}} n(\mathbf{r}_i)\hat{n}_{i,\sigma} - \sum_{i=1}^{N_{\text{bf}}} \Delta(\mathbf{r}_i)\hat{c}^\dagger_{i,\uparrow}\hat{c}^\dagger_{i,\downarrow} + \text{h.c.}, \end{aligned} \tag{2.21}$$

with local occupation number $n(\mathbf{r}_i)$ and pairing amplitude $\Delta(\mathbf{r}_i)$. The first term of $\hat{H}_{\text{I}}$ expresses the tendency of particles to bunch up, because of the attractive interactions, while the second term models the Cooper pairing. The pairing term is not particle number conserving, as it is responsible for particles or holes hopping in or out of the superonducting condensate.

The Hamiltonian is diagonalized by a Bogoliubov transformation

$$\hat{c}^\dagger_{i,\uparrow} = \sum_{n=1}^{N_{\text{bf}}} \left(u^*_n(\mathbf{r}_i)\gamma^\dagger_{n,\uparrow} - v_n(\mathbf{r}_i)\gamma_{n,\downarrow} \right) \tag{2.22}$$

$$\hat{c}^\dagger_{i,\downarrow} = \sum_{n=1}^{N_{\text{bf}}} \left(u_n(\mathbf{r}_i)\gamma_{n,\downarrow} + v^*_n(\mathbf{r}_i)\gamma^\dagger_{n,\uparrow} \right), \tag{2.23}$$

with fermionic creation operators of Bogoliubov quasi-particles $\gamma^\dagger_{n,\sigma}$, particle wave functions $u_n(\mathbf{r}_i)$ and hole wave functions $v_n(\mathbf{r}_i)$ that obey

$$\sum_{i=1}^{N_{\text{bf}}} \left(|u_n(\mathbf{r}_i)|^2 + |v_n(\mathbf{r}_i)|^2 \right) = \sum_{n=1}^{N_{\text{bf}}} \left(|u_n(\mathbf{r}_i)|^2 + |v_n(\mathbf{r}_i)|^2 \right) = 1, \tag{2.24}$$

so that the transformation is unitary.

The particle and hole wave functions are defined by the Bogoliubov-deGennes(BdG) equations

$$\begin{pmatrix} h & \Delta \\ \Delta^* & -h^* \end{pmatrix} \begin{pmatrix} u_n(\mathbf{r}_i) \\ v_n(\mathbf{r}_i) \end{pmatrix} = \epsilon_n \begin{pmatrix} u_n(\mathbf{r}_i) \\ v_n(\mathbf{r}_i) \end{pmatrix}. \tag{2.25}$$

with

$$hu_n(\mathbf{r}_i) = -t\sum_{\hat{\delta}} u_n(\mathbf{r}_i+\hat{\delta}) + (V_i-\mu - U\frac{n(\mathbf{r}_i)}{2})u_n(\mathbf{r}_i) \tag{2.26}$$

$$\Delta u_n(\mathbf{r}_i) = \Delta(\mathbf{r}_i)u_n(\mathbf{r}_i). \tag{2.27}$$

The BdG equations are particle-hole, time-reversal and chiral(sub-lattice) symmetric. Particle-hole symmetry of the BdG equations amounts to an eigenvector with positiv eigenenergy ϵ_n

$$|\epsilon_n\rangle = \begin{pmatrix} u_n \\ v_n \end{pmatrix}, \tag{2.28}$$

being related to an eigenvector with negative energy ϵ_n according to

$$|-\epsilon_n\rangle = \begin{pmatrix} -v_n \\ u_n \end{pmatrix}. \tag{2.29}$$

The number of degrees of freedom in the BdG equations are doubled with respect to the mean-field Hamiltonian (Eq. (2.21)). This is only a mathematical trick that allows to diagonalize the Hamiltonian within a first quantization formalism, even though the mean-field Hamiltonian is not particle number conserving. In Fig. 2.4 (left) the dispersion is shown for the clean case with $\Delta(\mathbf{r}) = 0$. Fig. 2.4 (right) shows the dispersion with finite pairing, which opens up a gap around the Fermi energy. In both cases the complete information is contained in the lower and upper half plane. We choose as the physical sector $\epsilon_n > 0$ to discard the redundant degrees of freedom. Note that in Fig. 2.4 (right) particle and hole states are mixed and the color coding corresponds to the predominant character of the states.

The mean-fields $\Delta(\mathbf{r}_i)$ and $n(\mathbf{r}_i)$ have to be determined such that the mean-field Hamiltonians $\hat{H}_{\mathrm{BdG}}$ approximates the many-body Hamiltonian $\hat{H}_{\mathrm{Hubbard}}$ in an optimal way. This is achieved by requiring that the free

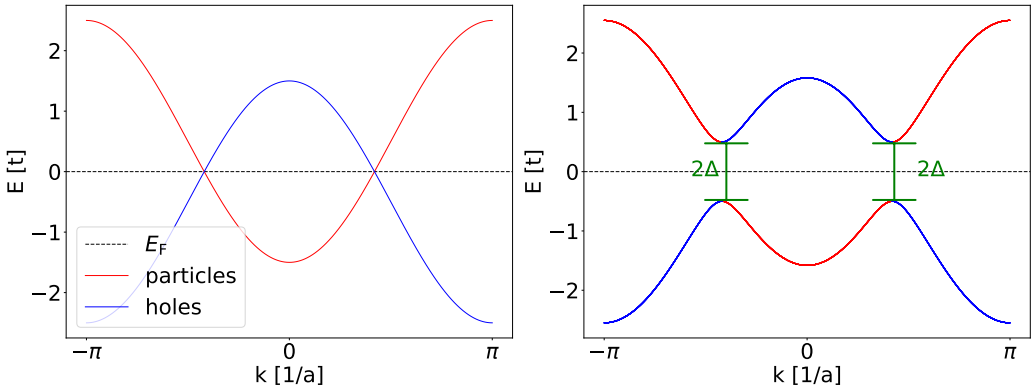

Figure 2.4: The dispersion with homogeneous potential $V_i = \text{const}$, as calculated from Eq. (2.25) with $\Delta(\mathbf{r}) = 0$ (left) and $\Delta(\mathbf{r}) = \Delta = 0.5$ (right).

energy $F = \langle \hat{H}_{\text{Hubbard}} \rangle - TS$ of $\hat{H}_{\text{Hubbard}}$ with respect to the eigenstates $|\Phi\rangle$ of $\hat{H}_{\text{BdG}}$

$$\langle \hat{H}_{\text{Hubbard}} \rangle = \frac{\sum_\Phi \langle \Phi | \hat{H}_{\text{Hubbard}} | \Phi \rangle \exp\left(-\beta E_\Phi\right)}{\sum_\Phi \exp(-\beta E_\Phi)}, \tag{2.30}$$

with eigenenergy E_Φ of state Φ and $\beta = \frac{1}{k_B T}$ is stationary. The resulting scf-conditions for the density $n(\mathbf{r})$ and the gap-function $\Delta(\mathbf{r})$ read

$$\Delta(\mathbf{r}_i) = U \left[u_n(\mathbf{r}_i) v_n^*(\mathbf{r}_i)(1 - 2f_n) \right], \tag{2.31}$$

$$n(\mathbf{r}_i) = 2 \sum_n \left[|v_n(\mathbf{r}_i)|^2 (1 - f_n) + |u_n(\mathbf{r}_i)|^2 f_n \right], \tag{2.32}$$

with Fermi function

$$f_n = \frac{1}{\exp(\beta \epsilon_n) + 1}. \tag{2.33}$$

In addition the chemical potential μ has to be determined self-consistently for a given filling factor n according to

$$n = \sum_{i=1,\sigma}^{N_{\text{bf}}} \frac{\langle \hat{n}_{i,\sigma} \rangle}{N_{\text{bf}}}. \tag{2.34}$$

The self-consistency requirement leads to non-linearity in the BdG equations. Such non-linearity is the origin of the richness but also difficulty that self-consistent field theories exhibit. The local density of states (LDoS) within

BdG theory reads

$$\rho(E, \mathbf{r}_i) = 2 \sum_n \left[|v_n(\mathbf{r}_i)|^2 \delta(E + \epsilon_n) + |u_n(\mathbf{r}_i)|^2 \delta(E - \epsilon_n) \right] \tag{2.35}$$

BCS theory

We will briefly discuss the BdG equations in the clean case. A full account can be found in standard textbooks[39]. In the special case of a homogeneous potential in Eq. (2.21)

$$V_i = \text{const } \forall i \ , \tag{2.36}$$

$\hat{H}_{\text{BdG}}$ reduces to the BCS Hamiltonian. With translational invariance the pairing amplitude takes a constant value in space and the Hartree shift can be absorbed in the chemical potential as it is homogeneous

$$\Delta(\mathbf{r}) = \Delta_0 \tag{2.37}$$

The resulting BCS Hamiltonian in real space reads

$$\hat{H}_{\text{BCS}} = - t \sum_{\langle i,j \rangle, \sigma} \hat{c}^\dagger_{i,\sigma} \hat{c}_{j,\sigma} + \text{h.c.} - \mu \sum_{i=1,\sigma}^{N_{\text{bf}}} \hat{n}_{i,\sigma} - \tag{2.38}$$

$$- \sum_{i=1}^{N_{\text{bf}}} \Delta_0 \hat{c}^\dagger_{i,\uparrow} \hat{c}^\dagger_{i,\downarrow} + \text{h.c.}, \tag{2.39}$$

Applying a Fourier transform (Eq. (2.12)) we arrive at the standard momentum-space representation of the BCS Hamiltonian

$$\begin{aligned}
\hat{H}_{\mathrm{BCS}} &= \hat{H}_{\mathrm{free}} - \sum_{i=1,\sigma}^{N_{\mathrm{bf}}} \mu \hat{c}^{\dagger}_{i,\sigma}\hat{c}_{i,\sigma} - \sum_{i=1}^{N_{\mathrm{bf}}} \Delta_0 \hat{c}^{\dagger}_{i,\uparrow}\hat{c}^{\dagger}_{i,\downarrow} + \mathrm{h.c.} = \\
&= \hat{H}_{\mathrm{free}} - \mu \sum_{i,m,n=1,\sigma}^{N_{\mathrm{bf}}} \hat{c}^{\dagger}_{\sigma}(\mathbf{k}_m)\hat{c}_{\sigma}(\mathbf{k}_n)e^{-i(\mathbf{k}_m-\mathbf{k}_n)\mathbf{r}_i} - \\
&- \sum_{i,m,n=1}^{N_{\mathrm{bf}}} \Delta_0 \hat{c}^{\dagger}_{\uparrow}(\mathbf{k}_m)\hat{c}^{\dagger}_{\downarrow}(\mathbf{k}_n)e^{-i(\mathbf{k}_m+\mathbf{k}_n)\mathbf{r}_i} + \mathrm{h.c.} = \qquad (2.40) \\
&= \sum_{m,\sigma}\left[\sum_{d=1}^{D} -2t\cos(\mathbf{k}_m \cdot \hat{r}_d) - \mu\right]\hat{c}^{\dagger}_{\mathbf{k}_m,\sigma}\hat{c}_{\mathbf{k}_m,\sigma} \\
&\quad -\Delta_0 \sum_{m=1}^{N_{\mathrm{bf}}} \hat{c}^{\dagger}_{\mathbf{k}_m,\uparrow}\hat{c}^{\dagger}_{-\mathbf{k}_m,\downarrow} + \mathrm{h.c.} = \\
&= \sum_{m,\sigma} \xi_{\mathbf{k}_m}\hat{c}^{\dagger}_{\mathbf{k}_m,\sigma}\hat{c}_{\mathbf{k}_m,\sigma} - \Delta_0 \sum_{m=1}^{N_{\mathrm{bf}}} \hat{c}^{\dagger}_{\mathbf{k}_m,\uparrow}\hat{c}^{\dagger}_{-\mathbf{k}_m,\downarrow} + \mathrm{h.c.},
\end{aligned}$$

whereby we used the Fourier transform of $\hat{H}_{\mathrm{free}}$ as already derived in Eq. (2.8). Note that in the standard formulation of BCS theory the pairing term is restricted to states close to the Fermi energy

$$\sum_{m=1}^{N_{\mathrm{bf}}} \Delta_{\mathbf{k}}\hat{c}^{\dagger}_{\mathbf{k}_m,\uparrow}\hat{c}^{\dagger}_{-\mathbf{k}_m,\downarrow} + \mathrm{h.c.}, \qquad (2.41)$$

with

$$\Delta_{\mathbf{k}} = \begin{cases} \Delta_0 & |\xi_{\mathbf{k}_m}| \leq \hbar\omega_{\mathrm{D}} \\ 0 & |\xi_{\mathbf{k}_m}| > \hbar\omega_{\mathrm{D}} \end{cases},$$

with Debye frequency ω_D. As a consequence states across the whole bandwidth B will be paired. $B/2$ replaces ω_{D} wherever it appears in BCS theory. Particles will still only be strongly paired around the Fermi energy. The hole character of the eigenstates in BCS theory follows

$$|v_{\mathbf{k}}|^2 = \frac{1}{2}\left[1 - \frac{\xi_{\mathbf{k}}}{(\Delta_0^2 + \xi_{\mathbf{k}}^2)^{\frac{1}{2}}}\right]. \qquad (2.42)$$

It quickly falls off around the Fermi energy, whereas far from the Fermi energy it retains power-law tails $\sim \xi_{\mathbf{k}}^{-2}$. The clean self-consistency equation reads

$$1 = -\frac{U}{2} \sum_{\mathbf{k}} \frac{\tanh(\beta \sqrt{\xi_{\mathbf{k}}^2 + \Delta_0^2}/2)}{\sqrt{\xi_{\mathbf{k}}^2 + \Delta_0^2}} \tag{2.43}$$

In the continuum limit we get

$$1 = -\frac{U}{2} \int_{-B/2}^{B/2} d\xi \frac{\tanh(\beta \sqrt{\xi_{\mathbf{k}}^2 + \Delta_0^2}/2)\rho(\xi)}{\sqrt{\xi^2 + \Delta_0^2}}, \tag{2.44}$$

with density of states $\rho(\xi)$. Whenever we refer to the BCS gap, we will calculate it employing this equation for $T \to 0$. The critical temperature is proportional to the zero temperature gap for BCS theory in the low-coupling limit. The clean correlation length is defined as

$$\xi = \frac{v_{\mathrm{F}}}{\pi \Delta_0}, \tag{2.45}$$

with the Fermi velocity v_{F}.

Chapter 3

Numerical Implementation

In this chapter we will outline how self-consistency is established numerically. We will first describe the self-consistency cycle. In the following chapters we will introduce the Kernel Polynomial Method (KPM) and its application to the BdG equations.

3.1 Self-consistency cycle

The Hamiltonian that we aim to establish self-consistency for (see Eq. 2.25 and 2.26) is defined as

$$\begin{pmatrix} h & \Delta \\ \Delta^* & -h^* \end{pmatrix} \begin{pmatrix} u_n(\mathbf{r}_i) \\ v_n(\mathbf{r}_i) \end{pmatrix} = \epsilon_n \begin{pmatrix} u_n(\mathbf{r}_i) \\ v_n(\mathbf{r}_i) \end{pmatrix}. \tag{3.1}$$

with

$$hu_n(\mathbf{r}_i) = -t\sum_{\hat{\delta}} u_n(\mathbf{r}_i+\hat{\delta}) + (V_i-\mu - U\frac{n(\mathbf{r}_i)}{2})u_n(\mathbf{r}_i) \tag{3.2}$$

$$\Delta u_n(\mathbf{r}_i) = \Delta(\mathbf{r}_i)u_n(\mathbf{r}_i). \tag{3.3}$$

The pairing amplitude $\Delta(\mathbf{r}_i)$ and the density $n(\mathbf{r}_i)$ do not only appear as matrix elements in the Hamiltonian but also as observables defined by the self-consistency equations (see (2.31) and (2.32))

$$\Delta(\mathbf{r}_i) = U\left[u_n(\mathbf{r}_i)v_n^*(\mathbf{r}_i)(1-2f_n)\right], \tag{3.4}$$

$$n(\mathbf{r}_i) = 2\sum_n \left[|v_n(\mathbf{r}_i)|^2(1-f_n) + |u_n(\mathbf{r}_i)|^2 f_n\right], \tag{3.5}$$

with Fermi function

$$f_n = \frac{1}{\exp(\beta\epsilon_n) + 1}. \tag{3.6}$$

The Hamiltonian is self-consistent, when the observables agree with the corresponding matrix elements. We establish self-consistency in an iterative fashion. The Hamiltonian is constructed with an initial guess for the mean-fields, followed by a computation of the mean-fields (Eq. (3.4) and (3.5)) from this Hamiltonian. With these new mean-fields we construct the Hamiltonian again and recompute the new mean-fields. We repeat this cycle until the observables $\Delta(\mathbf{r}_i)$ and $n(\mathbf{r}_i)$ agree with the corresponding matrix elements up to some tolerance α

$$\alpha < |1 - \Delta^{(m)}(\mathbf{r}_i)/\Delta^{(m-1)}(\mathbf{r}_i)| \; \forall \; \mathbf{r}_i, \tag{3.7}$$

where $\Delta^{(m)}(\mathbf{r}_i)$ is the mean-field of iteration m. At each iteration the chemical potential μ in Eq. (3.2) is adjusted to keep the mean particle density constant

$$n = \sum_i \frac{n(\mathbf{r}_i)}{N_{\mathrm{bf}}}, \tag{3.8}$$

with number of sites N_{bf}. Typical values we take are $\alpha = 0.1\%, 0.5\%, 1\%, 3\%$. Note that the average change α_{avg} per iteration cycle is much smaller than α, e.g. for a typical sample at moderate disorder $W = 2$ we have $\alpha_{\mathrm{avg}} = 0.014\%, 0.025\%, 0.05\%, 0.1\%$. The straight-forward approach to compute the mean-fields is by full diagonalization of the Hamiltonian. The asymptotic computational complexity of this operation is $\mathcal{O}(N_{\mathrm{bf}}^3)$. This limits the system sizes that are possible to be tackled within such an approach quite severly. For this reason we have developed an implementation of the self-consistency cycle based on an alternative approach to construct the mean-fields that scales considerable better with system size, which will be outlined in the following section.

3.2 The kernel polynomial method

For the general outline of the KPM we will for the most part follow the review by Weiße et al. [40]. We will then apply the method to the system that we study throughout this thesis. The idea of KPM is to expand observables in Chebyshev polynomials. Through a recursion relation of the polynomials the

next moment can be calculated from the previous one. The calculation of one moment corresponds to the action of one sparse matrix on a vector. The finite series of moments is then convoluted with a kernel to dampen Gibbs oscillations. These oscillations occur, when an infinite series is cancelled after a finite number of terms.

In principle every set of orthogonal polynomials could be used for such an expansion. Chebyshev polynomials are the best choice for most cases for two reasons: (i)They exhibit good convergence properties. (ii) They are closely related to the Fourier transform. This relation to the Fourier transform allows for the easy construction of an optimal kernel and for an efficient evaluation of the observable, when the expansion coefficients have been determined.

We will start with some properties of Chebyshev polynomials. Chebyshev polynomials of the first kind are defined by

$$T_0(x) = 1, \tag{3.9}$$
$$T_{-1}(x) = T_1(x) = x, \tag{3.10}$$
$$T_{m+1}(x) = 2xT_m(x) - T_{m-1}(x), \tag{3.11}$$

with $x \in [-1, 1]$. The associated scalar product reads

$$\langle f|g\rangle = \int_{-1}^{1} dx \frac{f(x)g(x)}{\pi\sqrt{1-x^2}}. \tag{3.12}$$

With respect to this scalar product Chebyshev polynomials are orthogonal to each other

$$\langle T_n|T_{n'}\rangle = \frac{1+\delta_{n,0}}{2}\delta_{n,n'}. \tag{3.13}$$

We can now expand any function f that is defined on the interval $[-1, 1]$ according to

$$f(x) = \sum_{n=0}^{\infty} \frac{\langle f|T_n\rangle}{\langle T_n|T_n\rangle} T_n(x) = \alpha_0 + 2\sum_{n=1}^{\infty} \alpha_n T_n(x), \tag{3.14}$$

with coefficients

$$\alpha_n = \langle f|T_n\rangle = \int_{-1}^{1} dx \frac{f(x)T_n(x)}{\pi\sqrt{1-x^2}}. \tag{3.15}$$

These are the standard definitions for Chebyshev polynomials. They are however not well suited to iterative matrix problems. This is due to the

factor $\frac{1}{\sqrt{1-x^2}}$, which is integrated over, in Eq. (3.15). Each power of x will correspond to one action with the Hamiltonian matrix H. A construction of the matrix $\frac{1}{\sqrt{1-H^2}}$ is impractical compuationally.

There is however a simple solution to that. Instead of directly using Chebyshev polynomials, we will use the orthogonal functions

$$\Phi_n(x) = \frac{T_n(x)}{\pi\sqrt{1-x^2}}. \tag{3.16}$$

They are orthogonal to each other according to another scaler product

$$\langle \Phi_n | \Phi_{n'} \rangle = \int_{-1}^{1} dx \pi \sqrt{1-x^2} \Phi_n(x) \Phi_{n'}(x) = \frac{1+\delta_{n,0}}{2} \delta_{n,n'}. \tag{3.17}$$

The expansion of a function $f(x)$ then reads

$$f(x) = \sum_{n=0}^{\infty} \frac{\langle f|\Phi_n\rangle}{\langle \Phi_n|\Phi_n\rangle} \Phi_n(x) = \frac{1}{\pi\sqrt{1-x^2}} \left[\mu_0 + 2\sum_{n=1}^{\infty} \mu_n T_n(x) \right], \tag{3.18}$$

with coefficients

$$\mu_n = \langle f|\Phi_n\rangle = \int_{-1}^{1} dx f(x) T_n(x). \tag{3.19}$$

As we will cancel the series after a number of moments $N_\mathcal{C}$, Gibbs oscillations will occur. These can be dampened by the convolution of the moments with a kernel

$$f(x) = \frac{1}{\pi\sqrt{1-x^2}} \left[g_0\mu_0 + 2\sum_{n=1}^{N_\mathcal{C}} g_n \mu_n T_n(x) \right], \tag{3.20}$$

with kernel g_n and μ_n defined according to Eq. (3.19).

For most applications, including the expansion of our mean-fields, the Jackson Kernel

$$g_n^J = \frac{(N-n+1)\cos\frac{\pi n}{N+1} + \sin\frac{\pi n}{N+1}\cot\frac{\pi n}{N+1}}{N+1}, \tag{3.21}$$

with total number of moments N is the optimal choice.

An expanded delta distribution convoluted with the kernel yields

$$\begin{aligned} \delta_{\mathrm{KPM}}(x-a) &= \langle K_N(x,y)|\delta(y-a)\rangle = \\ &= g_0^J \Phi_0(x) T_0(a) + 2\sum_{n=1}^{N-1} g_n^J \Phi_n(x) T_n(a). \end{aligned} \tag{3.22}$$

Resulting in the variance

$$\begin{aligned}\sigma^2 &= \int_{-1}^{1} x^2 \delta_{\mathrm{KPM}}(x-a)dx - \left(\int_{-1}^{1} x\delta_{\mathrm{KPM}}(x-a)dx\right)^2 = \\ &= \frac{g_0^J T_0(a) + g_2^J T_2(a)}{2}\left(g_1^J T_1(a)\right)^2 = \\ &= \frac{N-a^2(N-1)}{2(N+1)}\left(1-\cos\frac{2\pi}{N+1}\right) \approx \left(\frac{\pi}{N}\right)^2\left(1-a^2+\frac{3a^2-2}{N}\right),\end{aligned} \tag{3.23}$$

where we used $x = T_1(x)$ and $x^2 = [T_2(x) + T_0(x)]/2$. The expansion of a delta peak is approximated well by a Gaussian of width σ. The broadening changes smoothly from $\sigma = \pi/N$ at $x = 0$ to $\sigma = \pi/N^{\frac{3}{2}}$ at the boundaries.

3.3 Application to the BdG system

The general idea in applying the KPM to our Hamiltonian system is to expand some energy dependent observable $O(E)$ in Chebyshev polynomials. This expansion can then be formulated as a trace over powers of the Hamiltonian.

At first the Hamiltonian needs to be rescaled to the domain of the Chebyshev polynomials

$$\tilde{H} = (\hat{H} - b)/a, \tag{3.24}$$

with resulting energies

$$\tilde{E} = (E - b)/a. \tag{3.25}$$

The factors a and b are chosen according to

$$a = (E_{\max} - E_{\min})/(2-\epsilon), \tag{3.26}$$

$$b = (E_{\max} + E_{\min})/2, \tag{3.27}$$

where $E_{\max}$ is the largest and $E_{\min}$ the lowest eigenvalue of $\hat{H}$ The parameter ϵ is introduced to avoid stability problems at the boundaries. We choose it to be $\epsilon = 0.01$.

In the Chebyshev expansions of observables that we pursue in this thesis, the building blocks will be expectation values of Chebyshev polynomials with some vectors $|\alpha\rangle$ and $|\beta\rangle$

$$\mu_n = \langle\alpha|T_n(\tilde{H})|\beta\rangle. \tag{3.28}$$

We can simply calculate the resulting vector after n actions with the Hamiltonian

$$|\alpha_n\rangle = T_n(\hat{H})|\alpha\rangle, \tag{3.29}$$

following the recursion relation of the Chebyshev polynomials (Eq. (3.9)-(3.11))

$$\begin{aligned} |\alpha_0\rangle &= |\alpha\rangle, & (3.30)\\ |\alpha_1\rangle &= \tilde{H}|\alpha\rangle, & (3.31)\\ |\alpha_n\rangle &= 2\tilde{H}|\alpha_n\rangle - |\alpha_{n-1}\rangle. & (3.32) \end{aligned}$$

The moments can then be calculated by

$$\mu_n = \langle\beta|\alpha_n\rangle. \tag{3.33}$$

We can simplify Eq. (3.33) further if $|\alpha\rangle = |\beta\rangle$. For this we use a product relation of Chebyshev polynomials

$$2T_m(x)T_n(x) = T_{m+n}(x) + T_{m-n}(x). \tag{3.34}$$

Using Eq. (3.34) we can calculate two moments with every action of the Hamiltonian

$$\begin{aligned} \mu_{2n} &= \langle\alpha|\alpha_{2n}\rangle = \langle\alpha|T_{2n}(\tilde{H})|\alpha\rangle = & (3.35)\\ &= 2\langle\alpha|T_n(\tilde{H})T_n(\tilde{H})|\alpha\rangle - \langle\alpha|T_0(\tilde{H})|\alpha\rangle = 2\langle\alpha_n|\alpha_n\rangle - \mu_0, \end{aligned}$$

$$\begin{aligned} \mu_{2n+1} &= \langle\alpha|\alpha_{2n}\rangle = \langle\alpha|T_{2n+1}(\tilde{H})|\alpha\rangle = & (3.36)\\ &= 2\langle\alpha|T_{n+1}(\tilde{H})T_n(\tilde{H})|\alpha\rangle - \langle\alpha|T_1(\tilde{H})|\alpha\rangle = 2\langle\alpha_{n+1}|\alpha_n\rangle - \mu_1. \end{aligned}$$

The observables that we expand in order to construct our mean-fields are the LDoS and an equivalent object that carries the spectral information of the pairing

$$\Delta(E, \mathbf{r}_i) = U \sum_n \left[\delta(E - \epsilon_n) u_n(\mathbf{r}_i) v_n^*(\mathbf{r}_i)\right] \tag{3.37}$$

$$\rho(E, \mathbf{r}_i) = 2 \sum_n \left[\delta(E - \epsilon_n) |v_n(\mathbf{r}_i)|^2\right]. \tag{3.38}$$

An energy integral over Eq. (3.37) and (3.38) with the appropriate distribution functions directly yields the mean-fields defined in Eq. (3.4) and (3.5).

Note that the sum over eigenenergies ϵ_n is both over negative and positive energies. In the expansion scheme that we follow an expansion over the whole range of energies is unavoidable. In such an approach the complete information of the system is present both in the particle and the hole part of the wave function. This can be seen easily from the particle-hole symmetry in Eq. (2.28) and (2.29). The moments of the resulting Chebyshev expansion are

$$\begin{aligned}
\mu_m^{\Delta}(\mathbf{r}_i) &= \int_{-1}^{1} dE U T_m(E) \sum_n \left[\delta(E-\epsilon_n) u_n(\mathbf{r}_i) v_n^*(\mathbf{r}_i)\right] \\
&= U \sum_n \left[T_m(\epsilon_n) u_n(\mathbf{r}_i) v_n^*(\mathbf{r}_i)\right] = \\
&= \sum_n \langle \epsilon_n | T_m(\hat{H}) | v(\mathbf{r}_i)\rangle \langle u(\mathbf{r}_i) | \epsilon_n \rangle = \\
&= \langle u(\mathbf{r}_i) | T_m(\hat{H}) | v(\mathbf{r}_i)\rangle, \qquad (3.39)
\end{aligned}$$

$$\begin{aligned}
\mu_m^{\rho}(\mathbf{r}_i) &= \int_{-1}^{1} dE 2 T_m(E) \sum_n \left[\delta(E-\epsilon_n) |v_n(\mathbf{r}_i)|^2\right] = \\
&= 2 \sum_n \langle \epsilon_n | T_m(\hat{H}) | v_n(\mathbf{r}_i)\rangle \langle v_n(\mathbf{r}_i) | \epsilon_n \rangle \\
&= 2 \langle v(\mathbf{r}_i) | T_m(\hat{H}) | v(\mathbf{r}_i)\rangle. \qquad (3.40)
\end{aligned}$$

These matrix elements can then be computed recursively according to Eq. (3.33), (3.36) and (3.37).

After the coefficients have been determined, we can construct the energy-dependent quantities according to

$$f(x) = \frac{1}{\pi\sqrt{1-x^2}} \left(g_0 \mu_0 + 2 \sum_{n=1}^{N_C} g_n \mu_n T_n(x) \right). \qquad (3.41)$$

To arrive at the mean-fields we need to perform an integration over energy

with the corresponding distribution functions

$$\Delta(\mathbf{r}_i) = \int_0^1 dE \frac{(1-2f(E))}{\pi\sqrt{1-E^2}} \left(g_0\mu_0^{\Delta}(\mathbf{r}_i) + 2\sum_{n=1}^{N_\mathcal{C}} g_n\mu_n^{\Delta}(\mathbf{r}_i)T_n(E) \right) \quad (3.42)$$

$$n(\mathbf{r}_i) = \int_0^1 dE \frac{1-f(E)}{\pi\sqrt{1-E^2}} \left(g_0\mu_0^{\rho}(\mathbf{r}_i) + 2\sum_{n=1}^{N_\mathcal{C}} g_n\mu_n^{\rho}(\mathbf{r}_i)T_n(E) \right) + + \int_0^{-1} dE \frac{f(E)}{\pi\sqrt{1-E^2}} \left(g_0\mu_0^{\rho}(\mathbf{r}_i) + 2\sum_{n=1}^{N_\mathcal{C}} g_n\mu_n^{\rho}(\mathbf{r}_i)T_n(E) \right) \quad (3.43)$$

Both the construction of the spectral quantities (Eq. (3.41)) and the energy integration can be performed very efficiently. For this we use the close relation of Chebyshev polynomials to trigonometric functions. It holds

$$T_n(x) = \cos\left[n\arccos(x)\right]. \quad (3.44)$$

Now the abscissas of Chebyshev numerical integration [41] are

$$x_k = \cos\left(\frac{\pi(k+1/2)}{\tilde{N}}\right) \text{ with } k = 0, ..., (\tilde{N}-1). \quad (3.45)$$

For a sufficient accuracy of the integral we can take for instance $\tilde{N} = 2N_\mathcal{C}$. The values $f(x_k)$ (Eq. (3.41)) we can now get through a discrete cosine transform,

$$\gamma_k = \pi\sqrt{1-x_k^2}f(x_k) = \mu_0 g_0 + 2\sum_{n=1}^{N_\mathcal{C}} \mu_n g_n \cos\left(\frac{\pi n(k+1/2)}{\tilde{N}}\right). \quad (3.46)$$

This can be evaluated with an efficient divide-and-conquer algorithm of asymptotic complexity $\tilde{N}\ln\tilde{N}$. The computational effort to get these values is neglegible compared to the computation of the Chebyshev moments.

With these values, we can easily evaluate any integral

$$\int_{-1}^{1} f(x)g(x)dx = \int_{-1}^{1} \frac{\sqrt{1-x^2}f(x)g(x)}{\sqrt{1-x^2}}dx \approx \approx \frac{\pi}{\tilde{N}}\sum_{k=0}^{\tilde{N}-1}\sqrt{1-x_k^2}f(x_k)g(x_k) = \frac{1}{\tilde{N}}\sum_{k=0}^{\tilde{N}-1}\gamma_k g(x_k). \quad (3.47)$$

3.3.1 Error discussion

There is an error involved in the expansion, as we cancel the infinite series after the $N_{\mathcal{C}}$-th moment. This leads to a broadening of the δ peaks in Eq. (3.37) and (3.38). As $\Delta(E, \mathbf{r}_i)$ in Eq. (3.37) is antisymmetric and furthermore has its largest contributions close to zero energy, this broadening can lead to cancellation between positive and negative energy contributions. The error at some position $\mathbf{r}$ becomes significant as the broadening of the delta peaks (see Eq. (3.24)) becomes comparable to the spectral gap of the LDoS at this position. Thus for a given accuracy the necessary number of Chebyshev moments $N_{\mathcal{C}}$ increases with decreasing spectral gap. In practice the self-consistency cycle can be performed with a low number of moments $N_{\mathcal{C}}$ quickly, after which we increase the number of moments successively until full convergence is achieved.

3.3.2 Scaling and memory usage discussion

Parts of this discussion can already be found in an earlier publication with copyright by the American Physical Society[9]. The computationally demanding step limiting the code-performance is the calculation of the self-consistent fields that need to be evaluated in every iteration cycle of the self-consistency process. In straight-forward implementations the Hamiltonian is diagonalized in each iteration cycle to construct the self-consistent fields and restart the cycle with the updated Hamiltonian; the cost is $\mathcal{O}(N_{\mathrm{bf}}^3)$ operations, where N_{bf} is the dimension of the single-particle Hilbert space.

With our KPM implementation the expansion of one positional eigenstate amounts to $N_{\mathcal{C}}$ sparse-matrix multiplications that each exhibit an asymptotic complexity of $\mathcal{O}(N_{\mathrm{bf}} N_{\mathrm{nz}})$ with N_{nz} number of non-zero Hamiltonian matrix-elements per row. As this has to be repeated for all of the N_{bf} sites, we have achieved a reduction in scaling of one self-consistency cycle with respect to a full diagonalization approach to $\mathcal{O}(N_{\mathcal{C}} N_{\mathrm{bf}}^2 N_{\mathrm{nz}})$. For a dense matrix we have $N_{\mathrm{nz}}{=}N_{\mathrm{bf}}$, while for a very sparse matrix $N_{\mathrm{nz}} \approx N_{\mathrm{bf}}^0$. For example, for the BdG equations, we have $N_{\mathrm{nz}} = 2d + 2$, with $2d$ denoting the number of nearest neighbors on a cubic lattice in d dimensions. Typically we can choose $N_{\mathcal{C}} \ll N_{\mathrm{bf}}$ and furthermore $N_{\mathcal{C}}$ does not scale with system size. Thus we arrive at a scaling $\mathcal{O}(N_{\mathrm{bf}}^2)$.

Memory usage is not a significant issue for the system sizes that we have considered so far. As we use a sparse-matrix approach the memory usage does

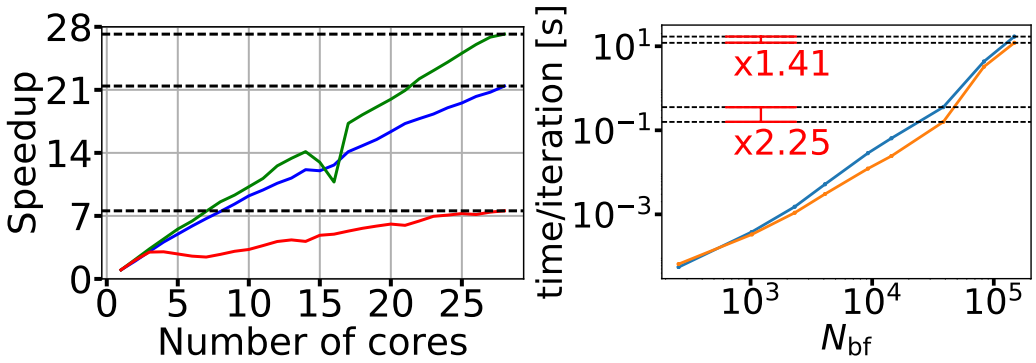

Figure 3.1: Benchmarking intra-node parallelization and code performance. Left: Speedup with the number of cores per process for different system sizes. The performance dips (green,blue: near 16; red: near 7,14,21,25) with rising number of cores we assign to a hardware issue related to caching. (Parameters: $L = 96$ (blue), $L = 192$ (green), $L = 288$ (red).) Right: Performance check comparing the matrix-free implementation (orange) with standard mkl_sparse_d_mm of the MKL Sparse BLAS library (blue). One iteration corresponds to one sparse matrix-vector product. The ratio of the timings of the MKL and matrix-free algorithms is shown in red at $L = 192$ and $L = 384$. These figures can already be found in an earlier publication with copyright by the American Physical Society[9].

only linearly increase with system size N_{bf}. For a lattice of size 192x192, we have for instance used less than 10 GB of RAM.

3.3.3 Further optimization and design considerations

This discussion can already be found in an earlier publication with copyright by the American Physical Society[9]. As almost all runtime is spent on the recursive matrix vector products, the code lends itself very well to being split in an efficient low-level (i.e. C) kernel embedded in a high-level (i.e. python) code that implements the rest of the self-consistency cycle in a convenient way with negligible loss of performance. The kernel has been optimized for both threading and vectorization. In Fig. 3.1 we show benchmarks performed on a compute node with two 14-core Haswell Xeon Processor E5-2697 v3; we monitor the time spent for performing a single sparse matrix-vector product. Fig. 3.1 (left) is illustrating the efficiency of our intra-node (OpenMP) parallelization. For the investigated system sizes $L < 288$ the memory-bound

runtime limit is not yet reached as is evidenced by the high speedup through parallelization. This makes it very advantageous to perform calculations in this size regime, where parallelization can still be utilized effectively. Fig. 3.1 (right) compares our matrix-free implementation with the standard MKL. As is seen from the data, our matrix-free implementation is advantageous already at system sizes as small as $N_{\mathrm{bf}} \sim 1000$ sites. Note, that at such small system sizes even full diagonalization routines can compete. As a technical remark we mention that, in principle, the matrix-free code should always be faster as compared to MKL implementations. The crossover size originates from our decision to use python as a platform, which leaves an interface to a C-based kernel. This interface is plagued with a small overhead that becomes negligible beyond the cross-over size.

An additional level of parallelism is obtained by running the expansion of different basis vectors independently on different nodes. The average over the disorder ensemble is performed via farming. This inter-node parallelization scales almost perfectly.

Matrix-free matrix-vector product

To speed up a single self-consistency iteration we optimize the Chebyshev expansion. Its performance critical part is constituted of the recursive action of the Hamiltonian on a basis vector, Eq. (3.29). An implementation of the sparse-matrix vector product custom-tailored to our system is crucial for an optimal performance. The sparse-martrix vector multiplication is memory-bound, i.e. the performance is limited by the time it takes to fetch data from memory. For this reason we devised a self-written "matrix-free" matrix vector product that outperforms standard state of the art sparse-matrix vector multiplication libraries.

The idea is the following: Conventional sparse matrix packages keep all non-zero elements, i.e. value and index, in memory. Matrix-free implementations become efficient if many of the non-zero elements have identical values storing only the different values that occur.

With matrix-free implementations the graph of the Hamiltonian has to be hard-coded in the matrix-vector product routine. For our Hamiltonian the amount of memory load operations of matrix data is reduced by a factor of 6 reflecting the number of non-zero elements per row of $\hat{H}_{\mathrm{BdG}}$. In addition, the integer indices corresponding to the matrix graph do not have to be loaded.

Altogether, this leads to a reduction of data to be loaded by a factor of 9. [i] We mention that recently a library has been made available that automatizes the implementation of such a matrix-free matrix-vector product for a given Hamiltonian [42].

Improved convergence of scf-cycle

We improve the code performance by reducing the number of iterations needed until the convergence of the scf-cycle. The main idea applies, e.g., when scanning the parameter space at fixed U for increasing disorder strength W. At strength W_1 a converged solution Ψ_1 is found for a given disorder realization. Thereafter, a sample at larger strength $W_2 > W_1$ is generated by rescaling the disorder in the first sample by a factor of W_2/W_1. Then, Ψ_1 will be used to initialize the scf-cycle for the second sample.

3.3.4 Similar implementations

Parts of this discussion can already be found in an earlier publication with copyright by the American Physical Society[9]. The KPM-aspect of our implementation is similar to other variants described in earlier work. They have been proven useful in applications of the BdG-equation for nanostructures with one or very few impurities, but have not been applied to disordered samples. Implementation differences are in details: Covaci, Peeters, and Berciu [43], Nagai, Ota, and Machida [44], and Nagai et al. [45] also use KPM to perform traces. In addition, Covaci, Peeters, and Berciu [43] also have employed a matrix-free implementation. While these authors expand the Green's function employing the Lorentz kernel, we expand the spectral function where the Jackson Kernel typically has better convergence properties [40]. In addition we will present a stochastic approach for the evaluation of the trace that has never been employed in the context of BdG theory. It provides a promising route to achieve even larger system sizes in the future.

[i] The datatype for values is double and for the indices is integer. Note, that the speed-up to be expected from the matrix-free implementation is less than a factor of 9. This is because not only the matrix but also the basis vectors have to be loaded from memory, so the reduction of memory load operations also depends on how many basis vectors are acted on in parallel.

3.4 Alternative expansion approaches

In this section we will shortly introduce alternative approaches of the Chebyshev expansion that might prove useful for either large system sizes or large tempertures in the future.

Random trace evaluation

The trace in Eq. (3.39) and (3.40) over energy eigenstates can be performed directly in a stochastic way.

$$\mu_n = \mathrm{Tr}\left[AT_n(\tilde{H})\right] \approx \frac{1}{R}\sum_{r=0}^{R-1}\langle r|AT_n(\tilde{H})|r\rangle. \tag{3.48}$$

The number of random states does not scale with the size of the system, or can even be reduced sometimes for larger systems. Such kind of an expansion is thus especially suited for very large systems.

We first define random vectors

$$|r\rangle = \sum_{i=0}^{N_{\mathrm{bf}}} \xi_{r,i}|i\rangle, \tag{3.49}$$

in some arbitrary basis $|i\rangle$. That the random trace converges to the exact trace in the limit $R \to \infty$ the numbers $\xi_{i,r}$ need to fulfill

$$\langle\langle \xi_{i,r}\rangle\rangle = 0, \tag{3.50}$$
$$\langle\langle \xi_{i,r}\xi_{j,r'}\rangle\rangle = \delta_{r,r'}\delta_{j,j'}, \tag{3.51}$$

where the statistical average is defined as

$$\langle\langle g(x)\rangle\rangle = \int_{-\infty}^{\infty} \mathcal{P}(x)g(x)dx, \tag{3.52}$$

with probability distribution $\mathcal{P}(x)$. Thus we get on average

$$\left\langle\left\langle \frac{1}{R}\sum_{r=0}^{R-1}\langle r|B|r\rangle \right\rangle\right\rangle = \frac{1}{R}\sum_{r=0}^{R-1}\sum_{i,j=0}^{D-1}\langle\langle \xi_{i,r}^{*}\xi_{j,r}\rangle\rangle B_{ij} = \sum_{i=0}^{D-1} B_{ii} = Tr(B). \tag{3.53}$$

The choice of random distribution can make a difference here, though it is usually not a huge effect. An example for an appropriate distribution is a box distribution of the form

$$\mathcal{P}(x) = \sqrt{12}\Theta(\frac{1}{2\sqrt{12}} - |x|), \tag{3.54}$$

with Heaviside function Θ.

An optimal choice of random vectors would be random phase vectors. As we can choose our Hamiltonian to be real, due to time reversal invariance, this is numerically not favorable in our case.

We have developed a pilot implementation of a random trace evaluation approach. There is an additional error caused by taking the trace over a finite number of random vectors. For the system sizes considered here this error is too large with a number of random vectors $R < N_{\mathrm{bf}}$. For very large systems this is no longer the case, as the necessary number of random vectors for a given accuracy does not scale with system size. In the very large system size limit one can achieve a scaling $\mathcal{O}(N_{\mathrm{bf}})$ with a random trace evaluation approach. Tests of our pilot implementation for very large systems are in progress.

Expansion of the Fermi function

Instead of expanding the LDoS or the spectrally resolved pairing, one can epxand the Fermi function in the self-consistency equations (Eq. (2.31) and (2.32)) and calculate the trace directly according to

$$\begin{aligned}
\Delta(\mathbf{r}_i) &= U \sum_n [u_n(\mathbf{r}_i) v_n^*(\mathbf{r}_i)(1 - 2f_n)] =, \\
&= U \sum_n \langle \epsilon_n | \, |u(\mathbf{r}_i)\rangle\langle v(\mathbf{r}_i)| (1 - 2f(\hat{H})) \, |\epsilon_n\rangle \qquad (3.55) \\
n(\mathbf{r}_i) &= 2 \sum_n \left[|v_n(\mathbf{r}_i)|^2 (1 - f_n) + |u_n(\mathbf{r}_i)|^2 f_n \right] = \\
&= 2 \sum_n \langle \epsilon_n | \, |v(\mathbf{r}_i)\rangle\langle v(\mathbf{r}_i)| (1 - f(\hat{H})) + |u(\mathbf{r}_i)\rangle\langle u_n(\mathbf{r}_i)| f(\hat{H}) \, |\epsilon_n\rangle \qquad (3.56)
\end{aligned}$$

The trace can either be evaluated by a random trace evaluation described above or by a trace over the positional eigenstates outlined in Section 3.3. For low temperatures a large number of moments $N_{\mathcal{C}}$ will be necessary to expand

the Fermi function, as it very sharply drops in the vicinity of the Fermi energy. Consequently we have found that at low temperature the expansion of $\Delta(E, \mathbf{r}_i)$ and $\rho(E, \mathbf{r}_i)$, as described in Section 3.3, is the better choice. As the number of necessary Chebyshev moments $N_\mathcal{C}$ to expand the Fermi function decreases with increasing temperature, such an approach becomes interesting for large temperatures.

Chapter 4

Single Impurity

In this chapter we will study superconductors in the presence of a single non-magnetic Anderson impurity. In particular we are interested in the resulting Friedel oscillations of the superconducting gap at the surface of a 3D and 2D system.

The response of the superconducting gap to impurities has recently received considerable attention both experimentally[46, 47, 48, 49] and theoretically[50, 51, 52, 53, 54]. The resulting Friedel oscillations provide a promising tool in determining properties of the underlying supercondcting state. For instance, they may reveal unconventional symmetry of the order parameter or the presence of topological edge states[53, 54].

Friedel oscillations in the density are a consequence of the screening of a potential impurity in a metal [55]. At low temperatures, due to the sharpness of the Fermi surface, the wave vector of the electrons that participate in the screening is the Fermi wave vector k_F. For that reason the density response is also modulated by a frequency determined by k_F. The density response $\delta n(\mathbf{r})$ far from a potential impurity follows to leading order [56]

$$\delta n(\mathbf{r}) \sim \frac{\cos\left(2k_F|\mathbf{r}| + \Phi\right)}{|\mathbf{r}|^D}, \tag{4.1}$$

with phase Φ and dimension D. Similarily, the response of the self-consistent pairing amplitude $\delta\Delta(\mathbf{r})$ far from a potential impurity in the bulk of a 3D s-wave superconductor [57] is described to leading order in $\mathbf{r}$ by

$$\delta\Delta(\mathbf{r}) \sim \frac{\cos\left(2k_F|\mathbf{r}| + \Phi\right)}{|\mathbf{r}|^2}\exp(-a|\mathbf{r}|/\xi), \tag{4.2}$$

with superconducting coherence length ξ and some constant factor a. Thus in 3D the pairing amplitude decays with $|\mathbf{r}|^{-(D-1)}$ in contrast to the $|\mathbf{r}|^{-D}$ behavior of the density. To arrive at this result the gap was calculated self-consistently.

The functional form of the pairing amplitude response is known only for the special case mentioned above. The reason that a more general description has not been found so far lies in the complications that the self-consistency requirement brings. At the same time self-consistency leads to unexpected properties: The decay of the pairing amplitude response does not simply follow the oscillations in the density. The response of the gap turns out to be more long-ranged.

Self-consistent numerical calculations have been conducted before [50, 51, 58, 54] for other dimensionalities than the analytically tractable case but the aforementioned exponents have never been determined. This is presumably due to the limitations in system size in previous studies.

To describe the pairing amplitude response to an Anderson impurity in 2D and for an impurity on a 3D surface, we will study the model Hamiltonian

$$\begin{aligned}
\hat{H}_{\text{Friedel}} &= \hat{H}_{\text{BdG}}|_{V_i=0} + \hat{H}_{\text{imp}} \qquad (4.3)\\
\hat{H}_{\text{BdG}}|_{V_i=0} &= -t\sum_{\langle i,j\rangle,\sigma}\hat{c}^\dagger_{i,\sigma}\hat{c}_{j,\sigma} - \sum_{i=1,\sigma}^{N_{\text{bf}}}\left(\frac{U}{2}n(\mathbf{r}_i)+\mu\right)\hat{n}_{i,\sigma} -\\
&- \sum_{i=1}^{N_{\text{bf}}}\Delta(\mathbf{r}_i)\hat{c}_{i,\uparrow}\hat{c}_{i,\downarrow} + \text{h.c.},\\
\hat{H}_{\text{imp}} &= -t\hat{c}^\dagger_{I,\sigma}\hat{c}_{1,\sigma} - \left(\frac{U}{2}n(\mathbf{r}_I)+\mu+V_{\text{imp}}\right)\hat{n}_{I,\sigma} -\\
&- \Delta(\mathbf{r}_I)\hat{c}_{I,\uparrow}\hat{c}_{I,\downarrow} + \text{h.c.},
\end{aligned}$$

consisting of the BdG Hamiltonian $\hat{H}_{\text{BdG}}|_{V_i=0}$, defined by equations (2.25) - (2.32), without the inhomogeneous potential V_i and $\hat{H}_{\text{imp}}$, which describes an added Anderson impurity of potential V_{imp} at site $\mathbf{r}_I$. In the case of a 2D system, $\hat{H}_{\text{BdG}}|_{V_i=0}$ will be periodic in both spatial directions. In the 3D case, we choose the x- and y-direction to be periodic and for the z-direction we impose open boundary conditions. The Anderson impurity will be located on one of the surfaces. The density $n(\mathbf{r})$, pairing amplitude $\Delta(\mathbf{r})$ and chemical potential μ are computed self-consistently on the whole system consisting of the periodic lattice and the added impurity site.

We define the response of an observable $O(\mathbf{r})$ as

$$\delta O(\mathbf{r}) = \langle \hat{O}(\mathbf{r}) \rangle_{\text{imp}} - \langle \hat{O}(\mathbf{r}) \rangle_0, \tag{4.4}$$

where $\langle . \rangle_{\text{imp}}$ is the trace with respect to $\hat{H}_{\text{Friedel}}$ and $\langle . \rangle_0$ with respect to $\hat{H}_{\text{BdG}}|_{V_i=0}$. The site of the impurity $\mathbf{r}_I$ is excluded from this response. Both the pairing amplitude and density will be neglegible there.

4.1 Results: Pairing amplitude response

All the results in this chapter have been computed with a full diagonalization solver as described in Chapter 3.

4.1.1 Thin film superconductors (2D)

In Fig. 4.1 a spatial map of the response as defined in Eq. (4.4) for the pairing amplitude $\Delta(\mathbf{r})$ is shown. As is the case for Friedel oscillations in the density, we assume an analogous form of the pairing amplitude response to the 3D case (Eq. 4.2) with a different exponent of the power-law decay. The interaction strength U is chosen such, that the superconducting correlation length $\xi = 54a \approx aL/2$. Through this we keep the contribution of the exponential small, while at the same time avoiding finite size effects. The red circles represent distances of integer multiples of half the Fermi wave length $\lambda_F/2$. The frequency of $2k_F$ of the oscillations in analogy to Eq. (4.2) is readily discernible. Note that at the impurity site the superconducting gap is enhanced by more than 20%. This is in qualitative agreement with the experimental data. As the experiments were conducted on a 3D superconductor, we refer to the next subsection for a quantitative analysis.

In Fig. 4.2 the oscillatory part of the pairing amplitude is shown in diagonal direction. We multiplied the pairing amplitude with the distance from the impurity. This is done under the assumption that in 2D the exponent will be reduced by one with respect to the 3D gap response (Eq. (4.2)), as is the case for Friedel oscillations in the density. There is no discernible decay and we conclude that an exponent of 1 of the power-law decay is consistent with our data. There seems to be a slower oscillation superimposed to the $2k_F$ oscillation. One might suspect a finite size effect but the analysis is ongoing. Similar simulations have been conducted before [50, 51, 54], although the authors did not extract the decay of the exponent.

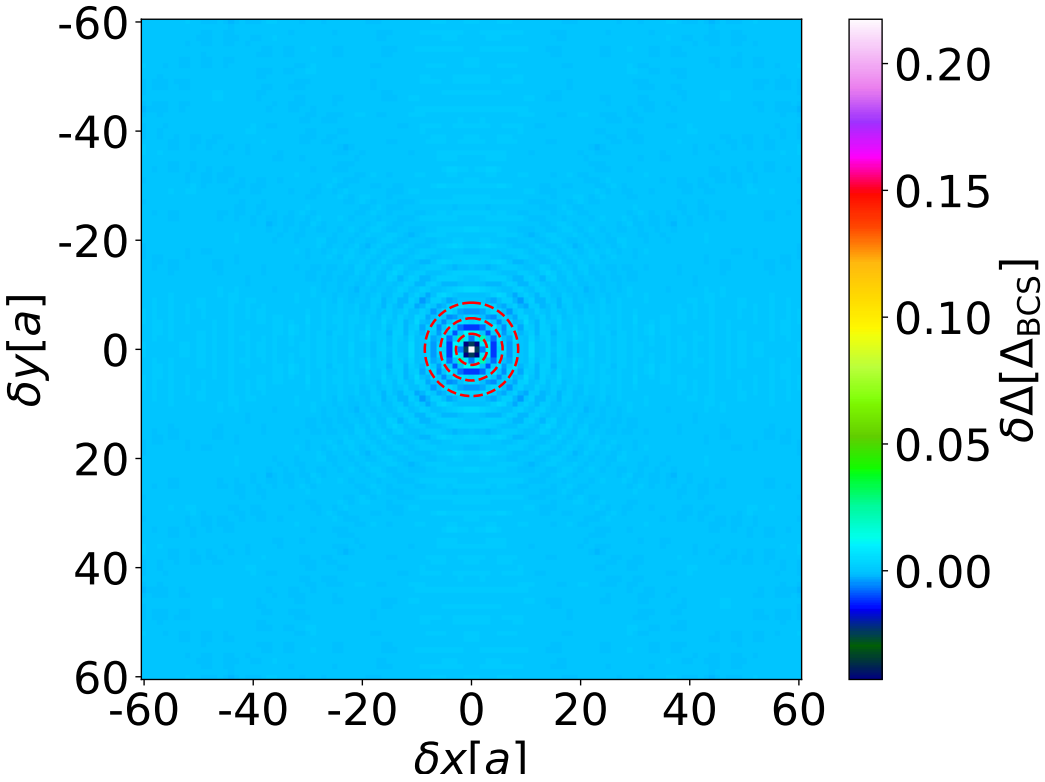

Figure 4.1: Spatial map of the response of the pairing amplitude in a thin film to an Anderson impurity (extra site) at $\delta x = \delta y = 0$. As a guide for the eye the red dashed lines represent multiples of half the Fermi wave length $\lambda_{\mathrm{F}}/2$ distance from the impurity. (Parameters: $n = 0.2$, $U = 1.6$, $V_{\mathrm{imp}} = -0.06t$, $\lambda_F \approx 1.42a$, (converged $\alpha = 0.001\%$))

4.1.2 Bulk superconductors (3D)

In this subsection we will investigate the influence of an Anderson impurity on the pairing amplitude and density response on the surface of a 3D bulk. In an upcoming paper we will contrast these results with experiments conducted by the Wulfhekel group at the Karlsruhe Institute of Technology [10].

In Fig. 4.3 the cross section of the system is shown in the xz plane. The surface itself causes Friedel oscillations, as has been noted before [59, 50, 51]. We see an enhancement of the gap of close to 6% below the impurity site, which is in qualitative agreement with the experimental findings. In Fig. 4.4 the logarithm of the pairing amplitude on the surface below the impurity is

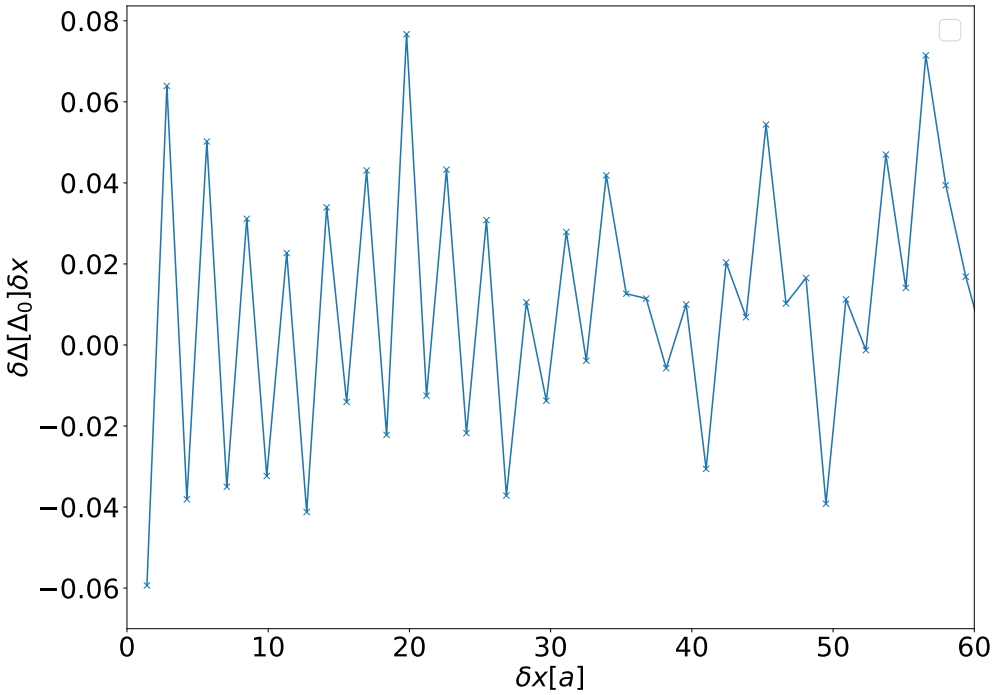

Figure 4.2: The pairing amplitude response along the diagonal of a surface below an Anderson impurity (extra site) multiplied by x^{-1}. (Parameters: $n = 0.2$, $U = 1.6$, $V_{\text{imp}} = -0.06t$, (converged $\alpha = 0.001\%$))

shown. The disorder potential is chosen to represent the difference in work function of Fe and Al on Al111 surface. The choice of interaction strength $U = 3.2$ leads to a correlation length of $\xi = 10.6 \approx L/2$, to minimize the effect of the exponential decay. The red circles represent multiples of half the Fermi wave length. Again a $2k_F$ oscillation is clearly visible. Similar simulations have been conducted before [50, 51], albeit on a very small 8^3 lattice. While the authors also observed an increase of the pairing amplitude at the impurity site, the size of the system did not permit an analysis of the decay.

In Fig. 4.5 map the absolute value of the pairing amplitude response on the surface is projected to a linear plot, according to the distance from the impurity. This is done to alleviate the finite size effects through a finer distance discretization. We find in Fig. 4.5 (left) that the decay of the pairing amplitde is compatible with a x^{-3} power law envelope, while in Fig. 4.5 (right) the density is in agreement with a x^{-4} decay. As seen before in the

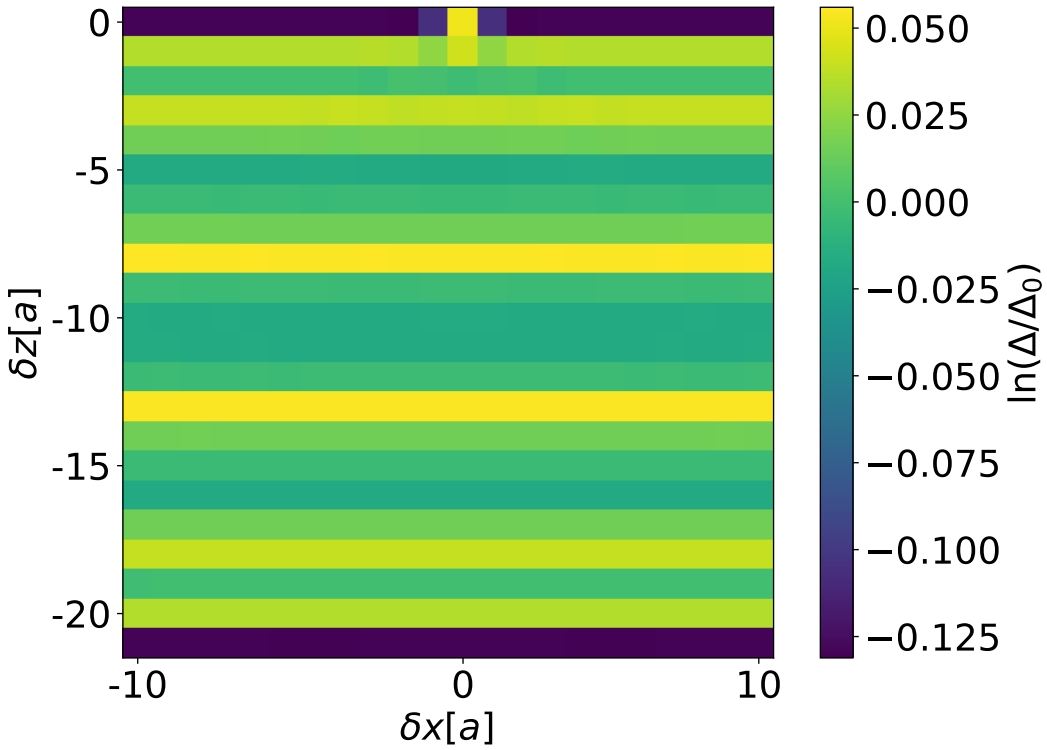

Figure 4.3: Left: Spatial map of a 2D slice of the response of the pairing amplitude on a 3D lattice to an Anderson impurity (extra site) at $\delta x = \delta z = 0$. Translational invariance is broken in z-direction. Δ_0 is the mean gap of the system without impurity. (Parameters: $n = 0.12$, $U = 3.2$, $W_{\text{imp}} = -0.06$, (converged $\alpha = 0.0001\%$))

2D case and 3D bulk case, the exponent of the decay of the pairing amplitude is reduced by one with respect to the exponent of the density. The behavior that does not seem to be in accordance with a simple $2k_F$ oscillation in Fig. 4.5 we attribute to finite size effects. There are only states in a few directions close to the Fermi surface, which leads to anisotropy. In addition, these states can vary in their in-plane Fermi wave length. While we were already able to show that an increase of the gap is to be expected, in the upcoming paper we will also compare the power-law decay of the experimental and numerical data [10].

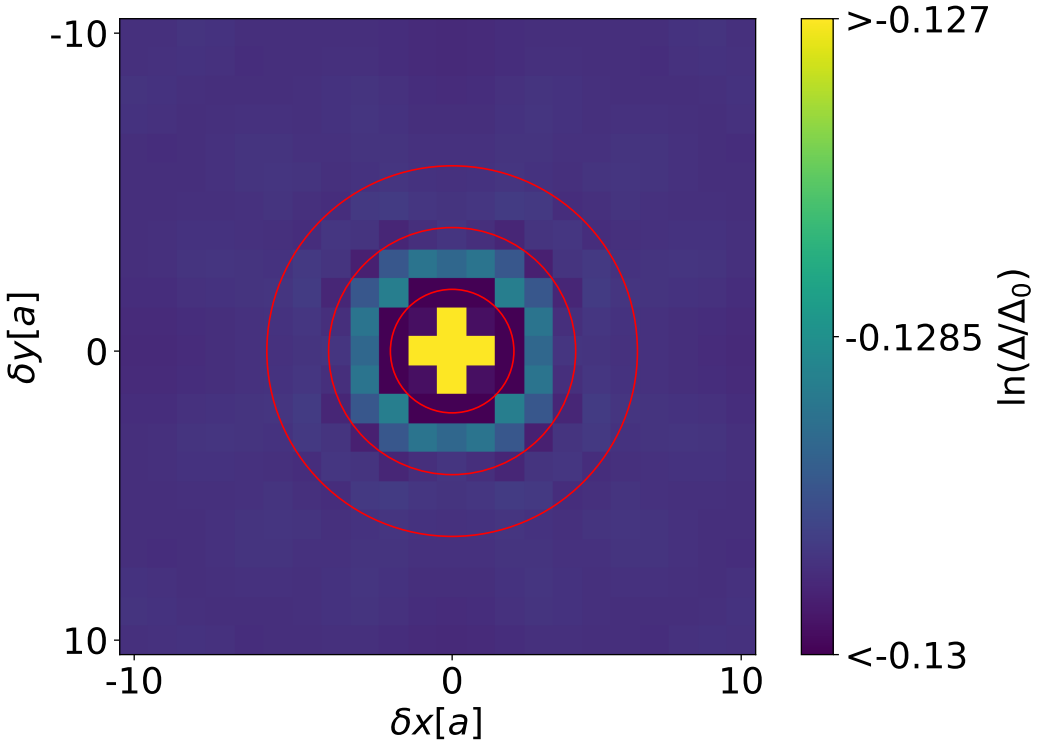

Figure 4.4: Spatial map of the response of the pairing amplitude on the surface of a 3D lattice to an Anderson impurity (extra site) at $\delta x = \delta y = 0$. The red lines represent the first three minima of a $2k_F$ oscillation. Δ_0 is the mean gap of the system without impurity. (Parameters: $n = 0.12$, $U = 3.2$, $W_{\text{imp}} = -0.06t$, (converged $\alpha = 0.0001\%$))

4.1.3 Discussion

We find that in all the considered cases the exponent of the power-law decay of the pairing amplitude response to an Anderson impurity is reduced by 1 with respect to the corresponding exponent in the density response. This is also true for the analytically tractable case of an impurity in a 3D bulk (see Eq. (4.2)). It is possible that this is a generic property of Friedel oscillations in the pairing amplitude.

While an analytical solution of the pairing amplitude response remains unknown in the 2D case to the best of our knowledge, we can hint at a technical explanation for the difference in exponent between density and pairing amplitude. In 2D the anomalous Green's function decays with x^{-1},

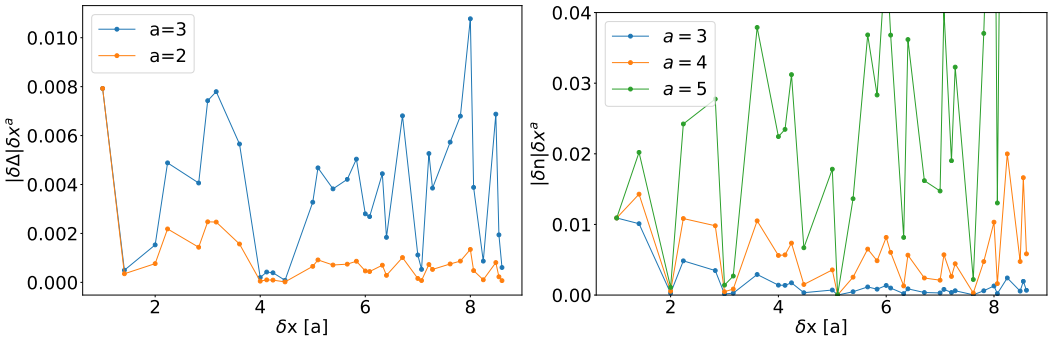

Figure 4.5: Absolute value of the pairing amplitude (left) and density (right) response on the surface below an Anderson impurity (extra site) multiplied by power-laws with exponent a. The pairing amplitude response is given in unites of the mean gap Δ_0 of the system without impurity. The 2d data has been mapped to a linear plot according to the distance of the respective sites from the impurity. (Parameters: $n = 0.12$, $U = 3.2$, $W_{\text{imp}} = -0.06$, (converged $\alpha = 0.0001\%$))

while the normal Green's function decays with x^{-2}. [60] It is tempting to assume that this is related.

All the results and also the analytical treatment of the 3D bulk involve the solution of the fully self-consistent gap equation. In the case of a periodic 1D system with a potential impurity it has been found that the self-consistency requirement can be relaxed, while still describing the response semi-quantiatively [50]. In the partial self-consistency scheme considered by the authors only the spectrum and not the eigenstates are renormalized in the self-consistency cycle. This approximation is exact in the case of plane waves. As the problem of a single impurity can be understood in terms of scattered plane waves it is no wonder that this approximation works well. One might expect a larger associated error in the case of a surface of a 3D bulk, as the Hartree potential is neglected in this approach. We will consider this partial energy-only self-consistency scheme further in the context of disordered superconductors in Chapter 5.

In the experiment detailed in the introduction an enhancement of $\sim 9\%$ was found at the impurity position. We find an increase of $\sim 6\%$ in the 3D case. Thus the experiment has been reproduced semi-quantitatively.

Chapter 5

Dirty Superconductors

In this chapter disordered s-wave superconductors and the Superconductor-Insulator-Transition will be discussed. We will start with a short overview of non-interacting Anderson transitions. In the next chapter an overview will be given of the literature on Superconductor-Insulator-Transitions, focussing on the aspects that are most relevant to this thesis. Finally we will present and discuss our results.

5.1 Anderson localization

We will give a brief overview of Anderson localization and the Anderson model, while presenting their most relevant features to this thesis. For an exhaustive review please refer to Evers and Mirlin [4].

As first described by Anderson [61], disorder may lead to a localization transition. The original model that was found to exhibit such a transition, the Anderson model, reads

$$\hat{H}_0 = \hat{H}_{\text{free}} + \sum_{i=1,\sigma}^{N_{\text{bf}}} (V_i - \mu)\, \hat{n}_{i,\sigma}, \tag{5.1}$$

with $\hat{H}_{\text{free}}$, as defined in Eq. (2.8) and random potential $V_i \in [-W, W]$ drawn from a box distribution with disorder strength W. The choice of distribution here is not unique. For instance a Gaussian or Lorentzian distribution will lead to the same kind of transition.

There is a critical disorder strength W_c which separates the phase where all states are localized from the phase where delocalized states remain in

some region of energy. In the delocalized phase the wave functions exhibit appreciable weights everywhere in space

$$|\Psi(\mathbf{r})|^2 \propto \text{const.} \tag{5.2}$$

In the localized phase the envelope of the probability amplitude falls off exponentially with distance $\mathbf{r}$

$$|\Psi(\mathbf{r})|^2 \propto \exp(-|\mathbf{r}-\mathbf{r}_0|/\xi_{\text{loc}}), \tag{5.3}$$

with a localization length ξ_{loc} around some localization center $\mathbf{r}_0$. At a given disorder strength $W < W_c$ a localization transition also happens, when shifting the Fermi energy away from the band center beyond an energy E_{c}, the mobility edge.

The effect of disorder on the system is strongly dependent on dimensionality. In this thesis we will focus on two- and three-dimensional systems. In $d = 3$ an Anderson transition takes place in every symmetry class. In $d = 2$ all states are localized for arbitrarily low disorder strength in the orthogonal symmetry class. It is important to note here that, while this is true in the thermodynamic limit, the localization length can be macroscopically large for experimentally relevant low disorder strengths[62]. Furthermore in all the other symmetry classes, e.g. if spin-rotational symmetry is broken by spin-orbit coupling, there is an Anderson transition also in 2D.

An aspect of the Anderson transition that is highly relevant for the SIT is wave function multifractality. The critical wave functions, i.e. wave functions at $W = W_{\text{c}}$ or $E = E_{\text{c}}$, exhibit a multifractal spatial distribution. Qualitatively we can imagine such a distribution as something that shows an intermediate behavior between extended and localized states. The wave function amplitudes can vary strongly from location to location and the lattice is only partially covered with appreciable amplitudes. At the same time the non-zero amplitudes of the wave function are not limited to a certain region of space.

The higher moments of the wave functions

$$P_q = \int d^d\mathbf{r} |\Psi(\mathbf{r})|^{2q}, \tag{5.4}$$

are convenient objects to describe this behavior quantiatively.

To understand the significance of this object, let us first describe its behavior in the case of localized or extended wave functions. For the localized

wave function we will assume

$$\Psi_{\text{loc}}(\mathbf{r}) = \delta(\mathbf{r} - \mathbf{r}_0). \tag{5.5}$$

Thus in the localized case we arrive at the moments

$$P_q = 1. \tag{5.6}$$

In the extended case we will assume the wave functions to follow

$$\Psi_{\text{ext}}(\mathbf{r}) = \frac{1}{L^d}, \tag{5.7}$$

with volume L^d. This leads to the moments

$$P_q = L^{-d(q-1)}. \tag{5.8}$$

Thus extended and localized wave functions can be distinguished by the scaling of their higher moments with system size.

As already described qualitatively before, multifractal wave functions show a behavior in between localized and extended states. Their moments scale as

$$P_q = L^{-d(q-1)-\Delta_q}, \tag{5.9}$$

with anomolous dimension Δ_q. The behvaior of Δ_q determines the critical behavior of the Anderson transition. The presence of multifractality of the single-particle wave functions is a key aspect of the type of inhomogeneous superconductors that we will investigate throughout this thesis.

It is important to note that even in the orthogonal symmetry in two dimensions, where Anderson localization occurs even for infinitesimal disorder strengths, there is a notion of multifractality. The wave functions exhibit what is called weak multifractality on the scale of the localization length [63]. In contrast to the multifractality at an Anderson transition the exponents that characterize the moments of the wave functions are not universal, i.e. they depend for instance on the disorder strength.

5.2 Superconductor-Insulator-Transitions

In this chapter we will review both the theoretical and experimental status of the SIT. There are multiple possible theoretical approaches being discussed. The relation between them remains unclear. There are a number of

comprehensive reviews that summarize the different approaches and related experiments [64, 65, 66]

The SIT scenarios are classified broadly in:

- Fermionic scenarios, in which Cooper pairs are broken through a renormalization of the Coulomb repulsion by disorder. The electrons then localize through conventional Anderson localization. Both an intermediate metallic phase or a direct SIT are being discussed.

- Bosonic scenarios, where Cooper pairs stay intact across a SIT driven by phase fluctuations. The SIT can either be direct or an intermediate Bose metal phase may develop. Theoretical descriptions vary and both screened and long-range Coulomb repulsion are being considered. Furthermore theories differ in their underlying fundamental objects: Either they start from interacting electrons or interacting bosons. Through the preformed Cooper pairs the insulating phase can exhibit considerably different phenomenology compared to a conventional Anderson insulator.

In addition to this classification one should distinguish between the SIT in thin films and 3D bulk materials. Another important aspect is the type of disorder: both granular and homogeneously disordered materials have been considered. Finally there are disorder and magnetic field driven SITs.

This thesis is primarily concerned with the disorder-driven bosonic scenario of the interplay of Anderson localization and superconductivity with screened Coulomb interaction in thin homogeneously disordered films. In terms of methodology our approach employs a microscopic mean-field theory of interacting electrons. There are a number of reviews that are particularily relevant to the scenario considered here. [67, 25, 32]

Theoretical status

We will start with a review of the theoretical status of this line of thought, focussing on the aspects that are most relevant to us. The theoretical discussion of the impact of disorder on superconductivity began shortly after BCS theory was developed. [68, 69] This lead to the Anderson theorem, which states that superconductivity is essentially unimpeded by non-magnetic disorder. For instance the mean-free path does not enter the expression for the critical temperature in BCS theory.

When localization is taken into account the situation becomes more interesting. In the 80s BCS and Ginzburg-Landau theory were studied with an underlying localized system. It was shown that a superconducting state is possible in an Anderson insulator[70, 71]. The highly localized regime on the other hand does not support a superconducting phase anymore.

It became apparent that these superconductors have properties quite dissimilar from a BCS superconductor. Strong spatial fluctuations of the pairing amplitude close to the critical temperature [72, 73] and also an increased susceptibility to phase fluctuations were found [74, 75].

Ma and Lee [76] devised a criterion, when this inhomogeneous superconducting state emerges and when it is destroyed by disorder. It is of conventional BCS type as long as there is a sufficient number of states in a localization volume

$$\rho\Delta\xi_{\mathrm{loc}}^{d} \geq 1, \tag{5.10}$$

with density of states ρ, superconducting gap Δ, dimensionality d and localization length ξ_{loc}. As the number of states get depleted and $\rho\Delta\xi_{\mathrm{loc}}^{d} < 1$ the pairing amplitde acquires strong spatial inhomogenity and eventually vanishes, which was found to be true even at zero temperature.

With the seminal papers by Ghosal, Randeria, and Trivedi [11, 12] full self-consistency could for the first time be taken into account. This led to a few remarkable findings: (i) With increasing disorder granularity of the pairing amplitude on the scale of the superconducting coherence length emerged even in the case of short-range disorder. The amplitudes of the pairing amplitude were found to be distributed very broadly. (ii) The spectral gap in the density of states became parametrically decoupled from the mean value of the pairing amplitde. (iii) Finally a depletion of the phase stiffness with increasing disorder was demonstrated.

The loss of phase coherence between superconducting islands in homogeneously disordered films has been demonstrated at finite temperature under the inclusion of thermal phase fluctuations. [13]

Another important phenomenon displayed by disordered superconductors with screened Coulomb repulsion is the enhancement of superconductivity by wave function fractality. In a field-theoretical framework it has been shown that fractality can lead to an increase in critical temperature [77, 78]. In a partially self-consistent mean-field approach M. V. Feigel'man et al. [25] and Kravtsov [79] showed that fractality can enhance the critical temperature. It does even lead to a power-law dependance of the critical temperature on the

interaction strength

$$T_c \propto \lambda^{1/\gamma}, \tag{5.11}$$

where γ is determined by the fractality of the eigenstates and λ is the dimensionless interaction strength. This result has been obtained for 3D system close to the Anderson transition. Employing the same formalism an enhancement of T_c has also been confirmed for weak multifractality [80]. Additionally there are numerical fully self-consistent calculations confirming an increase in the mean gap [18, 23].

Field-theoretically very strong mesoscopic fluctuations have been predicted in the density of states and local density of states[35].

There is also a number of works on the insulating phase. In the bosonic scenario with screened Coulomb repulsion a direct SIT is expected [81]. Key features are the persistence of a pseudogap across the transition [24, 25, 14], a giant magnetoresistance [82, 32] and unusual thermally activated transport [25, 83, 32]. These are all believed to be caused by incoherent Cooper pairs in the insulating phase.

Relation to other scenarios

Granular superconductors For granular materials a percolative nature of the SIT was considered [84, 85]. The finding of the emergent granularity in homogeneously disordered systems might suggest a relation between SITs in homogeneously disordered and granular system. This is still under dispute.

Fermionic scenarios The phenomenology of fermionic scenarios, as they were pioneered by Finkel'stein [86] in a non-linear-σ-model approach, is quite different from the bosonic scenario that we consider here. We want to mention two striking differences: (i) The gap is monotonically decreased by disorder in the fermionic scenario, while it can be increased in bosonic scenarios. (ii) The SIT is accompanied by a vanishing of the gap, whereas in the bosonic scenario global phase coherence is lost, while locally superconducting correlations stay intact.

If there is a relation between the two approaches it remains unknown. Even though we want to point to one recent formal connection between the two approaches: In the non-linear-σ-model treatment by Burmistrov, Gornyi, and Mirlin [78] both short-range and long-range interactions can be treated on the same footing. Thus in this field-theoretical model both approaches can be described.

Random Josephson junction arrays Another bosonic scenario pioneered by Efetov [87] revolves around discarding all other degrees of freedom but the phase of the order parameter. Originally it was applied to granular materials but later it was also considered for homgeneously disordered systems. This approach shares a lot of the phenomenology with our approach, as for instance the preformed Cooper pairs in the insulating phase. An assumed duality between vortices in the insulating and electrons in the superconducting phase, allows for far-reaching analytical predictions: We want to mention here the existence of a universal resistance at the SIT. This seems to be in disagreement with the experimental data on thin films that exhibit a range of critical resistances. This is perhaps not surprising. The charge-vortex duality is well justified in a system of Josephson junctions. Charge and phase are conjugated quantum mechanical variables in that case. In a continuous superconducting system on the other hand, there is no such argument.

Additionally there is no notion of Anderson localization and wave function fractality, when only the phase of the order parameter is taken into account. These ingredients seem integral to our approach. Consequently a relation remains unknown, although the discussion is still ongoing.

Self-consistency of related theories

Here we want to give an overview of the degree in which self-consistency is kept in the theories related to the scenario of the SIT that we are interested in.

BCS and Landau-Ginzburg BCS theory and Landau-Ginzburg theory with an underlying Anderson localized system have been widely used, when the effect of localization on superconductivity was first considered [70]. No self-consistency whatsoever is kept in the superconducting order parameter. In Section 5.7.1 we will compare the fluctuations of the LDoS in such an approach with our fully self-consistent results.

Energy-only self-consistency in the Hubbard model This approach was pioneered by Ghosal, Randeria, and Trivedi [11, 12] and considerably extended by M. V. Feigel'man et al. [25]. The Hartree potential is completely neglected and only the pairing between exact eigenstates of the underlying Anderson problem is considered. This simplification leads to a self-consistency requirement that is only renormalizing single-particle energies,

while the eigenstates are still those of the Anderson problem. The advantage is that this allows for analytical predictions. We will discuss further to what extent this approximation is justified in Sections 5.7.2-5.7.5.

Non-linear-σ-model In the non-linear-σ-model approach, self-consistency is established for the mean gap only after the disorder average. It is in that sense not fully self-consistent. As it is perturbative in disorder strength and thus only justified in the low disorder limit, the effect of the partial self-consistency approximation should not be very large. We plan to compare this theory to our fully self-consistent approach in the future. An interesting object for comparison would be the field-theoretical predictions made on the mesoscopic fluctuations of the LDoS.

BdG Treatment of the Hubbard model This approach pioneered by Ghosal, Randeria, and Trivedi [11, 12] is widely used in numerical treatments of the Hubbard model. Full self-consistency can be kept, though an analytical treatment remains to this day impossible.

Experimental status

There is a wide range of experiments that demonstrate the direct bosonic SITs that we are interested in. An important prerequisite for a transition corresponding to the theoretical mechanism discussed here is strong screening. A large number of experiments have been conducted with thin films including InO_x[88, 89, 90, 28, 91, 29, 92, 93, 94, 95, 93], TiN[27, 96, 97, 98, 99, 100], NbN[101, 102, 103], Be[104, 105] and Bi[106, 107, 108]. Especially in recent times novel materials have been investigated as well, many of which exhibit an even larger dielectric constant than the mentioned thin films [109, 110, 111, 112, 113, 114, 115, 116, 117, 118, 33]. We mention here also magnetic field tuned experiments, as they provide important insight on the nature of the insulating phase.

A very sharp transition[119, 100, 97] by an increase in sheet resistance has been reported. This points to a direct SIT. The critical resistance does not seem to be universal.

The superconducting phase bears strong inhomogeneities in the local density of states and consequently in the superconducting gap[27, 89, 103]. This effect increases with increasing disorder strength.

A strong decrease of superfluid stiffness by disorder has been measured [102, 108].

The insulating phase has been investigated extensively as well. There is evidence of preformed Cooper pairs before the coherent condensate is formed. Unusual activated transport[120, 100] and a giant magnetoresistance have been detected [121, 88, 99, 107, 97, 94], a pseudo-gap,[104, 122, 96, 28, 102, 94] and the surpression of the coherence peaks[122, 28, 94] have been reported. Recently also more direct evidence has become available. With Andreev spectoscropy it has been demonstrated that a separate pair binding energy exists in addition to the spectral gap in the insulating state beyond the SIT [29].

An increase in the superconducting transition temperature by disorder has been reported [33].

5.3 Mean-field SITs

Within BdG theory the self-consistent solution of the pairing amplitude will always have a homogeneous phase. This can be easily understood in terms of the Josephson effect. A phase difference in a superconducting sample gives rise to a supercurrent. This would lead to a continuous supercurrent, if the static mean-field would exhibit a phase difference. This can obviously not be the case in equilibirum, as long as time-reversal symmetry is preserved.

As fluctuations such phase differences and the resulting supercurrents are possible. In mean-field theory these fluctuations are neglected. For that reason a SIT, where global phase coherence is lost, is not seen within BdG theory. Important insights in the SIT can still be gained. One can expect the absolute value of the pairing amplitude to be close to what one would expect if phase fluctuations were taken into account. In addition many signatures of the transition like a depletion of the phase stiffness are seen to a degree also in mean-field theory. While it does never vanish completely it is decreased by orders of magnitude in the parameter regime where the transition would take place, if phase fluctuations were taken into account[12].

5.4 Disordered attractive Hubbard model

From here on we will study the BdG Hamiltonian (see Eq. (2.21))

$$\begin{aligned} \hat{H}_{\mathrm{BdG}} &= \hat{H}_0 + \hat{H}_{\mathrm{I}} \\ \hat{H}_0 &= -t \sum_{\langle i,j\rangle,\sigma} \hat{c}^\dagger_{i,\sigma}\hat{c}_{j,\sigma} + \mathrm{h.c.} + \sum_{i=1,\sigma}^{N_{\mathrm{bf}}} (V_i - \mu)\,\hat{n}_{i,\sigma} \\ \hat{H}_{\mathrm{I}} &= -\frac{U}{2}\sum_{i=1,\sigma}^{N_{\mathrm{bf}}} n(\mathbf{r}_i)\hat{n}_{i,\sigma} - \sum_{i=1}^{N_{\mathrm{bf}}} \Delta(\mathbf{r}_i)\hat{c}^\dagger_{i,\uparrow}\hat{c}^\dagger_{i,\downarrow} + \mathrm{h.c.}, \end{aligned} \tag{5.12}$$

with homogeneous random potential V_i drawn from a box distribution $V_i \in [-W, W]$ with disorder strength W. The self-consistent potentials are determined according to Eq. (2.31) and (2.32).

5.5 Results: Mesoscopic fluctuations

This section can already be found in an earlier publication with copyright by the American Physical Society[9]. As a first application of our technology, we investigate statistical properties of $\Delta(\mathbf{r})$ and of the local density of states (LDoS), $\rho(\mathbf{r}, E)$ (Eq. (2.35)), throughout the $U-W$-plane. To give a first impression we display in Fig. 5.1 (left) the gap function averaged over a suitable ensemble of disordered samples, $\overline{\Delta}(U, W)$; the overline indicates the ensemble average with N_E disorder configurations, typically $N_{\mathrm{E}} \approx 700 - 800$ samples. The data has been obtained on a square lattice and should be compared with an analogous plot produced on the honeycomb lattice by Potirniche et al. [18]. The gap increase has been interpreted in terms of analytical results from quantum-field theory[32], which also should apply to the square lattice. We do not reproduce the enhancement in Fig. 5.1. This is because the low-coupling regime, where an increase of the mean gap can be seen on a square lattice as well, is not reached due to finite size effects. The gap vanishes at $U \approx 1$, where the superconducting correlation length exceeds the system size. In Section 5.6 we will show results at larger system size and lower coupling, where the mean gap is increased by disorder.

Also displayed in Fig. 5.1 (right) is the density of states, $\rho(E) = \int_{L^2} d\mathbf{r}\rho(E, \mathbf{r})$, calculated for four samples in representative regions of the parameter plane.

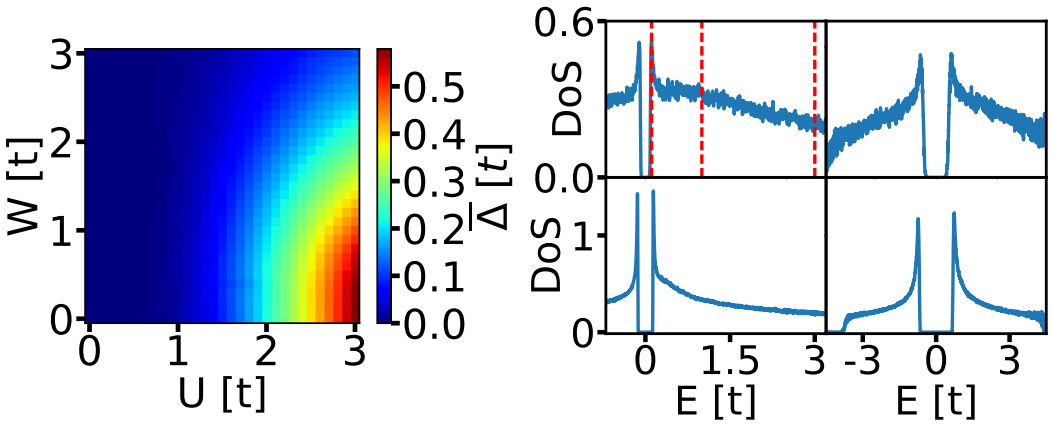

Figure 5.1: Left: Disorder averaged gap $\overline{\Delta(\mathbf{r})}$ in the $U-W$ parameter plane. Parameters: L=64; $N_{\mathrm{E}} = 500$, (converged $\alpha = 1\%$). Right: Density of states for typical samples shown at four characteristic parameter configurations. The red lines indicate the energies at which the LDoS is investigated in Fig. 5.2. Note that the energy is measured from the Fermi energy. Parameters: W=0.5 (bottom) , 1.5 (top) and U=1.5 (left) , 3.0 (right), L=192, $n = 0.875$, $T = 0$; $N_{\mathcal{C}} = 6144$, (converged $\alpha = 3\%$). These figures can already be found in an earlier publication with copyright by the American Physical Society[9].

At weak disorder the spectral gap and the coherence peaks are readily identified. Notice that only in the limit of weak disorder the spectral gap and $\overline{\Delta}$ scale with each other. [12]

To characterize the statistical properties of physical observables we focus in the following on autocorrelation and distribution functions. The numerical findings will be compared with predictions from analytical theories. This is especially relevant in regimes that go beyond the applicability of the analytical predictions.

5.5.1 Distribution functions of LDoS and local gaps

Parts of this subsection can already be found in an earlier publication with copyright by the American Physical Society[9].

LDoS. We begin the statistical analysis with the spatial fluctuations of the LDoS, $\rho(E, \mathbf{r})$. Fig.5.2 (left) displays an example showing how the

LDoS is spatially distributed over a typical sample with moderate disorder and interaction, $W \gtrsim U \gtrsim 1$. The logarithmically broad distribution of the LDoS is readily identified. The corresponding distribution function, $\mathcal{P}_{\rm ld}$, is displayed in Fig. 5.2 (right).

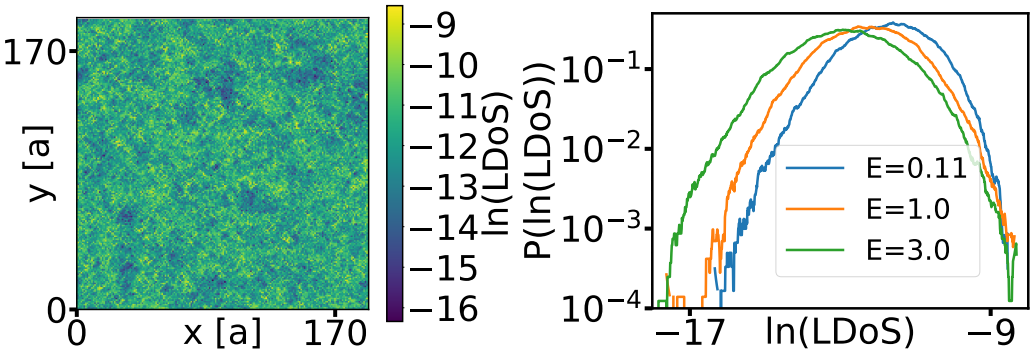

Figure 5.2: Distribution of the local density of states (LDoS), $\rho(E, \mathbf{r})$. Left: spatial distribution for a typical sample at peak energy of DoS (E=0.11, c.f. Fig. 5.1) Right: Corresponding distribution function of LDoS, $\mathcal{P}_{\rm ld}$, at energies E=0.11, 1.0, 3.0 illustrating the flow of the distribution with E. In Fig. 5.1 the corresponding DoS can be found. (Parameters: W=1.5, U=1.5, $n = 0.875$, $T = 0$; energy resolution 0.013; $N_{\mathcal{C}} = 6144$, (converged $\alpha = 3\%$)). These figures can already be found in an earlier publication with copyright by the American Physical Society[9].

With increasing energy the distribution shifts to smaller values, which is merely reflecting the decrease of the DoS $\rho(E)$, also seen in Fig. 5.1 (right). In contrast, the width of $\rho(E, \mathbf{r})$ is seen to grow. We assign this growths to the fact that the LDoS constitutes an average taken over a fixed-size energy window η. The number of eigenfunctions in the averaging window is estimated as $\rho(E)\eta L^2$ and therefore changes in energy if the DoS does. It is larger for energies near the coherence peak as compared to the bulk and for that reason the width of $\mathcal{P}_{\rm ld}$ should be expected to be reduced.

Local order parameter. The logarithmically broad distribution of the LDoS is concomitant with a similarly broad distribution of the local gap function $\mathcal{P}_{\rm lg}$, Fig. 5.3. The evolution of the latter function with interaction strength is very interesting. As long as disorder, W, and interaction, U, are weak the distribution of the local order parameter is close to Gaussian and

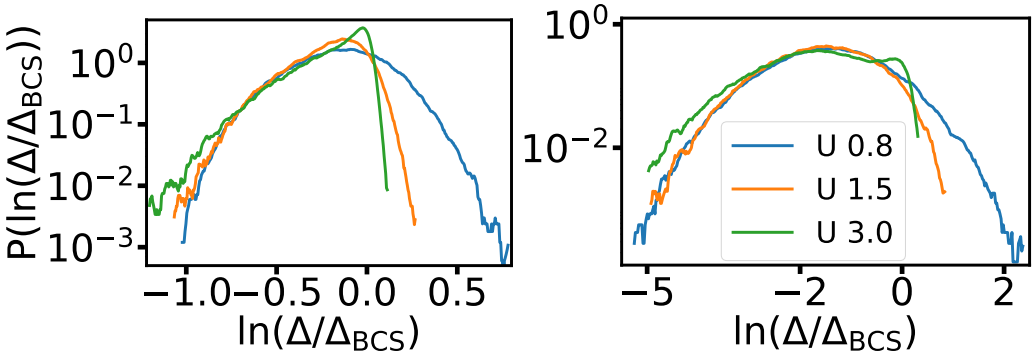

Figure 5.3: Distribution of the local gap function, $\mathcal{P}_{\rm lg}$, with interaction strength U for a typical sample with L=192 at weak disorder, W=0.5 (left plot), and stronger disorder, W=2.0 (right plot). As reference energy the pairing amplitude of the clean system, $\Delta_{\rm BCS}(U)$ has been chosen. (Parameters: U=0.8, 1.5, 3.0; $n = 0.875$, $T = 0$; $N_{\mathcal{C}} = 8192, 3072, 1024$, (converged $\alpha = 0.1\%$)). These figures can already be found in an earlier publication with copyright by the American Physical Society[9].

in this sense roughly following the statistics of the LDoS, see Fig. 5.3 (left). The typical value is seen to be very close to the pairing amplitude of the clean system, $\Delta_{\rm BCS}(U)$. However, with growing U the distribution becomes more skewed towards low values of Δ.

For increasing disorder and weak U more and more sites develop a pairing well below the clean limit, $\Delta(\mathbf{r}) \ll \Delta_{\rm BCS}$, consistent with observations made in Ref. [12]. Eventually, the shoulder is seen to dominate. In Fig. 5.3 (right) for strong disorder the distribution $\mathcal{P}_{\rm lg}$ becomes bimodal at stron interaction strenghts. It features a peak near $\Delta_{\rm BCS}$ and a logarithmically distributed background.

Discussion

The LDoS distribution in Fig. 5.2 (left) takes a log-normal form, already familiar for non-interacting disordered films with size smaller than a localization length, see e.g. Eq. (4.101) in Ref. Mirlin [123]. Analytical treatments of the LDoS distribution with superconducting interactions that are limited to the low disorder limit exist at temperatures above the critical temperature $T_{\rm c}$.[35] There a pronounced non-Gaussian character of the distribution was reported. Our observations at zero temperature are broadly consistent with

these results.

The order parameter distribution in Fig. 5.3 takes a log-normal form in the low-coupling ($U = 0.8$) case as well. In a partial self-consistency approach that is limited to low-disorder and low-coupling an analytical form could be derived for the distribution[80]. Both the position of the maximum and the width of the distribution are determined by the dimensionless conductance in this approach. Our numerical results show that the log-normal form carries over all the way in the strongly disordered limit.

The skewed form of the distribution for larger interaction strength in Fig. 5.3 has been observed in numerical calculations before in the very large interaction (U=5) limit[16]. The origin of such a distribution is not understood. We hypothesize that it might be related to the BCS-BEC crossover. Such a crossover takes place in the strongly interacting limit. There the picture of a superconducting condensate breaks down, as the correlation length approaches the lattice spacing. It becomes more instructive to think of Cooper pairs as separate hard-core bosons that comprise a Bose-Einstein condensate(BEC). For a review we refer to Chen et al. [124].

We mention here also that the superconducting gap and the LDoS are related. The low-lying excitations of the BdG system live in regions of high superconducting gap and the values of the gap in these regions determine the peak position of a BCS like LDoS[12]. At sites, where the superconducting gap has no appreciable weight on the other hand the LDoS does not follow a simple BCS like form and there is no obvious relation between superconducting gap and LDoS.

5.5.2 LDoS and DoS fluctuations

In this section we will analyze the mesoscopic fluctuations of the LDoS. A publication of our results is in preparation [125].

In Fig. 5.4 we present the LDoS of a representative sample along a line cut in real space around the Fermi energy for different values of disorder strength. The disorder strength increases from left to right. To contrast the results of one sample with disorder averaged quantities in Fig. 5.5 the disorder averaged DoS and standard deviation are shown. From top to bottom the disorder strength increases and from left to right the temperature is increased. If the DoS shows a clear coherence peak we mark it with a dashed black line, otherwise the line marks the delimination of the spectral gap.

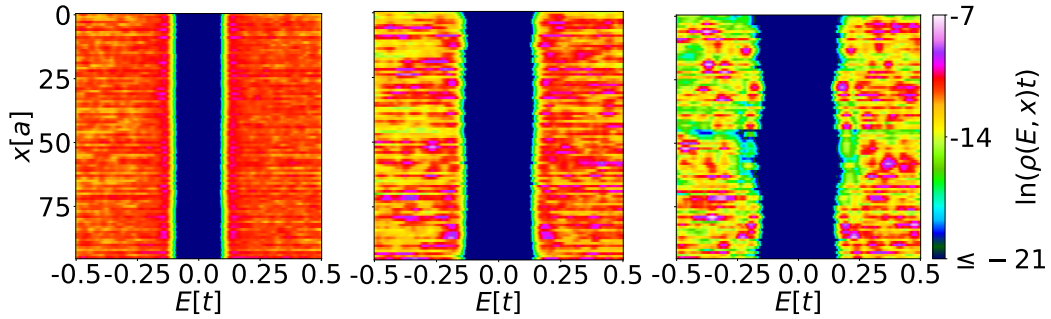

Figure 5.4: The LDoS along a line cut in real space around the Fermi energy of a representative sample as calculated from Eq. (2.35) on a logarithmic scale for different disorder values. From left to right: $W = 0.5, 1.25, 2.0$; $U = 2.2$, $n = 0.3$, $T = 0.0$; $L = 96$, (converged $\alpha = 0.01\%$)

The low disorder case in Fig. 5.4 (left) shows a spatially rather homogeneous spectral gap close to the clean BCS gap. Correspondingly the disorder averaged DoS in Fig 5.5 (top left, orange trace) exhibits a clear coherence peak and low standard deviation with respect to the value of DoS. For intermediate disorder stengths in Fig. 5.4 (center) the spectral gap is increased with respect to the BCS value and both the coherence peak positons heights can vary considerably. This translates in Fig. 5.5 to a disorder averaged DoS (center left, orange trace) with a strongly broadened coherence peak that is moved further away from the Fermi energy with respect to the BCS gap and a standard deviation of the LDoS (center left, blue trace) that is comparable to the DoS.

At high disorder strength in Fig. 5.4 (right) the line cut of the LDoS for a single sample is dominated by fluctuations. At some sites no clear coherence peak can be seen anymore and both position and height of the delimination of the gap fluctuates strongly. The spectral gap is on average enhanced even more strongly than in the intermediately disordered case. In correspondence in Fig. 5.5 the coherence peak of the disorder averaged DoS (bottom left, orange trace) has almost completely vanished, while the peak position has moved even further away from the Fermi energy. The standard deviation of LDoS (Fig. 5.5, bottom left, blue trace) exceeds the DoS by more than 50%.

An increase in temperature (from left to right) in Fig. 5.5 generically leads to an increase in standard deviation of the LDoS. This is in accordance with field theoretical results, where the critical temperature was approached

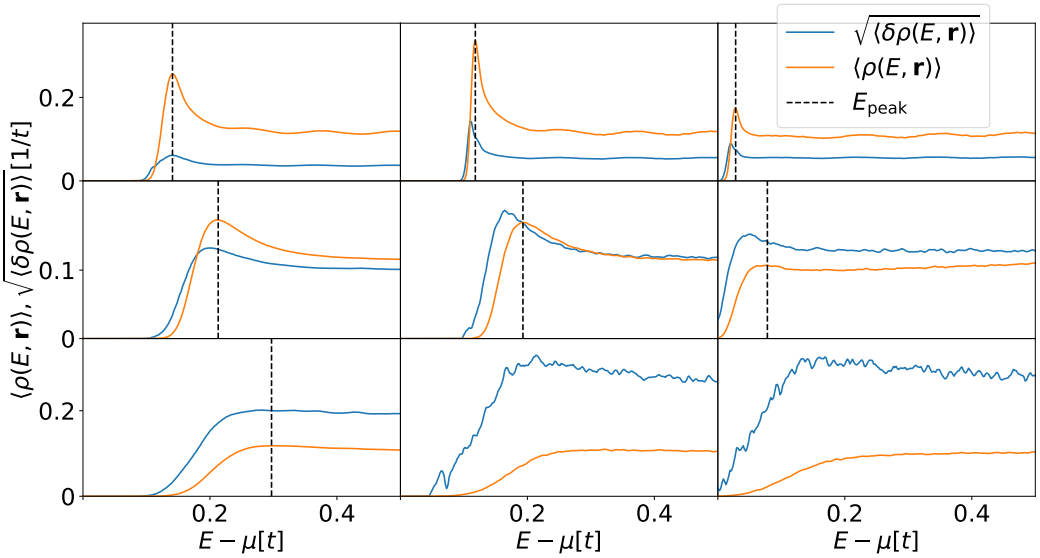

Figure 5.5: Disorder averaged DoS and standard deviation of the LDoS $\sqrt{\delta\rho(E,\mathbf{r})}$ for different values of disorder strength (W) and temperature (T) in units of the BCS critical temperature T_c^{BCS}. The dashed lines mark the coherence peak position, if applicable. From top to bottom (left to right): W=0.5($T = 0.0, 0.74T_c^{\text{BCS}}, 1.11T_c^{\text{BCS}}$), 1.25($T = 0.0, 0.89T_c^{\text{BCS}}, 1.78T_c^{\text{BCS}}$), 2.0($T = 0.0, 1.33T_c^{\text{BCS}}, 1.78T_c^{\text{BCS}}$);$U = 2.2$, $n = 0.3$; $T = 0$:$N_{\mathcal{C}} = 2048$, $T \neq 0 : N_{\mathcal{C}} = 8192$, (converged $\alpha = 0.01\%$)

from above and a substantial increase in the higher moments of the LDoS has been reported[35].

Discussion

The LDoS fluctuations in disordered superconductors are not well understood. Only field-theoretical calculations that are valid for weak disorder[35] exist. The tendency to increase the fluctuations, when the critical temperature is approached, are reproduced in our numerical findings in all disorder regimes.

The increase of the standard deviation of the LDoS with increasing temperature can be understood by the respective development of the spatial distribution of the pairing amplitude. The pairing amplitude develops a very inhomogeneous distribution with increasing temperature. The local density

of states at sites of low pairing amplitude is close to zero around the Fermi energy. At sites of high pairing amplitude on the other hand the LDoS exhibits a BCS-like form with peak position close to the pairing value at that site. The evolution of the spatial distribution of the pairing amplitude with temperature for a typical sample will be discussed in section5.6.

An analytical formalism that describes the LDoS fluctuations very well at weak disorder will be discussed in section 5.7.1.

5.5.3 Autocorrelations of gap function and coherence length

Parts of this subsection can already be found in an earlier publication with copyright by the American Physical Society[9]. We consider the disorder averaged spatial autocorrelator $\Phi_{\mathrm{lg}}(\mathbf{q}) = \overline{|\Delta(\mathbf{q})|^2}$ of the pairing function $\Delta(\mathbf{r})$ in Fourier space. At weaker disorder the correlation function displays a peak

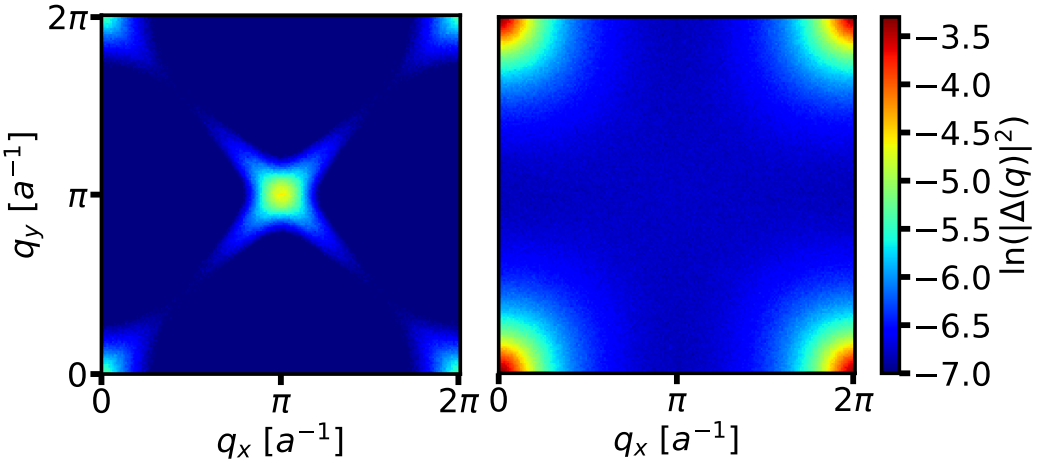

Figure 5.6: The gap autocorrelation function $\Phi_{\mathrm{lg}}(q)=\overline{|\Delta(q)|^2}$ in logarithmic representation for L=192 and U=1.5 at two values of disorder, W=0.5 (left) and W=2.5 (right); $n = 0.875$, $T = 0$, $N_{\mathrm{E}} \approx 900 - 1000$, $N_{\mathcal{C}} = 1024$, (converged $\alpha = 0.1\%$). These figures can already be found in an earlier publication with copyright by the American Physical Society[9].

at $(\pi/a, \pi/a)$, Fig. 5.6. It originates from us choosing the filling fraction 0.875 which is close to the commensurate value unity and thus should be seen as a signature of the square lattice; it disappears at stronger disorder,

e.g., at W=2.5. The same signature manifests in Fig. 5.7 where we show $\Phi_{\rm lg}(\mathbf{q})$ along two directions in $\mathbf{q}$-space, $(\pi/a, 0)$ and $(\pi/a, \pi/a)$: As already obvious from Fig. 5.6, at wavenumbers of order of the inverse lattice spacing, a^{-1}, and low W the correlator exhibits pronounced deviations from isotropy reflected by the collapse of open and closed symbols.

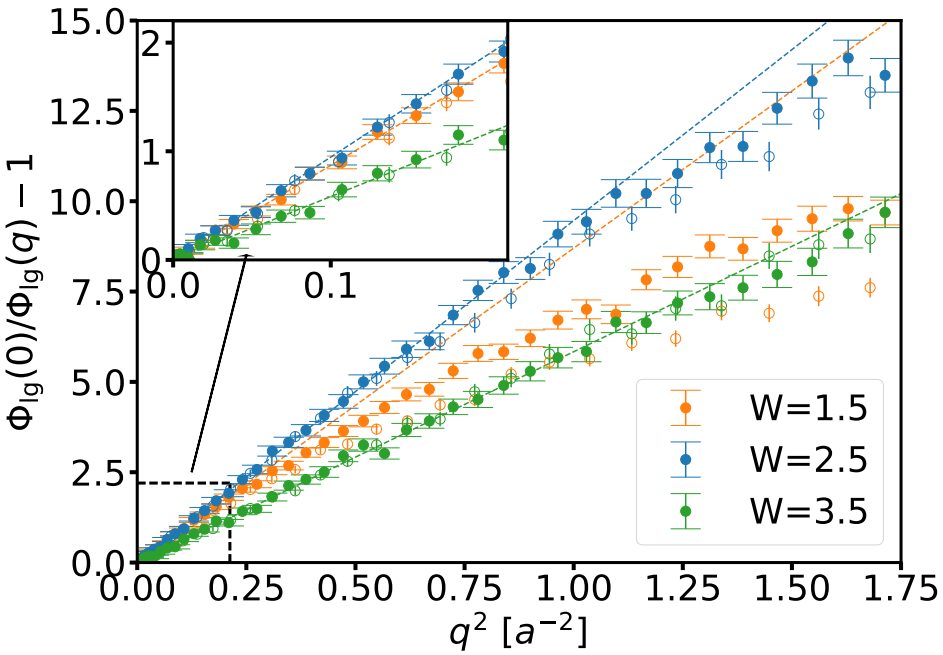

Figure 5.7: The non-trivial part of the inverted normalized gap autocorrelation function $\Phi_{\rm lg}^{-1}(\mathbf{q})=\overline{|\Delta(\mathbf{q})|^2}^{-1}$ evolving with W at fixed U. $\Phi_{\rm lg}$ is shown averaged over equivalent directions $(\pi/a, 0)$, $(0, \pi/a)$ (full symbols) and $(\pi/a, \pi/a)$, $(\pi/a, -\pi/a)$ (open). The inset shows a blowup of the small wave number regime where open and closed symbols collapse, so all traces are isotropic. (Parameters: U=1.5, W=1.5(orange), 2.5(blue), 3.5(green) L=192; $n = 0.875$, $T = 0$; $N_{\mathcal{C}} = 1024$, $N_{\rm E} \approx 600 - 1000$, (converged $\alpha = 0.5\%$)). This figure can already be found in an earlier publication with copyright by the American Physical Society[9].

Notwithstanding anisotropy at $q{\approx}a^{-1}$, in the limit of small wavenumbers

$q \ll a^{-1}$ the correlator $\Phi_{\rm lg}(q)$ is isotropic and with good accuracy we have

$$\frac{\Phi_{\rm lg}(0)}{\Phi_{\rm lg}(q)} = 1 + (q\xi)^2 + \dots \tag{5.13}$$

where $\Phi_{\rm lg}(0) := \Phi_{\rm lg}(q \to 0)$, given for different W in Fig. 5.8. $\Phi_{\rm lg}(\mathbf{q})^{-1}$ behaves nearly quadratically over the whole momentum range where $\Phi_{\rm lg}(\mathbf{q})$ exhibits isotropic behavior. Both the increase of $\Phi_{\rm lg}(0)$ (as approximated by $\Phi_{\rm lg}(\pi/L, 0)$) with disorder and the characteristic length ξ have been displayed in Fig. 5.8. To attain ξ we have used a linear fit of $\Phi_{\rm lg}(0)/\Phi_{\rm lg}(q^2)$ in the

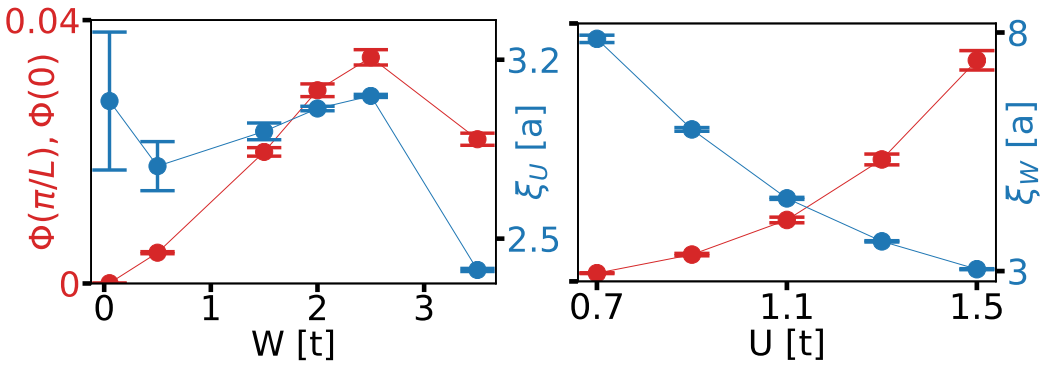

Figure 5.8: Variation of $\Phi_{\rm lg}(\pi/L, 0)$ and $\Phi_{\rm lg}(0)$ (red) and the correlation length, ξ (blue) with increasing disorder (left, U=1.5) and increasing interaction (right, $W = 2.5$). $\Phi_{\rm lg}(0)$ coincides with $\Phi_{\rm lg}(\pi/L)$ within the symbol size as portrayed here. The error bars depict the ensemble average error. The uncertainty due to cutoff α for ξ_W is discussed in the appendix. (Parameters (left): $n = 0.875$, $T = 0$, $N_{\mathcal{C}} = 1024$, $N_{\rm E} \approx 600-1000$, (converged $\alpha = 0.1\%$). Parameters (right):$n = 0.875$, $T = 0$, $N_{\mathcal{C}} = 16384$, $N_{\rm E} \approx 500$, (converged $\alpha = 3\%$).) These figures can already be found in an earlier publication with copyright by the American Physical Society[9].

isotropic regime. As with the range of this regime also the number of data points increases considerably with W, the uncertainty, i.e. the size of the error bars, of ξ is seen to decrease with rising W in Fig 5.8 (left). $\xi_U(W)$ exhibits a local non-monotonicity on its way from the clean to the dirty limit; the non-monotonic decay is readily seen also from the original data Fig. 5.7. This peculiar behavior should be interpreted in connection with the formation of superconducting islands. It occurs in the same parameter range and may relate to a percolation transition. It is also in this parameter

regime that the SIT has been found to take place in numerical simulations that take phase fluctuations in account[12].

Discussion

The correlations in the self-consistent fields of disordered mean-field theories so far remain only tractable in numerical simulations. Because of the complication that the self-consistency requirement brings analytical theories had to resort to partial self-consistency approaches in the past.

The non-monotonous shape of the correlation length in Fig. 5.8 has been reported in Ref. [19] albeit at unrealistically strong interactions U=5. Our results show that it carries over all the way into the physically more relevant regime of intermediate parameter values. As a hint on the origin of the non-monotonicity of the correlation length in Fig. 5.8 (left), we suggest that it might be a mean-field signature of a percolation transition. In granular materials a percolative nature of the SIT has long been suggested[84, 85]. The emergent granularity seen in the mean-field treatment of the Hubbard model[12] makes a relation to granular materials plausible.

The correlations on the length scale of the correlation length can be expected to play a particularily important role close to a phase transition. As a phase transition is approached this correlation length diverges and we expect long-range power-law correlations to emerge. In a linear system with correlated random on-site potential, it has been shown that novel criticality can be brought about by long-range correlations[8]. We expect an analogous effect at a phase transition within BdG theory.

5.6 Results: Enhancement of superconductivity

In this section we will consider the dependance of the pairing amplitude on temperature in a disordered superconductor.

In Fig. 5.9 the evolution of the mean gap with temperature is shown for various values of disorder. An increase of the gap at $T = 0$ can be seen for weak and intermediate disorder strength, with a pronounced maximum at intermediate disorder. The mean-field critical temperature on the other hand seems to be monotonically enhanced by disorder.

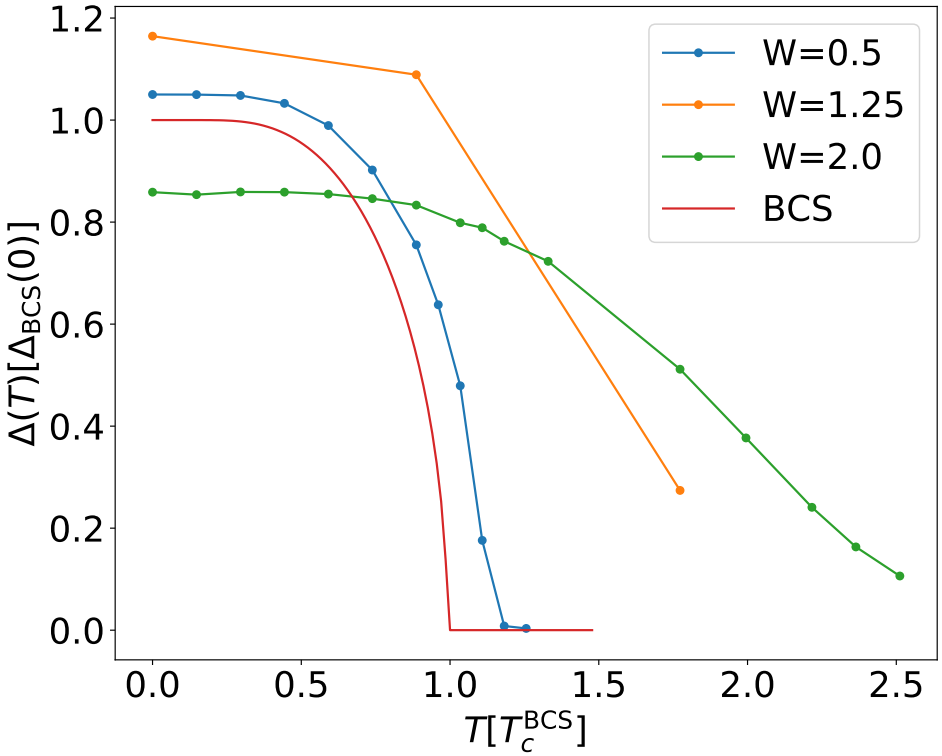

Figure 5.9: Temperature dependance of the disorder-averaged mean superconducting gap for various values of disorder. The BCS result has been obtained from the anayltical equation Eq. (2.44). (Parameters: $n = 0.3$, $U = 2.2$, $N_{\mathcal{C}} = 2048 - 8192$, $N_{\mathrm{E}} \approx 500$, (converged $\alpha = 0.01\%$))

In BCS theory there is a linear dependance between critical temperature the superconducting gap at zero temperature. This seems to be a reasonably estimate for the critical temperature in the low disorder case ($W = 0.5$), too. At larger disorder strength, the increase in critical temperature far exceeds the increase in the gap at zero temperature. T_{c} is even enhanced, when the gap at zero temperature is reduced by disorder, as can be seen from the green trace.

In Fig. 5.10 the evolution of the spatial distribution of the pairing amplitude with temperature is shown. In the low disorder case (top row) the pairing amplitude stays rather homogeneously distributed with increasing temperature. Only at high temperatures above the clean critical temperature a moderate inhomogeneity on a scale larger than the lattice spacing is

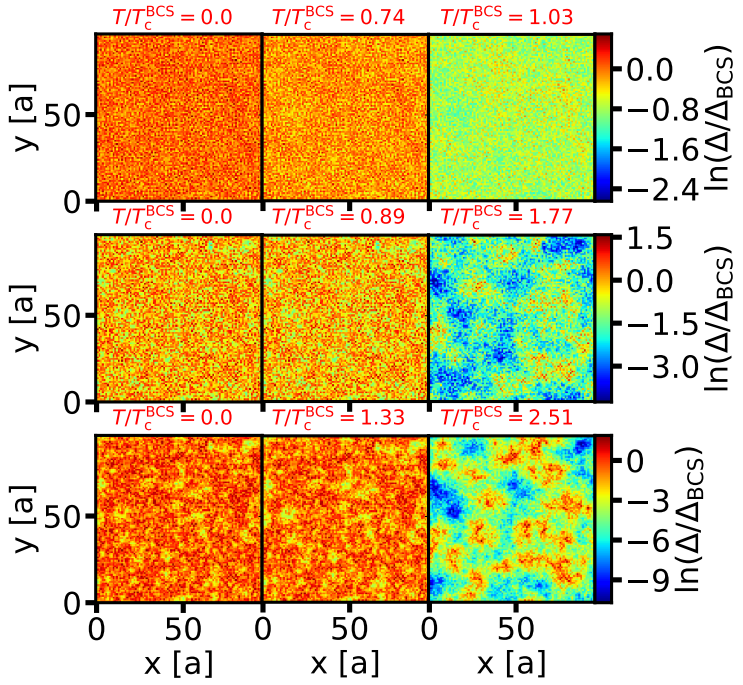

Figure 5.10: Temperature dependance of the spatial distribution of the gap of a representative sample for various values of disorder. Δ_{BCS} is the zero temperature gap and $T_{\mathrm{c}}^{\mathrm{BCS}}$ clean critical temperature as calculated from Eq. 2.44. (Parameters: $W = 0.5$(top),1.25(center),2.0(bottom); $n = 0.3$, $U = 2.2$, $N_{\mathcal{C}} = 2048 - 8192$, (converged $\alpha = 0.01\%$))

developed. Still the lowest values of the gap are on the order 10% of the zero temperature clean gap.

In the intermediate disorder (center row) case for temperature $T < T_{\mathrm{c}}^{\mathrm{BCS}}$, the gap is not affected very much by disorder as well close to the BCS critical temperature. For high temperatures superconducting islands develop and phase fluctuations would very likely destroy global phase coherence. Note that the maxima of the gap on the superconducting islands are still comparable to the values at zero temperature, even though the clean critical temperature is far exceeded.

In the highly disordered case the inhomogeneity does not increase substantially with increasing temperatures even across the clean critical temperature. It should be noted here that at zero temperature the phase stiffness

is already highly reduced by disorder, so even small changes might lead to a SIT here. For high temperatures superconducting islands persist but phase coherence would certainly be destroyed in this case with well seperated islands.

Discussion

The enhancement of the mean gap is brought about by multifractality, as has been demonstrated in partial self-consistency[25, 80] and field-theoretical approaches[30]. In our case we see weak multifractality, as it appears in 2D systems on the scale of the localization length[63].

An increase in the pairing amplitude through disorder has been seen before in the Hubbard model on a honeycomb lattice [18] and also on a square lattice [23]. On the square lattice it has so far only been found to be a small effect at very low disorder strength. Here we present a parameter regime, where the gap is strongly enhanced and complement our findings with a qualitative investigation of the actual increase of the mean-field critical temperature.

If the enhancement of the gap corresponds to an enhancement of the critical temperature is still under discussion. Some authors argue that through the impact of phase fluctuations the critical temperature is always montonically decreased by disorder[126], while others[25, 30, 80] argue that there is a parameter regime, where an increase of the critical temperature by disorder exists. The latter seems to be supported by recent experiments[33].

Our results on the development of the spatial distribution of the gap also seem to point to the possibility of an enhancement of the critical temperature. Generally the phase stiffness is decreased by inhomogeneity in the order parameter. In the low disorder case (Fig. 5.10, top right) the mean gap is still close to 50% of the zero temperature gap, when the clean critical temperature is already exceeded. Even the smallest values are still at $\sim 10\%$ of the zero temperature gap. It seems plausible that the phase stiffness is not reduced sufficiently by such a moderate inhomogeneity to lead to a loss of phase coherence. This is also consistent with field theoretical treatments of the disordered BKT transition. In the low disorder limit the critical temperature has been found to be very close to the BCS critical temperature[36]

$$T_{\mathrm{BKT}} = T_{\mathrm{BCS}}(1 - 4Gi), \tag{5.14}$$

with Ginzburg-Levanyuk number $Gi \ll 1$. The field-theoretical results are

for the case of a gap that is not enhanced at zero temperture. For a strong enhancement of the gap, as the one we see, we expect the enhanced mean-field critical temperature, which is at least $\sim 10\%$ enhanced with respect to the BCS critical temperature, to be close to T_{BKT} as well. In an upcoming paper we will complement the results shown here with a quantitative analysis of the phase stiffness[127].

5.7 Results: Impact of self-consistency

We return to a central theme of our interest, which is the impact of self-consistency on the calculation of physical observables.

5.7.1 LDoS fluctuations without self-consistency

We will first introduce an unpublished analytic formalism by Igor Burmistrov[125] for the variance of the LDoS, to compare it with our numerical results. It is based on introducing the non-interacting disordered eigenstates of the Anderson problem into a standard BCS formalism. In that sense it is non-self-consistent. The variance of the within this approach LDoS reads

$$\frac{\langle[\delta\rho(E,\boldsymbol{r})]^2\rangle}{\langle\rho(E,\boldsymbol{r})\rangle^2} = \frac{4}{\pi g}\left[\ln\frac{L}{l} + \frac{1}{8\epsilon^2}\ln\min\left\{1, \frac{\gamma^2}{\epsilon^2-1}\right\}\right], \tag{5.15}$$

with dimensionless conductance g, linear system size L, mean-free path l, $\epsilon = E/\Delta$ and $\gamma = g\delta/(4\pi\Delta)$, with mean level-spacing δ and superconducting gap Δ.

Comparison with full self-consistency

To compute the dimensionless conductance g and the mean-free path l, we compare the normalized variance of the LDoS for two different system sizes (see Fig. 5.11) for a given disorder strength at large energies. We choose large energies as then only the first term in Eq. (5.15) is relevant. In the derivation of the analytical formalism $T = 0$ is assumed. For $T \neq 0$ we choose the dimensionless conductance g such that the analytical description agrees with the numerical data at large energies, while keeping the mean-free path l as calculated for $T = 0$. We arrive at the following values:

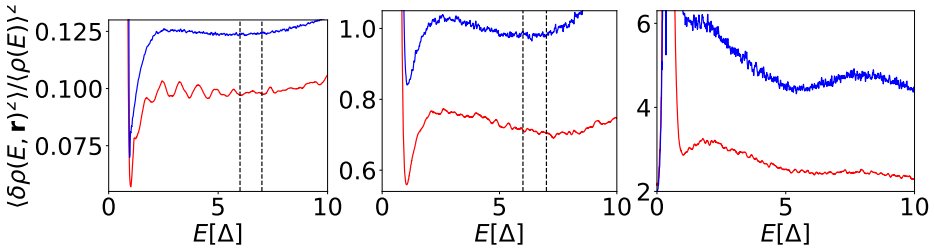

Figure 5.11: Disorder averaged variance of the LDoS normalized with the squared DoS for two different system sizes. The values encased by the dashed lines are averaged over and then used to compute g and l from (Eq. 5.15). Parameters: $L = 192$(blue), 96(red); $W = 0.5$(left),1.25(middle),2.0(right);$U = 2.2$, $n = 0.3, T = 0.0.$, $N_{\mathrm{E}} = 100$, (converged $\alpha = 0.001\%$)

	$T = 0.0$	$T = 0.74T_{\mathrm{c}}^{\mathrm{BCS}}$	$T = 0.89T_{\mathrm{c}}^{\mathrm{BCS}}$	$T = 1.11T_{\mathrm{c}}^{\mathrm{BCS}}$
$W = 0.5$	g=8.5,l=6.9	g=3.8,l=6.9		g=3.0,l=6.9
$W = 1.25$	g=0.8,l=15.6		g=0.6,l=15.6	

Note that the procedure yields a higher mean-free path l for intermediate disorder $W = 1.25$ than for $W = 0.5$. The physical mean-free path is monotonically decreased by disorder evidencing already that the procedure does not work in the intermediate disorder regime.

We now want to turn to a comparison of our fully self-consistent numerical results of the LDoS fluctuations with the analytical formalism without self-consistency (see Eq. (5.15)). In Fig. 5.12 the normalized variance of the LDoS as calculated numerically (red trace) is shown. The analytical prediction (see Eq. (5.15)) is added as a dashed black line. When there is no qualitative resemblence with the analytical prediction in the strong disorder case, the analytical prediction is omitted. In the low disorder case the analytical prediction fits very well to the numerical data. We want to stress here that the parameters have been determined in a way that the analytical formalism agrees with the data for large energies. The formalism still fits quantitatively for low energies. While we only derived a formalism for zero temperature, the simple rescaling of the prefactor of Eq. (5.15) such that it fits the data in the high energy limit yields a close to perfect agreement also for low energies.

For intermediate disorder there is still a minimum at low temperatures at the position of the coherence peak. As it is diminished by increasing the

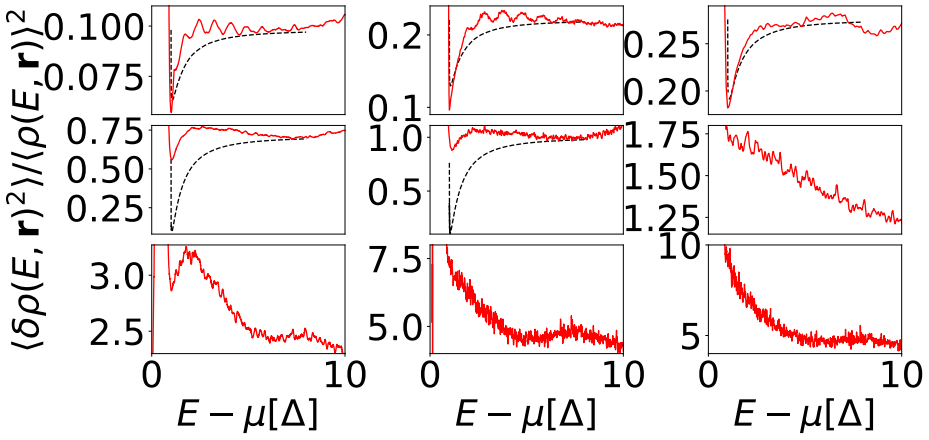

Figure 5.12: Variance of the disorder-averaged LDoS normalized with squared disorder-averaged DoS using the same parameters as plot 5.5. Dashed line is a plot of the analytical formula Eq. 5.15 using values in Table 5.7.1. From top to bottom (left to right): W=0.5($T = 0.0, 0.74T_c^{\mathrm{BCS}}, 1.11T_c^{\mathrm{BCS}}$), 1.25($T = 0.0, 0.89T_c^{\mathrm{BCS}}, 1.78T_c^{\mathrm{BCS}}$), 2.0($T = 0.0, 1.33T_c^{\mathrm{BCS}}, 1.78T_c^{\mathrm{BCS}}$);$U = 2.2$, $n = 0.3$; $T = 0$:$N_{\mathcal{C}} = 2048$, $T \neq 0 : N_{\mathcal{C}} = 8192$, (converged $\alpha = 0.01\%$)

temperature it vanishes. The same happens in the srongly disorderd case but already at a lower temperature, as the coherence peak is very washed out to begin with.

Discussion

We showed that in the low disorder case a simple approach based only on BCS theory and non-interacting disordered eigenstates without any self-consistency leads to a quantitative agreement with our data. In such an approach the variance of the LDoS is proportional to the DoS and a simple function that depends on the dimensionless conductance, the mean-free path, the BCS gap and the mean level spacing. This is no longer true already at intermediate disorder strengths. There self-consistency becomes important and an analytical description of the fluctuations of the LDoS remains unknown.

The low disorder case in Fig. 5.5 (top row) exhibits oscillations in the normalized variance of the LDoS. This is a finite size effect, as can be seen in Fig. 5.11 (left). For the blue trace ($L = 192$) the oscillations seen in the red trace ($L = 96$) vanish.

5.7.2 Partial (energy-only) self-consistency scheme

This subsection can already be found in an earlier publication with copyright by the American Physical Society[9]. The full BdG-problem is specified by the set of equations (2.25) - (2.32). It is highly complicated, e.g., because the scf-conditions (2.31) and (2.32) are non-linear. As is frequently done in such situations, the full scf-problem is replaced by a simplified variant exhibiting partial self-consistency.

Various possibilities for such simplifications are conceivable. The scheme we here describe is inspired by analytical calculations performed by Feigelman et al. [24, 25]. The overall procedure can be considered a generalization of BCS theory that allows for an inhomogeneous order parameter. To bring the self-consistency requirement into the familiar BCS form, additional approximations besides the mean-field decoupling are necessary.

We here derive equations for partial self-consistency starting from the mean-field Hamiltonian Eq. (2.21). We express the field operators employing as a basis the eigenstates $\psi_l(\mathbf{r}_i)$ of the non-interacting part of $\hat{H}_{\mathrm{BdG}}$, i.e. $\hat{H}_0$:

$$\hat{d}_{l,\sigma} = \sum_{i=1}^{N_{\mathrm{bf}}} \hat{c}_{i,\sigma}\psi_l^*(\mathbf{r}_i), \quad \hat{d}_{l,\sigma}^\dagger = \sum_{i=1}^{N_{\mathrm{bf}}} \hat{c}_{i,\sigma}^\dagger\psi_l(\mathbf{r}_i). \tag{5.16}$$

The corresponding eigenvalues of ψ_l are denoted ξ_l and will be measured with respect to the Fermi-energy E_{F}. Expressing $\hat{H}_{\mathrm{BdG}}$ in $\hat{d}, \hat{d}^\dagger$ we obtain

$$\begin{aligned}\hat{H}_{\mathrm{BdG}} = &\sum_{l=1,\sigma}^{N_{\mathrm{bf}}} \xi_l \hat{d}_{l,\sigma}^\dagger \hat{d}_{l,\sigma} + \sum_{l,m,n,o,\sigma} M_{lmno}\langle \hat{d}_{l,\sigma}^\dagger \hat{d}_{n,\sigma}\rangle \hat{d}_{m,\sigma}^\dagger \hat{d}_{o,\sigma} \\ &- U \sum_{l,m,n,o=1}^{N_{\mathrm{bf}}} M_{lmno}\langle \hat{d}_{n,\downarrow}\hat{d}_{o,\uparrow}\rangle \hat{d}_{l,\uparrow}^\dagger \hat{d}_{m,\downarrow}^\dagger + \mathrm{h.c.},\end{aligned} \tag{5.17}$$

where an abbreviation

$$M_{lmno} = \sum_i \psi_l^*(\mathbf{r}_i)\psi_m^*(\mathbf{r}_i)\psi_n(\mathbf{r}_i)\psi_o(\mathbf{r}_i), \tag{5.18}$$

has been introduced.

The main approximate step in partial self-consistency is to neglect all terms with more than two indices

$$M_{lmno} = \begin{cases} M_{ln}, & \text{if } l = m \text{ and } n = o \\ 0, & \text{otherwise} \end{cases}, \tag{5.19}$$

together with the Hartree term. The simplified mean-field Hamiltonian then reads

$$\hat{H}^{\mathrm{s}}_{\mathrm{BdG}} = \sum_{l=1,\sigma}^{N_{\mathrm{bf}}} \xi_l \hat{d}^{\dagger}_{l,\sigma} \hat{d}_{l,\sigma} + \sum_{l=1}^{N_{\mathrm{bf}}} \Delta_l \hat{d}^{\dagger}_{l,\uparrow} \hat{d}^{\dagger}_{l,\downarrow} + \mathrm{h.c.}, \tag{5.20}$$

with an s-wave pairing strength

$$\Delta_l = -U \sum_{m=1}^{N_{\mathrm{bf}}} M_{lm} \langle \hat{d}_{m,\uparrow} \hat{d}_{m,\downarrow} \rangle. \tag{5.21}$$

The Hamiltonian (5.20) is structurally equivalent to the BCS Hamiltonian in the sense that the kinetic term and Δ_l are diagonal in the same (real-space) basis; Cooper pairs form within a Kramer's doublet. The corresponding BCS gap-equation at temperature T reads

$$\Delta_l = \frac{U}{2} \sum_{m=1}^{N_{\mathrm{bf}}} M_{lm} \frac{\Delta_m}{\sqrt{\Delta_m^2 + \xi_m^2}} \tanh\left(\frac{\sqrt{\Delta_m^2 + \xi_m^2}}{2T} \right). \tag{5.22}$$

Converting back to real-space we have

$$\Delta(\mathbf{r}_i) = \frac{U}{2} \sum_{l=1}^{N_{\mathrm{bf}}} \frac{\Delta_l}{\sqrt{\Delta_l^2 + \xi_l^2}} \psi_l^2(\mathbf{r}_i). \tag{5.23}$$

The advantage of the partial ("energy-only") scf-scheme is that the pairing-amplitude can be calculated solely from the eigenstates and eigenvalues of the non-interacting reference Hamiltonian $\hat{H}_0$. This comes at the expense of ignoring changes in the wavefunctions related to pairing and the inhomogeneous Hartree shift.

5.7.3 Local-gap distribution

Parts of this subsection can already be found in an earlier publication with copyright by the American Physical Society[9]. We compare the results of full and energy-only self-consistency schemes for the local pairing amplitude $\Delta(\mathbf{r})$ for the Anderson Problem in 2D and 3D.

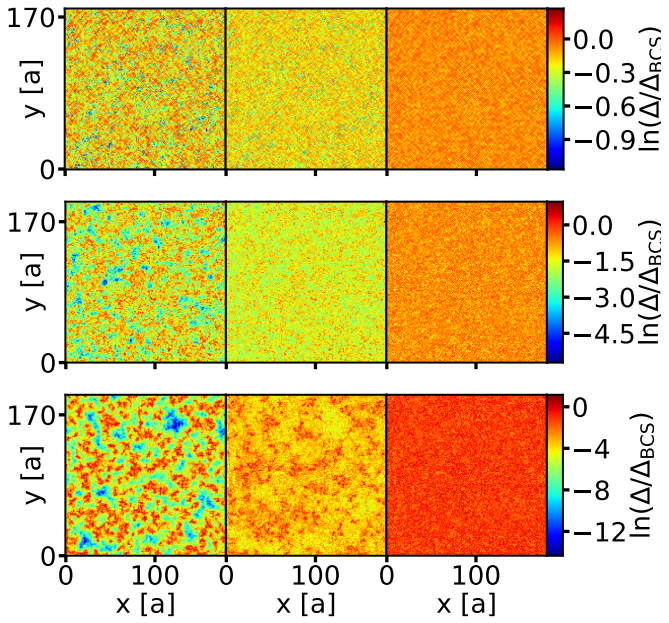

Figure 5.13: Evolution of islands with disorder increasing from top to bottom, W=0.5, 2.0, 3.5. Different self-consistency schemes are compared. Left column: full self-consistency. Center column: energy-only self-consistency with inhomogeneous Hartree shift. Calculation is done with the single-particle ("screened") potential as it results from the full scf-calculation, left. Right column: energy-only scheme. The energy-only data has been calculated employing full diagonalization (Parameters: U=1.5, n = .0875, $T = 0$; $N_{\mathcal{C}}$=1024, (converged α = 0.5%)). This figure can already be found in an earlier publication with copyright by the American Physical Society[9].

Thin films (2D)

Fig. 5.13 shows a spatial distribution of $\Delta(\mathbf{r})$ as obtained for typical sample at intermediate interaction and three disorder values. The calculation with full self-consistency, Fig. 5.13 (left) column exhibits a clear tendency towards the formation of superconducting islands. In contrast, with energy-only self-consistency, right column, a rather homogeneous speckle pattern is found missing any indications of island formation. Hence, already by inspecting individual samples we expect that distribution functions of physical observables will depend in a qualitative way on the applied scf-scheme in broad

parameter regions.

In order to highlight the effect of screening, we have displayed in Fig. 5.13 also the results of an intermediate scf-scheme. It operates in an energy-only mode, but adopts for the disorder the effective single particle potential ("screened" potential) as it is obtained as a result from the full scf-calculation. As is seen from Fig. 5.13, center column first indications of islands emerge, but the contrast is still largely underestimated. This result underlines the importance of full consistency in the scf-procedure.

Bulk systems (3D)

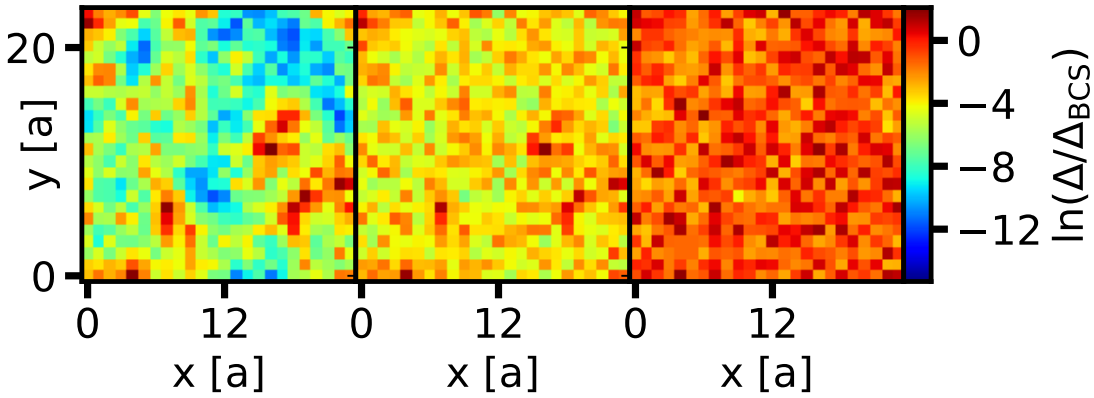

Figure 5.14: Corresponding plot to Fig. 5.13 in 3D. A representative 2D slice of a sample is shown. The data has been calculated employing full diagonalization (Parameters: $L = 24$ W=4.0, U=2.5, $n = 0.3$, $T = 0$; (converged $\alpha = 0.5\%$)). This figure can already be found in an earlier publication with copyright by the American Physical Society[9].

In analogy to the 2D case, we compare the results of full and energy-only self-consistency schemes for the local pairing amplitude $\Delta(\mathbf{r})$ in 3D. All 3D results have been computed with a conventional full diagonalization solver.

In the non-interacting 3D Anderson problem there is a phase transition at a critical disorder strength W_c, where all states become localized. For a disorder strength below W_c there exists an energy E_c, the mobility edge, which separates a fully localized band from a band of extended states. We note that as the Anderson Hamiltonian is symmetric around $E = 0$ this is also true for the mobility edge. We refer to B. Bulka [128] for the phase diagram.

Our interest is in the importance of self-consistency in the presence of attractive on-site interactions close to the mobility edge in the insulating band. For comparibility with authors that have considered an energy-only approach in this context before[25], we choose a Gaussian disorder distribution

$$p(V_i) = \frac{1}{\sqrt{2\pi}W}\exp\left[-\frac{V_i^2}{2W^2}\right] \tag{5.24}$$

of the random onsite energies V_i in Eq. 2.26.

Fig. 5.14 shows the spatial distribution of $\Delta(\mathbf{r})$ of a typical sample as obtained for moderate interaction and disorder strength and chemical potential in the localized band. The chosen filling factor n=0.3 corresponds to a chemical potential of $\mu \approx -6$ in the fully self-consistent case. The mobility edge without interactions is located at $E_c \approx -5.5$ for the disorder strength W=4 that is considered here[128]. As in the 2D case, the field obtained within the fully self-consistent calculation shows a pronounced formation of islands, Fig. 5.14 (left). The energy-only scheme in analogy to our 2D results exhibits a rather homogeneous spatial distribution, Fig. 5.14 (right). The results of the energy-only scheme with "screened" potential shown in Fig. 5.14 (center) again show first indications of island development with dramatically underestimated contrast. This highlights the importance of full self-consistency also in 3D.

Discussion

In both reduced self-consistency schemes the inhomogeneity is greatly underestimated with respect to the fully self-consistent result. To what extent the conclusions of earlier theoretical works that consider this scenario [24, 25] are affected remains to be seen. In these works the authors identified the neglection of the inhomogeneous Hartree shift as the biggest approximation in their partial self-consistency approach. We also observe that the inclusion of the inhomogeneous Hartree improves strongly upon the energy-only result without screening.

The energy-only mean-field pairing amplitude at the 3D Anderson transition (see Fig. 5.14) has been used as a reference point for a disordered Landau-Ginzburg theory [25]. As the phase stiffness is greatly diminished by spatial inhomogeneity, we expect that the impact of phase fluctuations would be underestimated in a theory based on the rather homogeneous mean-field

of our energy-only results. It is important to note that the authors considered the low-coupling limit, which we are not able to reach due to system size limitations in the 3D case.

5.7.4 Gap autocorrelator

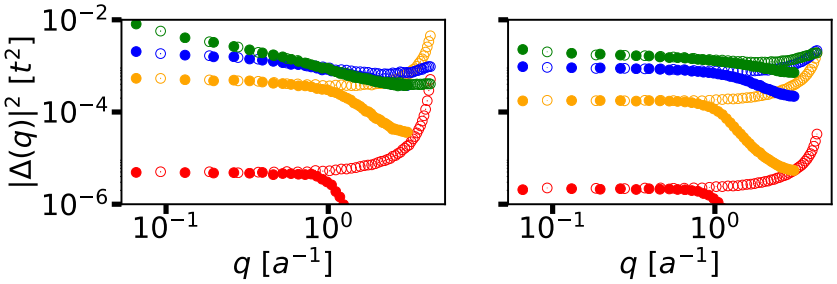

Figure 5.15: Gap autorcorrelation function $\Phi_{\rm lg}(\mathbf{q})=\overline{|\Delta(\mathbf{q})|^2}$ calculated employing two different energy-only self-consistency schemes. $\Phi_{\rm lg}$ is shown along directions $(\pi/a, 0)$ (full symbols) and $(\pi/a, \pi/a)$ (open); traces for four different disorder values are shown, W=0.05, 0.5, 1.5, 2.5, from bottom to top. Left: energy-only self-consistency with screened potential. Right: energy-only self-consistency. (Parameters: U=1.5, $T = 0$, $n = 0.875$, L=96; $N_{\rm E} = 1000$, (converged $\alpha = 0.1\%$)). This figure can already be found in an earlier publication with copyright by the American Physical Society[9].

Parts of this subsection can already be found in an earlier publication with copyright by the American Physical Society[9]. Fig. 5.15 shows data analogue to Fig. 5.7, now with energy-only self-consistencies. As is obvious already from individual sample, Fig. 5.13, the contrast parametrized by $\Phi_{\rm lg}(0)$ is much smaller as compared to the case of full self-consistency given in Fig. 5.6. As one would expect from Fig. 5.13, the contrast with screened potential, Fig. 5.13 (right) exceeds the bare scheme, Fig. 5.13 (left) considerably.

The most striking and perhaps unexpected feature, however, is a qualitative difference. In the full scf-calculation, $\Phi_{\rm lg}(q)$ follows Eq. (5.13) and exhibits a well defined parabolic shape in the vicinity of small wavenumbers. This feature is not reproduced within energy-only schemes. The bare scheme does not exhibit an appreciable curvature up to $q \approx a^{-1}$, so the coherence

length with energy-only self-consistency, ξ_{eo}, vanishes. In contrast, within the screened scheme $\Phi_{\mathrm{lg}}(q)$ does not show clear saturation at small wavenumbers within the range of q-values accessible.

Discussion

We interpret these results as a strong indication that wavefunction renormalization as it occurs within the full scf-scheme is crucial for understanding those aspects of qualitative physics that hinge on long-range spatial correlations. In particular close to a phase transition, where the correlation length diverges, we expect partial energy-only schemes to be insufficient in describing the relevant physics.

5.7.5 Gap enhancement by disorder

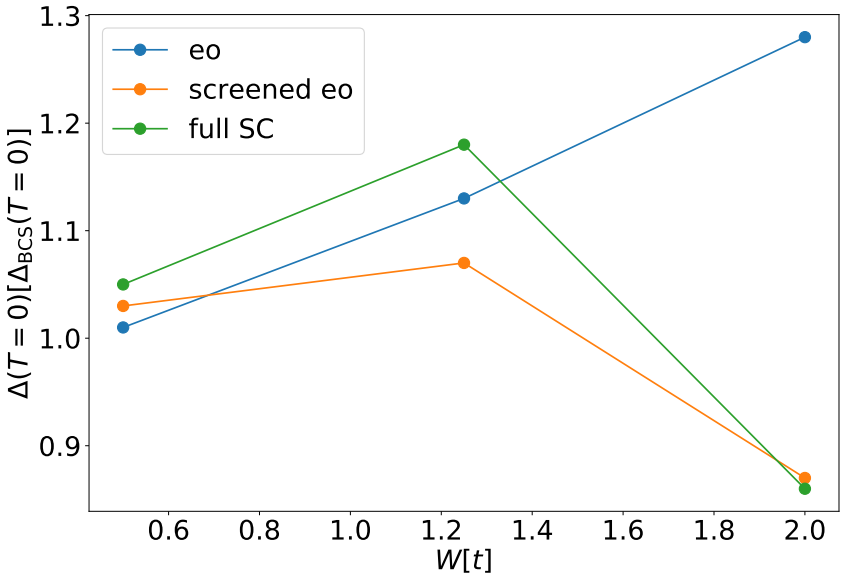

Figure 5.16: Comparison of the disorder-averaged zero temperature mean gap for different levels of self-consistency (eo: energy-only, screened eo: energy-only with Hartree potential, full SC: full self-consistency). The BCS gap has been obtained from Eq. 2.44. The data for the partial self-consistency schemes was obtained by full diagonalization. (Parameters: $n = 0.3$, $U = 2.2$, $N_{\mathcal{C}} = 2048$, $N_{\mathrm{E}} = 20$ (converged $\alpha = 0.01\%$))

We now want to turn to the effect of self-consistency on the gap enhancement brought about by disorder. In Fig. 5.16 the evolution of the zero temperature mean gap with disorder strength is shown for the different self-consistency schemes. At intermediate disorder strengths the gap enhancement is maximal for both the full and energy-only self-consistency with screening schemes. The energy-only scheme without screening exhibits a montonous increase of the mean gap on the other hand.

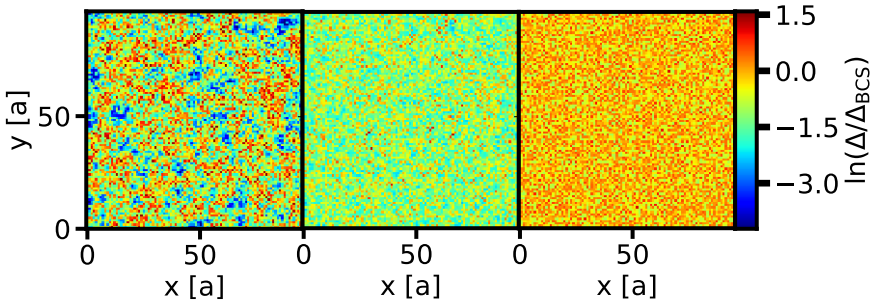

Figure 5.17: The spatial distribution of the gap with different levels of self-consistency (left: full self-consistency, center: energy-only with inhomogeneous Hartree potential, right: energy-only). The data for the partial self-consistency schemes was obtained by full diagonalization. (Parameters: $n = 0.3$, $U = 2.2$, $W = 2.0$, $T = 1.33T_c^{\mathrm{BCS}}$, $N_{\mathcal{C}} = 2048 - 8192$, (converged $\alpha = 0.01\%$))

In Fig. 5.17 the spatial distribution of the gap for the different self-consistency schemes at temperatures above the clean transition temperature is shown. The temperature is chosen such that it is close the energy-only critical temperature. For full self-consistency (left) the spatial inhomogeneity on a scale larger than the lattice constant is visible. To a degree such an inhomogeneity develops also in the screened energy-only self-consistency scheme (center) but it is far less pronounced. The spatial distribution for the energy-only self-consistency scheme (right) only displays a unstructered speckle pattern.

Discussion

The montonous enhancement of the gap in the energy-only self-consistency scheme is in disagreement with the evolution of the fully self-consistent gap

that exhibits a local maximum at intermediate disorder strength. We expect that this leads to an overestimation of the mean-field critical temperature at large disorder strengths. Furthermore, as no significant spatial inhomogeneity is developed in the partial energy-only scheme, the impact of phase fluctuations is strongly underestimated.

The energy-only self-consistency scheme with inhomogeneous Hartree shift on the other hand gives the correct qualitative behavior of the mean zero temperature gap. Such an approach might give a reasonable estimate for the mean-field critical temperature with full self-consistency. Phase fluctuations on the other hand would still be strongly underestimated, even in the energy-only scheme with screening.

Chapter 6

Conclusion

This thesis has been dedicated to the study of interactions in disordered metals. The interactions have been treated within mean-field theory. An interesting aspect of mean-field approaches to disordered systems is that they give rise to special ensembles of random Hamiltonians, namely Hamiltonians that satisfy self-consistency. They may exhibit interesting properties, as for instance long-range correlations in their matrix elements. We expect these ensembles to show novel kinds of criticality. The main focus of this thesis was to study (i) such critical behavior; (ii) in what way full self-consistency as opposed to partial self-consistency is necessary to faithfully describe the special properties of these ensembles.

To investigate such ensembles we have developed a state-of-the-art solver for self-consistent field equations based on the kernel polynomial method. The computational complexity could be reduced significantly with respect to full-diagonalization solvers that are conventionally used in this context. This allowed us to reach system sizes two orders of magnitude larger than those that have been reported in the literature. The computationally expensive operation of the KPM is the sparse matrix-vector product. A matrix-free implementation of this product allowed us to achieve a further speed-up of more than a factor of 2 with respect to state-of-the-art sparse-matrix libraries. Our software was designed for the solution of general self-consistent-field theories and is not limited to the systems studied in this thesis.

As the first application of our technology we considered the effect of a single impurity on thin film (2D) and bulk (3D) superconductors. We are motivated by a collaboration with the experimental group of Wulf Wulfhekel of the Karlsruhe Institute of Technology. In this group scanning tunneling

microscopy measurements have been performed around an Fe impurity on the surface of a Al(111) bulk superconductor. The experimentally observed enhancement as well as the induced Friedel oscillations of the gap around the impurity were reproduced semi-quantitatively in our simulations. An exhaustive and detailed comparison with the experiment including the decay of the response is in progress[10].

The main part of the thesis dealt with dirty thin film superconductors with screened Coulomb interaction. Experimentally these systems have been found to exhibit a spatially highly inhomogeneous superconducting gap that is correlated on a scale of the coherence length[27, 28]. Recently an enhancement of the critical temperature by disorder has been measured[33]. The inhomogeneity[12, 80, 35], island formation[12] and critical temperature enhancement[25, 30, 79, 80] have theoretically been observed previously. However the available predictions either do not reach the experimentally most relevant parameter regime(i) or require approximations in their self-consistency property(ii) that have not been systematically investigated so far. With our results we close this gap. In the following we will give examples of our findings with respect to (i).

We have observed the local gap in the low-coupling limit to follow a log-normal distribution for strong disorder. Previous results have been limited to the low disorder case[80]. The perturbative field theoretical result of enhanced LDoS fluctuations close to the critical temperature[30] were shown to carry over to the strong disorder limit as well.

The correlation length was demonstrated to exhibit a non-monotonous evolution with disorder strength already for moderate interaction strength, demonstrating that earlier results carry over from the strong coupling regime[16]. We attribute the non-monotonicity to island formation, which has not been pointed out before. Close to a phase transition, when the correlation length diverges, we expect the resulting long-range correlations to impact the critical behavior exhibited by disordered superconductors.

We have identified a regime of strong gap enhancement (up to $\sim 20\%$), where an increase of the critical temperature is plausible even in the presence of phase fluctuations. This is important, as there is no consensus if an increase in the zero temperature gap can increase the critical temperature.

With respect to (ii) we gained multiple insights. At low disorder phenomena like the LDoS fluctuations are represented semi-quantitatively even without any self-consistency. Already at moderate disorder key features like island formation are not represented by partial energy-only approaches. Based on

the results presented under (i) we believe there should be qualitative changes for analytical theories that rely on partial self-consistency[25].

Chapter 7

Outlook

We have further improvements of our numerical implementation in mind. The evaluation of the trace that is involved in the KPM can be performed stochastically. In such an approach the number of necessary random vectors to reach a given accuracy does not increase with system size. Consequently such a solver is particularily suited for very large systems. We have already developed a pilot implementation of the random trace evaluation. Preliminary tests look quite promising for an application in the very large system size limit.

With a machine learning algorithm we aim to optimize the starting guesses for the self-consistent fields with which the self-consistency cycle is initialized. Such an algorithm could be trained to increase the accuracy of its predictions with previously calculated converged self-consistent fields. This might reduce the number of self-consistency cycle iterations until convergence.

With our established program package thus developed we have many open physical questions in mind that we would like to address. In the following we would like to give a few examples. Within non-self-consistent approaches the critierion for superconductivity to be possible in an underlying localized system has been proposed [76] as

$$\Delta\rho(E_\mathrm{F})\xi_\mathrm{loc}^d \gg 1, \tag{7.1}$$

with superconducting gap Δ, density of states at the Fermi energy $\rho(E_\mathrm{F})$ and localization volume in d dimensions ξ_loc^d. Thus if the number of states in a localization volume within an energy window of the superconducting gap is sufficiently small, a localization transition takes place. Later on it

could be shown that the criterion is too restrictive, especially in a multifractal regime[25]. We are currently working on a paper, where we investigate the localization criterion for the first time within a fully self-consistent approach[127].

It is very promising to investigate other symmetry classes than the one considered in this thesis as well. Thin film superconductors with spin-orbit coupling provide a particularily interesting example. With a p-wave order parameter these systems can support a topological phase. Very little is known about the effect of self-consistency on topological edge states. Furthermore in the symmetry class with broken spin-rotational symmetry an Anderson transition is possible even in 2D. We expect interesting physics for a superconductor close to this transition, as has already been seen in partial self-consistency approaches at the 3D Anderson transition[25]. In addition the existence of a diffusive phase allows for the calculation of conventional random matrix theory properties like level spacing distributions. When only symmetry is taken into account such a distribtuion takes a universal form. It has never been investigated to what extent deviations from universality are brought about by self-consistency.

Finally we also hope that the numerical insights gained with our technology will pave the way for analytical advances. The incorporation of self-consistency in analytical theories of disordered metals would be a major breakthrough. We expect this to be an important basis for a critical theory of the SIT. Achieving this goal will be the focus of my postdoc period at the Landau Institute from September 2020 till August 2021.

Chapter 8

Appendix

8.1 Self-consistency cutoff discussion

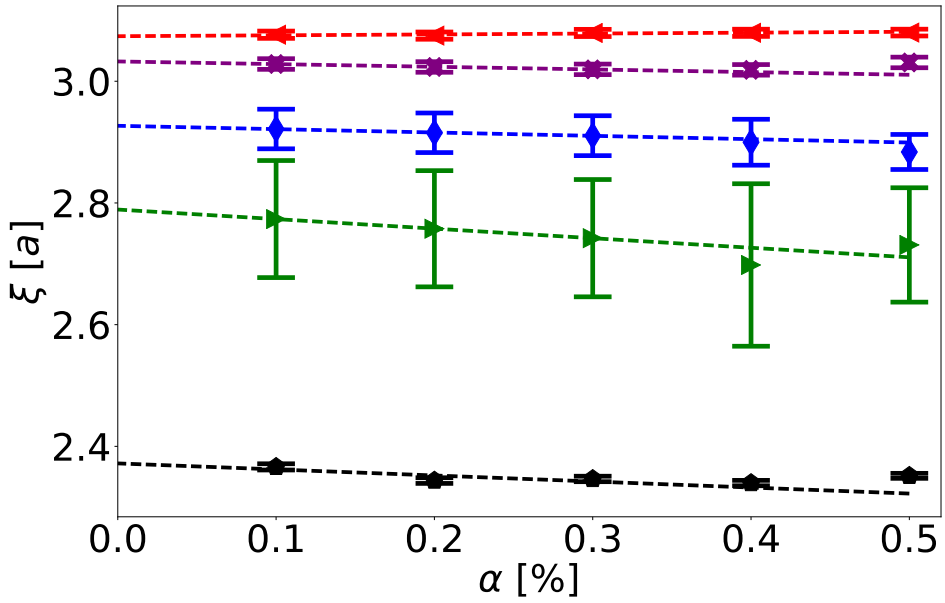

Figure 8.1: Development of ξ with cutoff α for disorder strengths $W = 0.5$ (green), 1.5 (blue), 2.0 (purple), 2.5(red), 3.5 (black); error bars depict the uncertainty stemming from the ensemble average. The dashed lines show a linear fit accounting for the three smallest α values. (Parameters: U=1.5 L=192; $N_{\mathrm{E}} \approx 600 - 1000$)

In Fig. 8.1 the dependence of ξ on α at fixed W is shown. The data demonstrates good convergence behavior of ξ in terms of the cutoff-parameter α; in particular, the α-dependency of ξ is seen to be small as compared to the variation with W. Figure 8.2 re-plots the data shown in Fig. 8.1, so the evolution of ξ with W is more clearly illustrated. In particular, it is seen that the non-monotonic behavior is very well converged in the cutoff α. The stronger change of ξ with α seen at low disorder strengths, e.g. at $W = 0.05, 0.5$, is related to the fact that the distribution of local values, $\Delta(\mathbf{r})$ is narrow at small W. In this case, the convergence requirement allowing for a maximal percentage α of change from cycle to cycle has implications for a substantial fraction of all sites; with broad distributions, convergence of most sites will be much better than α.

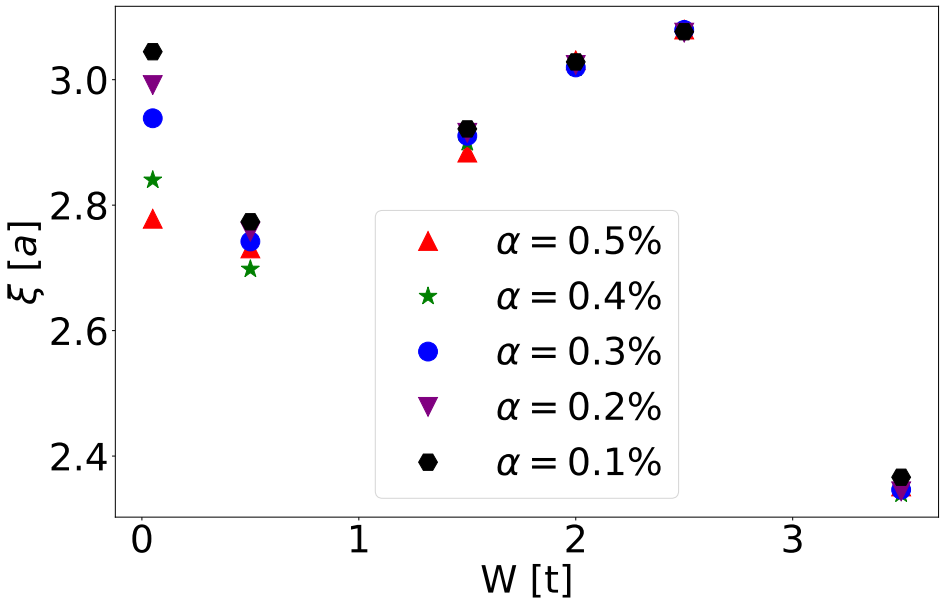

Figure 8.2: Re-plot of the data Fig. (8.1) to illustrate the (converged) variation of ξ with W.

Acknowledgements

I would like to thank my advisor Professor Evers for giving me the opportunity to work on this project. I have learned a lot in the past 4 years, thank you for that Ferdinand! Besides the professional aspect, I will certainly miss being a part of the Evers group in a personal way, too. Especially the group parties will be dearly missed.

I want to also thank the rest of the gang: Maria, Patrick, Felix, Nithin, Christian and Jan you are fantastic! Special thanks are reserved for Daniel: Thank you for all the time that you spent educating me and of course also the fun that we had.

To my office mates Magda and Maria: It has been a pleasure!

Furthermore I want to thank Professor Fabian for agreeing to act as referee for my thesis.

I am grateful to Soumya Bera, Igor Burmistrov, Christoph Strunk and Thomas Vojta for numerous inspiring discussions; also I'd like to express my gratitude to Ivan Kondov and Bruno Lang for sharing mathematical and computational expertise. Support from the DFG under EV30/11-1, EV30/12-1 and SFB-1277(Projects A03, B01) is acknowledged. I gratefully acknowledge the Gauss Centre for Supercomputing e.V. (www.gauss-centre.eu) for funding this project by providing computing time on the GCS Supercomputer SuperMUC at Leibniz Supercomputing Centre (www.lrz.de). This work was performed on the supercomputer ForHLR funded by the Ministry of Science, Research and the Arts Baden-Württemberg and by the Federal Ministry of Education and Research.

Bibliography

[1] M.R. Zirnbauer. "Riemannian symmetric superspaces and their origin in random-matrix theory". In: *J. Math. Phys.* 37 (1996), p. 4986.

[2] A. Altland and M. R. Zirnbauer. "Nonstandard symmetry classes in mesoscopic normal-superconducting hybrid structures". In: *Phys. Rev. B* 55 (1997), p. 1142.

[3] P. Heinzner, A. Huckleberry, and M.R. Zirnbauer. "Symmetry Classes of Disordered Fermions". In: *Commun. Math. Phys.* 257 (2005), p. 725.

[4] Ferdinand Evers and Alexander D. Mirlin. "Anderson transitions". In: *Rev. Mod. Phys.* 80 (4 Oct. 2008), pp. 1355–1417.

[5] A.D. Mirlin et al. "Transition from localized to extended eigenstates in the ensemble of power-law random banded matrices". In: *Phys. Rev. E* 54 (1996), p. 3221.

[6] A.D. Mirlin and F. Evers. "Multifractality and critical fluctuations at the Anderson transition". In: *Phys. Rev. B* 62 (2000), p. 7920.

[7] A. D. Mirlin and F. Evers. "Multifractality and critical fluctuations at the Anderson transition". In: *Phys. Rev. B* 62 (12 Sept. 2000), pp. 7920–7933.

[8] F.M. Izrailev, A.A. Krokhin, and N.M. Makarov. "Anomalous localization in low-dimensional systems with correlated disorder". In: *Physics Reports* 512.3 (2012), pp. 125–254.

[9] Matthias Stosiek, Bruno Lang, and Ferdinand Evers. "Self-consistent-field ensembles of disordered Hamiltonians: Efficient solver and application to superconducting films". In: *Phys. Rev. B* 101 (14 Apr. 2020), p. 144503.

[10] Matthias Stosiek et al. In: *unpublished* (expected:2020).

[11] A. Ghosal, M. Randeria, and N. Trivedi. "Role of Spatial Amplitude Fluctuations in Highly Disordered s-Wave Superconductors". In: *Phys. Rev. Lett.* 81 (1998), p. 3940.

[12] A. Ghosal, M. Randeria, and N. Trivedi. "Inhomogeneous pairing in highly disordered s-wave superconductors". In: *Phys. Rev. B* 65 (2001), p. 014501.

[13] Yonatan Dubi, Yigal Meir, and Yshai Avishai. "Nature of the Superconductor insulator transition in disordered superconductors". In: *Nature* 449 (2007), p. 876.

[14] Karim Bouadim et al. "Single- and two-particle energy gaps across the disorder-driven superconductor-insulator transition". In: *Nat. Phys.* 7 (2011), p. 884.

[15] G. Seibold et al. "Superfluid Density and Phase Relaxation in Superconductors with Strong Disorder". In: *Phys. Rev. Lett.* 108 (2012), p. 207004.

[16] G. Lemarié et al. "Universal scaling of the order-parameter distribution in strongly disordered superconductors". In: *Phys. Rev. B* 87 (2013), p. 184509.

[17] T. Cea et al. "Optical excitation of phase modes in strongly disordered superconductors". In: *Phys. Rev. B* 89 (2014).

[18] I.-D. Potirniche et al. "Superconductivity of disordered Dirac fermions in graphene". In: *Phys. Rev. B* 90 (2014), p. 094516.

[19] G. Seibold et al. "Amplitude, density, and current correlations of strongly disordered superconductors". In: *Phys. Rev. B* 92 (2015), p. 064512.

[20] T. Cea et al. "Nonrelativistic Dynamics of the Amplitude (Higgs) Mode in Superconductors". In: *Phys. Rev. Lett.* 115 (2015), p. 157002.

[21] Yen Lee Loh et al. "Superconductor-Insulator Transition and Fermi-Bose Crossovers". In: *Phys. Rev. X* 6 (2016), p. 021029.

[22] Maria N. Gastiasoro and Brian M. Andersen. "Enhancing superconductivity by disorder". In: *Phys. Rev. B* 98 (18 Nov. 2018), p. 184510.

[23] Bo Fan and Antonio M. García-García. "Enhanced phase-coherent multifractal two-dimensional superconductivity". In: *Physical Review B* 101.10 (Mar. 2020).

[24] M. V. Feigel'man et al. "Eigenfunction Fractality and Pseudogap State near the Superconductor-Insulator Transition". In: *Phys. Rev. Lett.* 98 (2007), p. 027001.

[25] M. V. Feigel'man et al. "Fractal superconductivity near localization threshold". In: *Ann. Phys-New York* 325 (2010), p. 1390.

[26] M. V. Feigel'man and L. B. Ioffe. "Superfluid density of a pseudogapped superconductor near the superconductor-insulator transition". In: *Phys. Rev. B* 92 (2015), 100509(R).

[27] B. Sacépé et al. "Disorder-Induced Inhomogeneities of the Superconducting State Close to the Superconductor-Insulator Transition". In: *Phys. Rev. Lett.* 101 (15 Oct. 2008), p. 157006.

[28] B. Sacépé et al. "Localization of preformed Cooper pairs in disordered superconductors". In: *Nature Physics* 7 (3 2011), p. 239.

[29] T. Dubouchet et al. "Collective energy gap of preformed Cooper pairs in disordered superconductors". In: *Nature Physics* 15 (3 2019), p. 233.

[30] I.S. Burmistrov, I.V. Gornyi, and A.D. Mirlin. "Enhancement of the Critical Temperature of Superconductors by Anderson Localization". In: *Phys. Rev. Lett.* 108 (2012), p. 017002.

[31] I.S. Burmistrov, I.V. Gornyi, and A.D. Mirlin. "Multifractality at Anderson transitions with Coulomb interaction". In: *Phys. Rev. Lett.* 111 (2013), p. 066601.

[32] I.S. Burmistrov, I.V. Gornyi, and A.D. Mirlin. "Superconductor insulator transitions: Phase diagram and magnetoresistance". In: *Phys. Rev. B* 92 (2015), p. 014506.

[33] K. Zhao et al. "Disorder-induced multifractal superconductivity in monolayer niobium dichalcogenides". In: *Nature Physics* 15 (9 2019), p. 904.

[34] Y. Noat et al. "Unconventional superconductivity in ultrathin superconducting NbN films studied by scanning tunneling spectroscopy". In: *Phys. Rev. B* 88 (1 July 2013), p. 014503.

[35] I.S. Burmistrov, I.V. Gornyi, and A.D. Mirlin. "Local density of states and its mesoscopic fluctuations near the transition to a superconducting state in disordered systems". In: *Phys. Rev. B* 93 (2016), p. 205432.

[36] E. J. König et al. "Berezinskii-Kosterlitz-Thouless transition in homogeneously disordered superconducting films". In: *Phys. Rev. B* 92 (21 Dec. 2015), p. 214503.

[37] J. Hubbard. "Electron correlations in narrow energy bands". In: *Proc. R. Soc. London, Ser. A* 276 (1963), p. 238.

[38] P. G. de Gennes. *Superconductivity of Metals and Alloys*. Westview Press, 1999.

[39] M. Tinkham. *Introduction to Superconductivity*. Dover Publications Inc., 2004.

[40] A. Weiße et al. "The kernel polynomial method". In: *Rev. Mod. Phys.* 78 (2006), p. 275.

[41] M. Abramowitz and I. A. Stegun. *Handbook of Mathematical Functions*. Dover Publications Inc., 1970.

[42] Andreas Pieper, Georg Hager, and Holger Fehske. "A domain-specific language and matrix-free stencil code for investigating electronic properties of Dirac and topological materials". In: *arXiv:1708.09689v2* (2017).

[43] L. Covaci, F. M. Peeters, and M. Berciu. "Superconductivity of disordered Dirac fermions in graphene". In: *Phys. Rev. Lett.* 105 (2010), p. 167006.

[44] Yuki Nagai, Yukihiro Ota, and Masahiko Machida. "Efficient Numerical Self-Consistent Mean-Field Approach for Fermionic Many-Body Systems by Polynomial Expansion on Spectral Density". In: *J. Phys. Soc. Jpn* 81 (2012), p. 024710.

[45] Yuki Nagai et al. "Numerical Contruction of a Low-Energy Effective Hamiltonian in a Self-Consistent Bogoliubov-de Gennes Approach of Superconductivity". In: *J. Phys. Soc. Jpn* 82 (2013), p. 094701.

[46] D. A. Bonn et al. "Comparison of the influence of Ni and Zn impurities on the electromagnetic properties of $YBa_2Cu_3O_{6.95}$". In: *Phys. Rev. B* 50 (6 Aug. 1994), pp. 4051–4063.

[47] H. F. Fong et al. "Effect of Nonmagnetic Impurities on the Magnetic Resonance Peak in $YBa_2Cu_3O_7$". In: *Phys. Rev. Lett.* 82 (9 Mar. 1999), pp. 1939–1942.

[48] S. H. Pan et al. “”Imaging the effects of individual zinc impurity atoms on superconductivity in Bi2Sr2CaCu2O8+δ””. In: *Nature* 403 (6771 2000), p. 746.

[49] V. Thampy et al. “Friedel-Like Oscillations from Interstitial Iron in Superconducting $Fe_{1+y}Te_{0.62}Se_{0.38}$”. In: *Phys. Rev. Lett.* 108 (10 Mar. 2012), p. 107002.

[50] K. Tanaka and F. Marsiglio. “S-wave superconductivity near a surface”. In: *Physica C: Superconductivity* 384.3 (2003), pp. 356–368.

[51] K Tanaka and F Marsiglio. “Microscopic study of inhomogeneous superconductors”. In: *Journal of Physics and Chemistry of Solids* 63.12 (2002). Proceedings of the Conference on Spectroscopies in Novel Superconductors, pp. 2287–2293.

[52] A. V. Balatsky, I. Vekhter, and Jian-Xin Zhu. “Impurity-induced states in conventional and unconventional superconductors”. In: *Rev. Mod. Phys.* 78 (2 May 2006), pp. 373–433.

[53] Emanuele G. Dalla Torre et al. “Friedel oscillations as a probe of fermionic quasiparticles”. In: *Phys. Rev. B* 93 (20 May 2016), p. 205117.

[54] Lars Lauke et al. “Friedel oscillations and Majorana zero modes in inhomogeneous superconductors”. In: *Phys. Rev. B* 98 (13 Oct. 2018), p. 134502.

[55] J. Friedel. “XIV. The distribution of electrons round impurities in monovalent metals”. In: *The London, Edinburgh, and Dublin Philosophical Magazine and Journal of Science* 43.337 (1952), pp. 153–189.

[56] Gabriele Giuliani. *Quantum Theory of the Electron Liquid*. Cambridge University Press, 2005.

[57] Alexander L. Fetter. “Spherical Impurity in an Infinite Superconductor”. In: *Phys. Rev.* 140 (6A Dec. 1965), A1921–A1936.

[58] Wei-Feng Tsai et al. “Impurity-induced bound states in iron-based superconductors with s-wave $\cos k_x \cdot \cos k_y$ pairing symmetry”. In: *Phys. Rev. B* 80 (6 Aug. 2009), p. 064513.

[59] T. Giamarchi, M. T. Béal-Monod, and Oriol T. Valls. “Onset of surface superconductivity”. In: *Phys. Rev. B* 41 (16 June 1990), pp. 11033–11046.

[60] D. N. Aristov, S. V. Maleyev, and A. G. Yashenkin. "RKKY interaction in layered superconductors with anisotropic pairing". In: *Z. Phys. B* 102 (1997), p. 467.

[61] P.W. Anderson. "Absence of Diffusion in Certain Random Lattices". In: *Phys. Rev. B* 109 (1958), p. 1492.

[62] A. MacKinnon and B. Kramer. "The scaling theory of electrons in disordered solids: Additional numerical results". In: *Zeitschrift für Physik B Condensed Matter* 53 (1 1983), p. 1.

[63] V. I Fal'ko and K. B Efetov. "Multifractality: Generic Property of Eigenstates of 2D Disordered Metals". In: *Europhysics Letters (EPL)* 32.8 (Dec. 1995), pp. 627–632.

[64] A. M. Goldman and N. Marković. "Superconductor-insulator transitions in the two-dimensional limit". In: *Phys. Today* 51.39 (1998).

[65] A. M. Goldman. "Superconductor-Insulator Transitions". In: *International Journal of Modern Physics B* 24.20n21 (2010), pp. 4081–4101.

[66] Vsevolod F Gantmakher and Valery T Dolgopolov. "Superconductor–insulator quantum phase transition". In: *Physics-Uspekhi* 53.1 (Jan. 2010), pp. 1–49.

[67] Michael V Sadovskii. "Superconductivity and localization". In: *Physics Reports* 282.5 (1997), pp. 225–348.

[68] A.A. Abrikosov and L.P. Gorkov. "On The Theory of Superconducting Alloys I. the Electrodynamics of Alloys at absolute zero". In: *Sov. Phys. JETP* 8 (1958), p. 1090.

[69] P.W. Anderson. "Theory of dirty superconductors". In: *J. Phys. Chem. Solids* 11 (1959), p. 26.

[70] L. N. Bulaevskii and M. V. Sadovski. "Localization and superconductivity". In: *Pisma ZhETF* 39.524 (1984).

[71] L. N. Bulaevskii and M. V. Sadovskii. In: *J. Low Temp.* 59 (1985), p. 89.

[72] L. N. Bulaevskii and M. V. Sadovskii. In: *JETP Lett.* 43 (1986), p. 99.

[73] L. N. Bulaevskii, S. V. Panyukov, and M. V. Sadovskii. In: *Sov. Phys. JETP* 65 (1987), p. 380.

[74] A. Kapitulnik and G. Kotliar. In: *Phys. Rev. Lett.* 54.473 (1985).

[75] A. Kapitulnik and G. Kotliar. In: *Phys. Rev. B* 33.5 (1985).

[76] M. Ma and P.A. Lee. "Localized superconductors". In: *Phys. Rev. B* 32 (1985), p. 5658.

[77] I. S. Burmistrov, I. V. Gornyi, and A. D. Mirlin. "Enhancement of the Critical Temperature of Superconductors by Anderson Localization". In: *Phys. Rev. Lett.* 108 (1 Jan. 2012), p. 017002.

[78] I. S. Burmistrov, I. V. Gornyi, and A. D. Mirlin. "Superconductor-insulator transitions: Phase diagram and magnetoresistance". In: *Phys. Rev. B* 92 (1 July 2015), p. 014506.

[79] V E Kravtsov. "Wonderful life at weak Coulomb interaction: increasing of superconducting/superfluid transition temperature by disorder". In: *Journal of Physics: Conference Series* 376 (July 2012), p. 012003.

[80] James Mayoh and Antonio M. García-García. "Global critical temperature in disordered superconductors with weak multifractality". In: *Physical Review B* 92.17 (Nov. 2015).

[81] Mats Wallin et al. "Superconductor-insulator transition in two dimensional dirty boson systems". In: *Phys. Rev. B* 49 (17 May 1994), pp. 12115–12139.

[82] Yonatan Dubi, Yigal Meir, and Yshai Avishai. "Theory of the magnetoresistance of disordered superconducting films". In: *Phys. Rev. B* 73 (5 Feb. 2006), p. 054509.

[83] M. V. Feigel'man, L. B. Ioffe, and M. Mézard. "Superconductor-insulator transition and energy localization". In: *Phys. Rev. B* 82 (2010), p. 184534.

[84] K. Sheshadri et al. "Percolation-Enhanced Localization in the Disordered Bosonic Hubbard Model". In: *Phys. Rev. Lett.* 75 (22 Nov. 1995), pp. 4075–4078.

[85] E. Shimshoni, A. Auerbach, and A. Kapitulnik. "Transport through Quantum Melts". In: *Phys. Rev. Lett.* 80 (15 Apr. 1998), pp. 3352–3355.

[86] A. M. Finkel'stein. *Electron Liquid in Disordered Conductors*. CRC Press, 1990.

[87] K B Efetov. "Phase transition in granulated superconductors". In: *Sov. Phys. - JETP (Engl. Transl.); (United States)* 51 (May 1980).

[88] V. F. Gantmakher et al. “Giant negative magnetoresistance of semi-insulating amorphous indium oxide films in strong magnetic fields”. In: *Zh. Eksp. Teor. Fiz.* 109 (1996), p. 1765.

[89] K. H. Sarwa B. Tan, Kevin A. Parendo, and A. M. Goldman. “Evidence of spatially inhomogeneous pairing on the insulating side of a disorder-tuned superconductor-insulator transition”. In: *Phys. Rev. B* 78 (1 July 2008), p. 014506.

[90] David Kowal and Zvi Ovadyahu. “Disorder induced granularity in an amorphous superconductor”. In: *Solid State Communications* 90.12 (0038-1098 1994), pp. 783–786.

[91] B. Sacépé et al. “High-field termination of a Cooper-pair insulator”. In: *Phys. Rev. B* 91 (22 June 2015), p. 220508.

[92] D. Shahar and Z. Ovadyahu. “Superconductivity near the mobility edge”. In: *Phys. Rev. B* 46 (17 Nov. 1992), pp. 10917–10922.

[93] G. Sambandamurthy et al. “Superconductivity-Related Insulating Behavior”. In: *Phys. Rev. Lett.* 92 (10 Mar. 2004), p. 107005.

[94] D. Sherman et al. “Measurement of a Superconducting Energy Gap in a Homogeneously Amorphous Insulator”. In: *Phys. Rev. Lett.* 108 (17 Apr. 2012), p. 177006.

[95] Myles Steiner and Aharon Kapitulnik. “Superconductivity in the insulating phase above the field-tuned superconductor-insulator transition in disordered indium oxide films”. In: *Physica C: Superconductivity* 422.1 (0921-4534 2005), p. 16.

[96] B. Sacépé et al. “Pseudogap in a thin film of a conventional superconductor”. In: *Nature Communications* 1 (1 2010), p. 140.

[97] T.I. Baturina et al. “Quantum-critical region of the disorder-driven superconductor-insulator transition”. In: *Physica C: Superconductivity* 468.4 (2008). Proceedings of the Workshop on Fluctuations and Phase Transitions in Superconductors, pp. 316–321.

[98] T. I. Baturina et al. “Superconductivity on the localization threshold and magnetic-field-tuned superconductor-insulator transition in TiN films”. In: *Journal of Experimental and Theoretical Physics Letters* 79 (7 2004), p. 337.

[99] T. I. Baturina et al. "Quantum Metallicity on the High-Field Side of the Superconductor-Insulator Transition". In: *Phys. Rev. Lett.* 98 (12 Mar. 2007), p. 127003.

[100] T.I. Baturina et al. "Localized Superconductivity in the Quantum-Critical Region of the Disorder-Driven Superconductor-Insulator Transition in TiN Thin Films". In: *Phys. Rev. Lett.* 99 (2007), p. 257003.

[101] S. P. Chockalingam et al. "Tunneling studies in a homogeneously disordered *s*-wave superconductor: NbN". In: *Phys. Rev. B* 79 (9 Mar. 2009), p. 094509.

[102] Mintu Mondal et al. "Phase Fluctuations in a Strongly Disordered *s*-Wave NbN Superconductor Close to the Metal-Insulator Transition". In: *Phys. Rev. Lett.* 106 (4 Jan. 2011), p. 047001.

[103] A. Kamlapure et al. "Emergence of nanoscale inhomogeneity in the superconducting state of a homogeneously disordered conventional superconductor". In: *Scientific Reports* 3 (2013), p. 2979.

[104] E. Bielejec, J. Ruan, and Wenhao Wu. "Hard Correlation Gap Observed in Quench-Condensed Ultrathin Beryllium". In: *Phys. Rev. Lett.* 87 (3 June 2001), p. 036801.

[105] V. Yu. Butko and P. W. Adams. "Quantum metallicity in a two-dimensional insulator". In: *Nature* 409 (2001), p. 161.

[106] N. "Marković et al. "Superconductor-insulator transition in two dimensions". In: *Phys. Rev. B* 60 (6 Aug. 1999), pp. 4320–4328.

[107] H. Q. Nguyen et al. "Observation of Giant Positive Magnetoresistance in a Cooper Pair Insulator". In: *Phys. Rev. Lett.* 103 (15 Oct. 2009), p. 157001.

[108] S. M. Hollen et al. "Collapse of the Cooper pair phase coherence length at a superconductor-to-insulator transition". In: *Phys. Rev. B* 87 (5 Feb. 2013), p. 054512.

[109] A. D. Caviglia et al. "Electric field control of the LaAlO3/SrTiO3 interface ground state". In: *Nature* 456 (2008), p. 624.

[110] A. T. Bollinger et al. "Superconductor-insulator transition in La2 - xSr x CuO4 at the pair quantum resistance". In: *Nature* 472 (2011), p. 458.

[111] Yuichi Kasahara et al. "Enhancement of Pairing Interaction and Magnetic Fluctuations toward a Band Insulator in an Electron-Doped Li_xZrNCl Superconductor". In: *Phys. Rev. Lett.* 103 (7 Aug. 2009), p. 077004.

[112] Hisashi Kotegawa et al. "Strong suppression of coherence effect and appearance of pseudogap in the layered nitride superconductor Li_xZrNCl: ^{91}Zr- and ^{15}N-NMR studies". In: *Phys. Rev. B* 90 (2 July 2014), p. 020503.

[113] R. Schneider et al. "Superconductor-Insulator Quantum Phase Transition in Disordered FeSe Thin Films". In: *Phys. Rev. Lett.* 108 (25 June 2012), p. 257003.

[114] R Schneider et al. "Excess conductivity and Berezinskii–Kosterlitz–Thouless transition in superconducting FeSe thin films". In: *Journal of Physics: Condensed Matter* 26.45 (Oct. 2014), p. 455701.

[115] Joseph A. Sulpizio et al. "Nanoscale Phenomena in Oxide Heterostructures". In: *Annual Review of Materials Research* 44.1 (2014), pp. 117–149.

[116] Y. Taguchi, A. Kitora, and Y. Iwasa. "Increase in T_c upon Reduction of Doping in Li_xZrNCl Superconductors". In: *Phys. Rev. Lett.* 97 (10 Sept. 2006), p. 107001.

[117] Kouji Taniguchi et al. "Electric-field-induced superconductivity at 9.4 K in a layered transition metal disulphide MoS2". In: *Applied Physics Letters* 101.4 (2012), p. 042603.

[118] J. T. Ye et al. "Superconducting Dome in a Gate-Tuned Band Insulator". In: *Science* 338.6111 (2012), pp. 1193–1196.

[119] G. Sambandamurthy et al. "Experimental Evidence for a Collective Insulating State in Two-Dimensional Superconductors". In: *Phys. Rev. Lett.* 94 (1 Jan. 2005), p. 017003.

[120] Wenhao Wu and E. Bielejec. *Measuring the Localization Length through the superconductor-insulator transition in ultrathin amorphous beryllium films*. 2005.

[121] D. Shahar and Z. Ovadyahu. "Superconductivity near the mobility edge". In: *Phys. Rev. B* 46 (17 Nov. 1992), pp. 10917–10922.

[122] S. P. Chockalingam et al. "Tunneling studies in a homogeneously disordered *s*-wave superconductor: NbN". In: *Phys. Rev. B* 79 (9 Mar. 2009), p. 094509.

[123] A.D. Mirlin. "Statistics of energy levels and eigenfunctions in disordered systems". In: *Phys. Rep.* 326 (2000), p. 259.

[124] Qijin Chen et al. "BCS-BEC crossover: From high temperature superconductors to ultracold superfluids". In: *Physics Reports* 412.1 (2005), pp. 1–88.

[125] Matthias Stosiek, Igor Burmistrov, and Ferdinand Evers. In: *unpublished* (expected:2020).

[126] Nandini Trivedi et al. "Emergent granularity and pseudogap near the superconductor-insulator transition". In: *Journal of Physics: Conference Series* 376 (July 2012), p. 012001.

[127] Matthias Stosiek, Igor Burmistrov, and Ferdinand Evers. In: *unpublished* (expected:2021).

[128] B. Kramer B. Bulka M. Schreiber. "Localization, quantum interference, and the metal-insulator transition". In: *B.Z. Physik B - Condensed Matter* 66 (1987), p. 21.